

Determining Key Parameters and Guidelines for the Design of an Electrically Activated
Concrete Slab for Peak Shifting in a Light-Weight Residential Building in a Northern
Climate

Dave Olsthoorn

A Thesis Report

In

The Department

Of

Building, Civil and Environmental Engineering

Presented in Partial Fulfillment of the Requirements
For the Master of Engineering (Building/Civil) Program at
Concordia University
Montreal, Quebec, Canada

August 14th, 2018

© Dave Olsthoorn, 2018

CONCORDIA UNIVERSITY

Department of Building, Civil and Environmental Engineering

This is to certify that the thesis prepared

By: **Dave Olsthoorn**

Entitled: **Determining Key Parameters and Guidelines for the Design of an Electrically Activated Concrete Slab for Peak Shifting in a Light-Weight Residential Building in a Northern Climate**

and submitted in partial fulfillment of the requirements for the degree of

Master of Applied Science (Building Engineering)

conforms to the regulations of the University and meets the accepted standards with respect to originality and quality.

Signed by the final examining committee:

<u>Dr. Hoi Dick Ng</u>	Examiner
<u>Dr. Radu Zmeureanu</u>	Examiner
<u>Dr Fuzhan Nasiri</u>	Examiner
<u>Dr. Haghghat</u>	Supervisor
<u>Mr. Alain Moreau</u>	Co-Supervisor

Approved by

Dr. Haghghat
Graduate Program Director, Department of Building, Civil & Environmental Engineering

Dr. Amir Asif
Dean of Faculty

Date:

June 19th, 2018

Abstract

A thermal storage system for residential buildings in a Northern climate is developed for electrical peak shifting and shaving. To facilitate implementation, only commercially available products are used for the system in conjunction with common construction methods. A thermal model is created with the TRNSYS simulation software and validated using data from a two-year monitoring campaign. The thermal model is used to identify key system parameters and propose system design guidelines. It is determined that, for residential buildings with a footprint varying between 80 m² to 200 m², the basement floor slab can be used for thermal storage with electrical heating cables and that the entire basement heating load can, during the peaks, be shifted to off peak periods. The optimal assembly for the basement floor is composed of 102 mm of extruded polystyrene insulation followed by 152 mm of concrete. The electric heating cables are positioned at the bottom of the concrete layer. This assembly can be controlled with the air set point temperature. The air setpoint temperature of basement rooms during charging needs to be 2°C higher than the air setpoint temperature during normal operating conditions. The required charging time for building footprints of 80, 120 160 and 200 m² corresponds to 6.00, 5.51, 5.05 and 4.66 hours, respectively.

Acknowledgements

I would like to express my deepest gratitude to my supervisor Dr. Fariborz Haghighat for his continuous support, his guidance and up and foremost, for his trust in me. He has been a great inspiration both on a professional and a personal level.

I would like to acknowledge the contribution of Hydro-Québec's research institute (Laboratoire des technologies de l'énergie) for supplying monitoring equipment for the study as well as invaluable knowledge through the involvement of their experts; more specifically Alain Moreau and Stéphane Boyer. I would also like to thank Ouellet Canada Inc. for their involvement in the project which included heating equipment, a house to monitor, ventilation equipment as well as specialists such as Gino Lacroix and Philippe Beaulieu.

I am grateful for the financial support offered by the Natural Science and Engineering Research Council of Canada (NSERC) through the Alexandre Graham Bell Canada Graduate Scholarships as well as Hydro Québec's Scholarship for the Engineering Faculty.

Last but not least, I would like to thank all my friends and family for their continuous support and encouragements.

Table of Contents

CHAPTER 1: INTRODUCTION	1
1.1 Background	1
1.2 Scope and Objective.....	3
CHAPTER 2: TECHNICAL LITERATURE REVIEW	5
2.1 Means of Thermal Mass Activation.....	5
2.1.1 Surface Activation.....	6
2.2 Forced-Air Activation.....	12
2.1.3 Hydronic Activation.....	17
2.1.4 Electrical Activation.....	23
2.2. Thermal Performance and Control of Activated Thermal Mass.....	24
2.3. Barriers to Application.....	30
2.4. Summary	32
CHAPTER 3: METHODOLOGY	34
3.1 Monitoring Campaign	34
3.1.1 Description of the Building.....	34
3.1.2 Selection of Parameters.....	36
3.1.3 Data Quality Validation	36
3.2 Model Development.....	37
3.2.1 Modelling Software Description	37
3.2.2 Approaches to Produce Reliable Model Input	38
3.2.3 Model Validation	39
3.3 Peak Shave Potential	41

3.3.1 Description of the Thermal Storage System	42
3.3.2 Description of the Control Strategy	43
3.3.3 Performance Evaluation	44
3.3.4 Reference Scenario.....	46
3.3.5 Peak Shave Potential of Current Configuration.....	47
3.3.6 Optimal System Configuration for the Monitored Building.....	47
3.3.7 Optimal System Configuration for Buildings of Various Footprints.....	48
CHAPTER 4: RESULTS.....	50
4.1 Monitored Data Quality Validation	50
4.2 Model Validation	52
4.2.1 Energy Losses	52
4.2.2 Thermal Time Constant	54
4.2.3 Building Energy Consumption.....	55
4.3 Peak Shave Potential	58
4.3.1 Reference Power Consumption.....	58
4.3.2 Peak Shave Potential of Current Configuration.....	59
4.3.3 Optimal System Configuration for Monitored Building.....	61
4.3.4 Optimal System Configuration for Buildings of Various Footprints.....	65
CHAPTER 5: CONCLUSION	69
BIBLIOGRAPHY.....	72
APPENDIX A – Optimal System Configuration Selection.....	92
A.1 Building with an 80 m ² Footprint.....	93
A.2 Building with a 120 m ² Footprint.....	94
A.3 Building with a 160 m ² Footprint.....	95

A.4 Building with a 200 m ² Footprint.....	96
APPENDIX B – Monitoring Equipment Installation	97
B.1 SS-CH1 (Basement Bedroom 1)	98
B.2 SS-SF (Basement Family Room)	99
B.3 SS-SDB (Basement Bathroom)	100
B.4 SS-CH2 (Basement Bedroom 2)	101
B.5 SS-GAR (Basement Storage and Laundry Room)	102
B.6 RDC-SF (Ground Floor Family Room and Dining Area).....	103
B.7 RDC-CUI (Ground Floor Kitchen, Dining Area, Mudroom).....	104
B.8 RDC-GAR (Ground Floor Garage).....	105
B.9 ET-SDB1 and ET-SDB2 (2 nd Floor Bathrooms).....	106
B.10 ET-CH1, ET-CH2 and ET-CH3 (2 nd Floor Bedrooms).....	107
B.11 ET-BUR (2 nd Floor Office and Gym).....	108
B.12 ET-COU (2 nd Floor Hallway).....	109
B.13 Hot Water Tank	110
B.14 Heat Exchanger	111
APPENDIX C – Construction Drawings	113
APPENDIX D – Modelling Notes	129
D.1 Heat Transfer through Walls and Assemblies.....	130
D.2 Heat Exchange between Surfaces	131
D.3 Windows and Doors	131
D.4 Attic Thermal Network	132
D.5 Heat Exchanger	132
D.6 Vertical Air Shafts.....	132

D.7 Integrating Infiltration Test Measurements	132
D.8 Modelling Electric Heating Cables in TRNSYS	134
D.9 Convective Heat Transfer Coefficients	135
D.10 Hot Water Tank	138
D.11 Thermostats	138
D.11.1 PI-Controller Structure	139
D.11.2 Stage Controller Structure	140
D.11.3 Optimisation Process	140
D.11.4 Simulated Thermostats	142
D.12 Internal Heat Gains	143
APPENDIX E – Infiltration Test Report	146
E.1. General Information	148
E.2. Building Description	149
E.2.1 Location	149
E.2.2 Construction	149
E.2.3 Condition of Openings in Building Envelope	150
E.2.4 HVAC System	151
E.3. Procedure	153
E.3.1 Technique Employed	153
E.3.2 Test Equipment Used	153
E.3.3 Calibration Date of Fan Pressurization Device	153
E.3.4 Calibrated Density	153
E.4. Measurement Data	154
E.4.1 Fan Pressurization Measurements	154

E.4.2 Ancillary Data.....	155
E.5. Calculations	156
E.5.1 Means and Standard Deviations	156
E.5.2 One-Point Method	156
E.5.3 Two-Point Method.....	157
E.5.4 Manual Curve	158
E.5.5 Error Calculations.....	158
E.6. Calibration Certificates.....	160
E.6.1 Statement of Means of Calibration	160
E.6.2 Statement of Precision and Bias of Instruments	160
APPENDIX F – House Parameters.....	161
F.1 House Plans.....	162
F.1.1 Basement.....	162
F.1.2 Ground Floor.....	163
F.1.3 Second Floor	164
F.2 Heated Floor Construction.....	165
F.3 Hot Water Tank.....	169
F.4 Air Exchanger	170
F.6 Laundry Chute	171
F.7 Assemblies	171
F.8 Heating Systems.....	173

List of Figures

Figure 1 : Annual Surplus Destined for Exportation From 2008-2028	3
Figure 2 : Front View (Left) and Back View (Right) of the House.....	34
Figure 3: Workflow for Geometry File Creation.....	39
Figure 4 : Sample Workflow for TRNSYS Input File Creation.....	39
Figure 5 : Thermal Storage Assembly	43
Figure 6 : Implemented Control Strategy with Arbitrary Charging Set Point Temperature	44
Figure 7 : Temperature Profiles of Rooms Heated with an Electric Heating Floor: Basement Living Room (Left) and Ground Floor Kitchen (Right).....	51
Figure 8 : Temperature Profiles of Rooms Heated by Baseboards: Basement Family Room (Left) and Ground Floor Family Room (Right).....	52
Figure 9 : Volume Weighted Average Building Temperature.....	53
Figure 10 : Average Basement Slab Surface Temperature.....	54
Figure 11 : Simulated versus Actual Building Electrical Consumption for Space Heating	56
Figure 12 : Daily Building Electricity Demand as a Function of Outdoor Temperature .	58
Figure 13 : Average Peak Potential as a Function of Outdoor Air Temperature for the Morning Peak (left) and the Evening Peak (right).....	60
Figure 15 : Average Daily Energy Consumption Profile of the Three Coldest Days of Simulation Period.....	61
Figure 16 : Average Peak Potential as a Function of Outdoor Air Temperature for the Morning Peak (left) and the Evening Peak (right) of Optimal System Configuration	64
Figure 18 : Average Daily Energy Consumption Profile of the Three Coldest Days of Simulation Period.....	65

Figure 19 : Average Peak Potential as a Function of Outdoor Air Temperature for the Morning Peak of Optimal System Configuration for Buildings of 80, 120, 160 and 200 m² Footprints 67

Figure 20 : Average Peak Potential as a Function of Outdoor Air Temperature for the Evening Peak of Optimal System Configuration for Buildings of 80, 120, 160 and 200 m² Footprints 68

Figure 23 : SS_CH1 Thermostat and Smart Reader Install. Thermostat ID: SS-CH1-01 98

Figure 24 : SS-SF Thermostat and Smart Reader Install. Thermostat ID: SS-SF-04 (Left), SS-SF-04, SS-SF-03 and SS-SF-02 (Middle), SS-SF-01 (Right)..... 99

Figure 25 : SS-SDB Thermostat and Smart Reader Install. Thermostat ID: SS-SDB-01 100

Figure 26 : SS-CH2 Thermostat Installation. Thermostat ID: SS-CH2-01 (left) and SS-CH2-02 (Right). 101

Figure 27 : Thermostat and Smart Reader Install. Thermostat ID: SS-GAR-01 and SS-GAR-02 (Left) and Sinope In-Line Web Enabled Electrical Switch (Right). 102

Figure 28 : Thermostat and Smart Reader Install (Left) and 2nd Baseboard (Right). Thermostat ID: RDC-SF-01..... 103

Figure 29 : RDC-CUI Thermostat and Smart Reader Install. Thermostat ID: RDC-CUI-01 (Left) and RDC-CUI-01 (Right)..... 104

Figure 30 : RDC-GAR Thermostat and Smart Reader Install (Left) and Driveway Smart Reader Install (Right)..... 105

Figure 31 : ET-SDB1 (Left) and ET-SDB2 (Right) Thermostat and Smart Reader Install 106

Figure 32 : ET_CH1 (Left), ET-CH2 (Middle) and ET-CH3 (Right) Thermostat and Smart Reader Install 107

Figure 33 : ET-BUR Thermostat and Smart Reader Install..... 108

Figure 34 : ET-COU Thermostat and Smart Reader Install 109

Figure 35 : Sinope In-line Switch Installation	110
Figure 36 : a) Temperature Reading Locations b) Measurement Device	111
Figure 37 : Thermostat Install for Heat Exchanger	112
Figure 38 : Comparison of Infiltration Models as A Function of Wind Speed Recorded at Airport and Time.....	134
Figure 39 : Conventional Floor Assembly in TRNSYS (Left) And the Discretization of the Floor Assembly with Fictitious Zone (Right).....	135
Figure 40 : Discretization of Electric Heating Floor into Two Layers and a Wall Gain.	135
Figure 41 : Total Building Electricity Consumption Versus Space Heating Consumption	144
Figure 42 : Residual Electricity Consumption and Snow Fall.....	144
Figure 43 : Residual Consumption as a Function of the Hour of Day.....	145
Figure 44 : A) Envelope Penetrations on East Facade (Top Left), B) Envelope Penetration on North Facade (Top Right), C) Other Envelope Penetration on East Facade (Bottom Left) And D) Envelope Penetration on South Facade (Bottom Right).....	152
Figure 45 : Building Envelope Leakage Rate as a Function of Blower Induced Pressure	157
Figure 46 : Comparison of Infiltration Curve as a Function of Test Procedure	158
Figure 47 : Statement of Calibration of Test Apparatus	160
Figure 48 : Heating Cables for SS-CH2, SS-SF-STAIRS and SS-SF	165
Figure 49 : Heating Cables for SS-SDB, SS-SF and SS-CH1	166
Figure 50 : Heating Cables for SS-SF and SS-CH1	166
Figure 51 : Temperature Probe for SS-SF-04.....	167
Figure 52 : Temperature Probe for SS-SDB-01.....	167
Figure 53 : Temperature Probe for SS-CH1	168

Figure 54 : Temperature Probe for SS-SF-01	168
Figure 55 : Temperature Probes for SS-GAR-01 and SS-GAR-02	169
Figure 56 : DHW Tank Label	169
Figure 57 : Heat Exchanger Installation (Left) and Label (Right).....	170
Figure 58 : Laundry Chute Spanning All Storeys: Basement Laundry Room (Left), Ground Floor Garage (Middle) and 2 nd Floor Office (Right).	171

List of Tables

Table 1 : Peak Shaving and Cost Saving Potential of Various Studies Involving Surface Activation.....	11
Table 2 : Peak Shaving and Cost Saving Potential of Various Studies Exploring Forced-Air Thermal Mass Activation	16
Table 3 : Peak Shaving and Cost Saving Potential of Various Studies Exploring Hydronic Thermal Mass Activation.....	21
Table 4 Parameters Monitored during the Campaign.....	36
Table 5 : Parameters Investigated and their Associated Range	47
Table 6 : Temperature Difference between Thermostat and Thermocouple Readings (°C)	50
Table 7: Model Performance from Temperature Profile Comparison.....	53
Table 8 : Building Actual Versus Simulated Thermal Time Constant	54
Table 9 : Model Performance	55
Table 10 : Charging and Discharging Time as a Function of Air Setpoint Temperature Design Charging Period.....	59
Table 11 : Charging Depth and Charging Time Required as a Function of Air Setpoint Temperature During Charging, Insulation Thickness and Concrete Thickness	62
Table 12 : Discharge Time and Maximum Air Temperature as a Function of Air Setpoint Temperature During Charging, Insulation Thickness and Concrete Thickness	63
Table 13: Discharge Time and Maximum Air Temperature as a Function of Air Setpoint Temperature During Charging, Insulation Thickness and Concrete Thickness	66
Table 14 : Charging Depth and Charging Time Required as a Function of Air Setpoint Temperature during Charging, Insulation Thickness and Concrete Thickness for an 80 m ² Building.....	93

Table 15 : Discharge Time and Maximum Air Temperature as a Function of Air Setpoint Temperature during Charging, Insulation Thickness and Concrete Thickness for an 80 m ² Building.....	93
Table 16 : Charing Depth and Charging Time Required as a Function of Air Setpoint Temperature during Charging, Insulation Thickness and Concrete Thickness for a 120 m ² Building.....	94
Table 17 : Discharge Time and Maximum Air Temperature as a Function of Air Setpoint Temperature during Charging, Insulation Thickness and Concrete Thickness for a 120 m ² Building.....	94
Table 18 : Charing Depth and Charging Time Required as a Function of Air Setpoint Temperature during Charging, Insulation Thickness and Concrete Thickness for a 160 m ² Building.....	95
Table 19 : Discharge Time and Maximum Air Temperature as a Function of Air Setpoint Temperature during Charging, Insulation Thickness and Concrete Thickness for a 160 m ² Building.....	95
Table 20 : Charing Depth and Charging Time Required as a Function of Air Setpoint Temperature during Charging, Insulation Thickness and Concrete Thickness for a 200 m ² Building.....	96
Table 21 : Discharge Time and Maximum Air Temperature as a Function of Air Setpoint Temperature during Charging, Insulation Thickness and Concrete Thickness for a 200 m ² Building.....	96
Table 22 : Correlation Between Thermostat Reading and Heat Exchanger Operation ..	112
Table 23 : Convective Heat Transfer Coefficients for Heated Floors Found in Literature	136
Table 24 : Surface Averaged Exterior Convective Heat Transfer Coefficients.....	137
Table 25 : Optimisation Parameter Description.....	142
Table 26 : Simulated Baseboard Thermostat Optimisation Results	142
Table 27 : Simulated EHF Thermostat Optimisation Results.....	143

Table 28 : Livable Space per Room and Storey	149
Table 29 : Volume per Room and Storey	150
Table 30 : Recorded Conditions of the Building Elements	150
Table 31 : Recorded Air Leakage at Primary Pressure Station	154
Table 32 : Recorded Air Leakage at Secondary Pressure Station	154
Table 33 : Recorded Air Leakage at Various Pressures	154
Table 34 : Calculated Means and Standard Deviations of Data Points for Primary Pressure Station	156
Table 35 : Calculated Means and Standard Deviations of Data Points for Primary Pressure Station	156
Table 36 : Envelope Leakage Rate and ACH at 50 Pa	156
Table 37 : Logarithmic Coefficients from Two-Point Method.....	157
Table 38 : Recommended Bias	158
Table 39 : Precision Indexes and Estimated Biases from Single-Point Method.....	159
Table 40 : Measurement Uncertainty of Single-Point Method.....	159
Table 41 : Precision Indexes and Estimated Biases from Two-Point Method	159
Table 42 : Measurement Uncertainty of Two-Point Method.....	159
Table 43 : Assemblies of the Monitored Building and Their Constituting Materials and Properties	172
Table 44 : Heating Systems Installed in the Residence	174

Abbreviations

ACH	Air change per hour
AHU	Air handling unit
ASHP	Air source heat pump
BFHS	Buried floor heating system
BITES	Building integrated thermal energy storage
CFD	Computational fluid dynamics
CHS	Convective heating system
CMHC	Canadian Mortgage and Housing Corporation
COP	Coefficient of performance
CVRMSE	Coefficient of variance of root mean squared error
DHW	Domestic hot water
DOAS	Dedicated outdoor air system
DR	Demand response
E	Experimental
GHG	Greenhouse gases
HVAC	Heating, ventilation and air-conditioning
IAQ	Indoor air quality
IEA	International Energy Agency
LHTES	Latent heat thermal energy storage
MPC	Model predictive control
NBCC	National building code of Canada
NMBE	Normalized mean bias error
PCM	Phase change material
R&D	Research and development
S	Simulated
SFHS	Surface floor heating system
TABS	Thermo-active building systems
TES	Thermal energy system

TM	Thermal mass
TOU	Time of use
TOU-CPP	Time of use with critical peak pricing
VAV	Variable air volume
ZEB	Zero energy building(s)

CHAPTER 1: INTRODUCTION

1.1 Background

The building and infrastructure sector is accountable for 40% of the total worldwide energy consumption (Gan et al., 2007) and one third of the worldwide GHG emissions. In developed countries, the total energy consumption has increased, despite energy efficiency measures. This trend has been reported in many countries such as in Canada (Natural Resources Canada, 2011), the United States (U.S. Energy Information Administration, 2009), Italy (ENEA, 2015) and Saudi Arabia (Al-Sanea et al., 2012). In Canada, for instance, statistics indicate that there is an increase in the average liveable space per family (11.2%), appliance per house (40%), and percent of building stock equipped with air-conditioning (91.3%), which all equates to a higher energy consumption per habitant (Natural Resources Canada, 2011). National energy efficiency reports mention that between the 1990s and 2009, the influence of improved energy efficiency actions is measurable, whether it is in the industrial, commercial or residential sector. However, the population increase has led to higher nation-wide energy consumption. In addition, the standard of living has increased.

In Canada, 17% of the primary and secondary energy use can be attributed to the residential sector (Natural Resources Canada, 2011). In the province of Quebec, typical residential electricity consumption profiles include a significant peak power consumption in morning hours (Lanoue, 2014). Similar electricity demand profiles are seen in many countries in cold regions (Upshaw et al., 2015) such as Germany (Kalz et al., 2010). In a context where electricity consumption increases continuously, three solutions to this situation introduce themselves:

- 1) Increase the electricity production and accordantly increase the distribution capacity of the grid,
- 2) Increase the thermal resistance of building envelopes, thus decreasing the total energy consumption with respect to space conditioning,
- 3) Reduce the peak consumption by shifting the profile to off peak periods.

A significant amount of research has been conducted on energy efficiency measures for buildings (Ruparathna, Hewage, & Sadiq, 2016). Many suggestions have been proposed

for retrofitting residential buildings and also for new constructions like “additional roof insulation”, “additional façade insulation” and “limit air infiltration” (Nemry et al., 2010). New classes of buildings are seen like zero energy buildings (ZEB). They can be defined as buildings that consume as much energy as they produce via renewable energy sources (Kylili & Fokaides, 2015). The application of such approaches, nonetheless, is very expensive (Aste et al., 2016).

On a more local scale, a Commission was set up to analyse energy efficiency measures for the province of Quebec in response to an inquiry made by the Ministry of Natural Resources in 2014. An electronic version of the report is available online (Lanoue, 2014). An important conclusion from this commission is that the province of Quebec has an excess amount of electricity for most of the year, which is renewable at 99.8% since the closure of the nuclear plant Gentilly-2. Several factors are identified that can explain this scenario:

- 1) The economic crisis in the United States in 2008 caused many industries to close in Ontario, Quebec and Northern States reducing the overall demand for energy.
- 2) The cost of electricity produced from natural gas in the Northern States reduced considerably due to abundance of natural gas, thus reducing the demand for electricity produced by Hydro-Quebec.
- 3) Widespread adoption of energy efficiency measures from the population caused the demand for electricity to be much lower than what was estimated. Despite an increase in the level of living and of population size as previously discussed, the 2013 electricity consumption was lower than in 2007.

Despite all required energy being available, the province of Quebec has issued many contracts with small to medium size private producers (biomass, wind, etc.) in part due to social pressure in the 1990s. (ex.: the group Grand Conseil des Cris striking against hydroelectricity). Figure 1 shows the historical surplus of energy as well as the estimated surplus of energy for upcoming years for the province of Quebec (Lanoue, 2014).

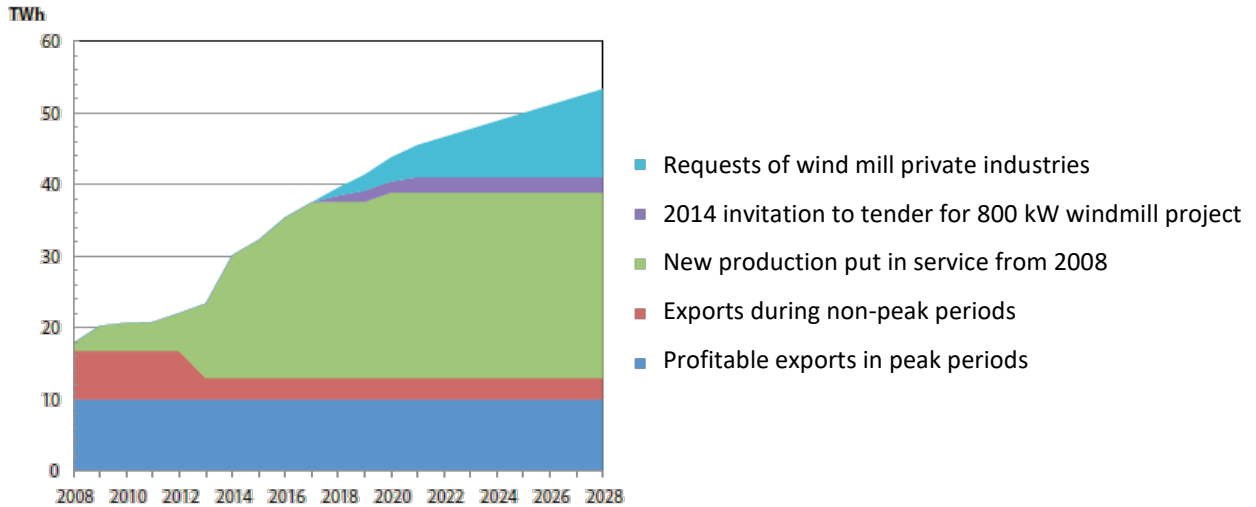


Figure 1 : Annual Surplus Destined for Exportation From 2008-2028

The solution to the energy crisis for the province of Quebec is therefore more related to managing supply and demand rather than energy efficiency. One of the solutions proposed by the Commission of Energy Efficiency is to first, create a political entity with, as an objective, the sustainable development of energy use. Such a political entity would require sufficient executive power. Another solution is research & development of various energy storage technologies through subsidies and research grants.

The purpose of this thesis is not to undermine the potential of energy efficiency driven incentives but to acknowledge the fact that these approaches are a benchmark of building design that require considerable initial investment. Both increasing energy efficiency and shifting peak power consumption can be solutions to reduce the stress on the electrical grid and are therefore worth investigating from a sustainability standpoint. Solutions which produce the greatest energy storage potential with the least amount of capital investment will be the ones that are easiest to implement considering political, cultural and economic challenges.

1.2 Scope and Objective

This thesis' novelty is the development of an electrically-activated thermal storage system for a residential building in a northern climate for peak shaving. The main objective is to provide the simplest storage system to implement, to demonstrate that peak shaving can be achieved using off the shelf products. This means that the proposed system needs

to be based on commercially available products, be easy to implement and construct and involve little to no differences with the current methods of house construction.

There are numerous challenges involved in this project which include:

- Quebec residential buildings have limited thermal mass. All above ground assemblies are light weight wood constructions. Only below ground assemblies are thermally heavy (concrete foundation). To prevent the use of any additional concrete, already existing thermally heavy assemblies need to be used, in this case the basement floor slab assembly.
- The climate of the investigation is very cold: a high heat capacity and heat flux is needed to condition the buildings.
- All surfaces, including the basement floor, need not exceed 28°C because of comfort issues. This prescribes maximum energy storage in the concrete.
- There are two peaks to address within the day: the morning peak (6:00 a.m. to 10:00 a.m.) and the evening peak (4:00 p.m. to 10:00 p.m.). The storage capacity is a compromise between the thermal capacity and the charging/discharging rate.
- The materials and systems used in this project must be off-the-shelf products to facilitate implementation.

CHAPTER 2: TECHNICAL LITERATURE REVIEW

The process of using thermal mass for space conditioning is an approach that can be referred to as demand response (DR), which is the process of managing the energy consumption of the user. The thermal mass can modify the demand curve and effectively shift the peak demand consumption (Liu et al., 2012). The thermal mass can also correct the mismatch between demand and supply when dealing with renewable energy sources like wind and solar (Reynders et al., 2013). Thermal energy systems (TES) are believed to be the most cost effective method for demand side management at the moment (Ruddell et al., 2014). The objective of this literature review is to create an up-to-date ensemble of research work related to the use of building integrated thermal mass used for peak shaving and shifting of electrical power consumption. Issues related to its design configuration, control, and achievable peak shave are discussed as well as barriers to its application. Both cooling and heating-related studies are presented because the thermodynamics between the storage and building air are very similar despite the fact that the charging mechanisms are different.

2.1 Means of Thermal Mass Activation

Many studies have emerged in the past two decades about thermo-active building systems (TABS) (Ma et al., 2015). However, literature is not consistent on the naming of this system: it can be referenced as slab cooling and heating system, concrete core conditioning, embedded hydronic pipe systems, thermally active mass, chilled beams, thermo-active building systems, hybrid systems (Henze et al., 2008) and active building integrated thermal energy storage (BITES) (Chen et al., 2013) to name a few. A distinctive difference between TABS and conventional space conditioning systems is that due to the high thermal mass, the temperature within a room does not stay constant, rather it lies within a comfort range (Olesen, 2012). Most often, the thermal mass is associated with a high temperature cooling or low temperature heating, which means that the cooling/heating time is stretched over a longer duration of the day. In addition, the heating and/or cooling of the thermal mass during off peak hours can be done by running the mechanical system at full capacity. Therefore, the mechanical system can be designed smaller since it runs at maximum efficiency most of the time (Braun, 2003); (Olesen & Pittarello, 2007); (Olesen,

2001). In literature, there are 4 reasons for which the use of thermal mass in conjunction to the conditioning control presents more opportunities compared to conventional methods: (Braun, 2003)

- 1) Reduction in demand costs,
- 2) The use of off peak lower tariffs,
- 3) Lower mechanical conditioning due to use of cooler night time air (summer ventilation), and
- 4) Increased mechanical efficiency due to better use of equipment part loads.

Even though much literature introduces thermal mass as a tool for better energy efficiency, it is often presented as an obstacle in practice because the effect of the conditioning equipment is not as instantaneous (Xu et al., 2004). However, as this thesis will show, there are many approaches available to render thermal mass an effective tool for both comfort and load management. Four ways of activating the thermal mass include; surface activation, air flow through cavities, water pipes, and electric heating cables.

2.1.1 Surface Activation

This method aims at shifting the peak power consumption by pre-cooling or pre-heating the building thermal mass (Turner, Walker, & Roux, 2015). This approach can be considered as thermal mass activation because the mass can be charged or discharged at the convenience of a control strategy governing the zone air temperature. Indirectly, the thermal mass of the building is activated because the conditioning of the thermal zone air also conditions the thermal mass. Therefore, the room conditioning approach/control dictates the state of charge/discharge of the thermal mass. Table 1 classifies recent studies involving surface activation and the obtained energy shave during peaks and energy related cost saving potential.

An advantage of this technique is that it requires absolutely no additional mechanical equipment, as the only system it relies on is the HVAC system (Turner et al., 2015). However, the potential of this approach is limited to the thermal comfort of the occupants of the building, and therefore only variations of a few degrees can be tolerated (Cetin et al., 2016). Some studies have shown that significant peak demand reductions can

be obtained, in the order of 80-100% in the case of cooling (Xu et al., 2004) for partially unoccupied buildings. Care must be taken when playing with set point temperatures or demand control because the wider variations of operative temperatures require the cooling coil or heating coil to operate at higher capacity when turned on. The control strategy should be designed as a function of the system size and performance to make sure that it is sufficiently powerful. Also, pre-cooling and pre-heating strategies can accentuate variations of air temperatures across rooms due to unbalanced dampers since the HVAC system runs continuously during the charging phase (Xu et al., 2004).

Significant research was conducted in the 1990s concerning pre-cooling and pre-heating. Ruud et al. (1990) studied the effect of pre-cooling a single storey of a high rise commercial building on peak cooling loads. They studied a single storey but also controlled the storey above and below in order to limit their influence on the investigated zone. Note that only 10% peak shaving was obtained. Rabl and Norford (1991) also found similar results, of the order of 10-20%. Possible reasons for this low performance was discussed by Braun (2003) as he described the control strategy as rudimentary. Also, the convective coupling between the various storeys might have been too strong and the building thermal mass too small.

Blondeau et al. (1997) obtained energy savings of 12% and up to 50% of peak demand shaving just from effective use of night ventilation in an office building with a diurnal exterior temperature swing of only 8.4°C. Geros et al. (1999) obtained up to 80% energy consumption decrease in Athens due to night ventilation. Bojić et al. (2005) concluded that the thermal mass of a building cannot be effectively used with night ventilation if energy losses to the environment are too high. They investigated the depth of use of a building's thermal mass as a function of insulation and obtained peak energy reductions of up to 38%.

Andresen et al. (1992) also studied pre-cooling strategies through simulation of a single zone of an office building. They obtained peak shaving potential of the order of 10-50% compared to turning off the HVAC system at night. Note, however, that the results of the three investigated control strategies were highly dependent on the relationship between the air and the thermal mass. Mahajan et al. (1993) further studied a classroom in a

university with night ventilation and they were able to achieve a 100% peak reduction between 2:00 p.m. and 6:30 p.m. Andrews et al. (1993) developed a pre-cooling strategy in laboratory conditions where, once pre-cooled, the building had an implemented control based on humidity during occupancy periods rather than temperature. As long as latent loads were managed, the set point temperature was permitted to float in a defined range. Savings due to this approach reached the 35% mark. Xu et al. (2004) managed to shift 80-100% of the load for a ~7450 m² governmental office building by varying the control strategy.

Morris et al. (1994) later demonstrated that night set back strategies could be outperformed with optimal control strategies. In this case, two control strategies were implemented, one that was oriented towards minimizing total energy costs and the other towards peak shaving, which resulted in a 41% peak shaving potential compared to a constant set point control. They further strengthened the need to pay attention to the heat transfer coefficient between the air and the thermal mass as this considerably influences the role of the thermal mass. Kintner-Meyer et al. (1995) investigated the potential of an optimal control using a combination of both the building's thermal mass and a cold storage. The optimisation was based on minimizing costs on a horizon of 24 hours. Peak shaving potential of up to 40% was achieved using a simulated "heavy" high-rise office building. In addition, the authors conducted a sensitivity analysis in order to determine factors that could influence the performance of the optimal control on shifting loads to off peak periods to reduce costs by effective use of electrical tariffs. Interestingly, the humidity in the air had a considerable influence on the results due to the additional conditioning required to remove the latent loads, which also addresses part of the sensible loads. This means that a smaller fraction of the sensible load can be addressed by the stored energy in the thermal mass, limiting its potential influence.

In another context, Becker et al. (2002) attempted to show if pre-cooling could be worthwhile in buildings with large internal loads, light to medium thermal weight and with a climate where summers are mild with small diurnal temperature variations. Their study concluded that either a combination of night ventilation and intensive cooling or only intensive cooling could be used. The thermal mass required to be cooler than the interior

air for a prolonged period of time for it to have any influence on the peak demand consumption. Kolokotroni et al. (1999), on the other hand, demonstrated a potential varying between 21% and 40% depending on the ACH of the night ventilation. There are also considerable cost savings related to pre-cooling a building which can equate to reductions of 40% for night set back pre-cooling strategies as opposed to regular night setback (Braun et al., 2001).

Up to the early 2000s, there was limited evidence that there existed potential for all commercial buildings since most of the literature only considered large scale office buildings. For this reason, a case study of a building that was not necessarily a good candidate was used for their case study; The Iowa Energy Center was selected because it is a single-storey building with a high exterior surface to volume ratio. Still, energy savings during peak periods of 31% were achieved demonstrating that peak shaving strategies can be applied to a geometrically-wide range of building stock (Braun et al., 2002). Lee and Braun thoroughly investigated the effect of varying building zone temperature set points on peak period shaving (Lee & Braun, 2006); (Lee & Braun, 2008). They acknowledged the fact that varying the set point temperature had a positive influence on peak shaving. It was shown that by managing the rate at which the set point temperature increased or decreased, the total cooling or heating demand could be minimized. This is particularly useful with conditioning equipment with varying part load performance. Similar studies were conducted by Yin et al. (2010): they concluded that the best trajectory for increasing the set point trajectory was exponential or step-wise.

One of the reasons why pre-cooling and pre-heating strategies are applied so often in office buildings is because most of them have high thermal mass. However, systems or materials can also be added to thermally light buildings. Phase change materials (PCMs) are often cited as the material for buildings of the future because of their high thermal capacity with respect to the volume they occupy. The IEA published a best practice guide as part of the Annex 23 project in relation to the application of these products in buildings for architects and engineers as the primary sought reader (Haghighat et al., 2013). These materials, however, are still relatively new and their market price is very high. Current scientific gaps are mostly related on demonstrating the cost analysis methods and economic

evaluations of PCMs (Akeiber et al., 2016). As demonstrated by Kenisarin et al. (2016), most real applications are still at the scale of test cabins.

There are many recent studies that have investigated surface activation applications of PCMs in buildings. For example, Xu et al. (2005) and Entrop et al. (2011) studied the thermodynamic properties of PCMs when they are integrated in a building's floor. But, their focus was more on absorption of solar radiation to prevent daily temperature swing and occupant discomfort. Applications on roofs (Alqallaf & Alawadhi, 2013) and window curtains (Ismail & Henriquez, 2001) are also reported.

In terms of peak shaving and shifting, Bastani et al. (2015) developed a tool that enables to determine the optimal wallboards' physical properties in order to obtain a desired charging/discharging time. Feustel et al. (1997) analyzed a PCM wallboard's ability to reduce cooling loads during peak periods but the performance criterion was the operative temperature reduction during this period. The authors mentioned that wallboards have the advantage of having a high surface to storage capacity ratio and that wall surface area is much more abundant than floor area. But, the convective heat transfer is still low and could be increased by placing ventilation ports near the walls. Many studies promote the passive cooling opportunities that PCM wallboards can offer (Jiao & Xu, 2015); (Santamouris et al., 1999); Roucoult et al., 1999) but again the performance indicator is the decrease rate of room air operative temperature rather than the cooling load decrease or energy cost savings. Stovall et al. (1995) discussed the peak shaving and shifting potential of PCM integration in wall boards applications but did not conclude to any physical specifics of the PCMs. Peippo et al. (1991) conducted a simulation-based study on the peak shaving potential of PCMs. Of their remarks, one of the most important parameters in PCM application to buildings is defining the melting point of the cells. In their study, it was determined that a range of 1-3°C above the maximum set point is a good design criterion. Their simulation considered two cities: Helsinki, Finland and Madison, Wisconsin, United States of America. They managed to have a 6% energy savings for Helsinki and 15% for Madison. With the economics at the time of the study, this corresponded to a payback period of 20 years and 10 years, respectively. This is in accordance with other studies (Tomlinson & Heberle, 1990); Stetiu & Feustel, 1996).

There are a number of residential applications for peak shaving and shifting. Turner et al. (2015) investigated a prototype house in 12 different climate zones and identified a potential of up to 50% peak shaving by varying the mechanical ventilation set points for a pre-cooling approach. Some scenarios involving extensive pre-cooling did shave up to 99% of the load during peak periods, but the authors questioned the advantage of doing so as this significantly increases the total daily cooling loads (up to 67% increase). A study conducted by the Davis Energy Group for the California utility company showed that a peak shave of 97% is possible and that on a general basis 88% peak shavings are obtainable when conciliating a 26% total annual increase in energy consumption (Springer & Spiegel, 2013). Another study investigated the peak shaving due to dynamic time of use with critical peak pricing (TOU-CPP) rates and showed, through a 2-year investigation, that 58% of the peak can be shaved in the residential sector using only the thermal mass of the building and with an acceptable occupant comfort (Herter, 2014).

Table 1 : Peak Shaving and Cost Saving Potential of Various Studies Involving Surface Activation

Location of Project	Building Type	Control Type	Method	Shaving Potential	Cost Saving Potential	Case Study
Jacksonville, Florida, United States	Commercial, high-rise	Night set back	E	0-10%	-	(Ruud et al., 1990)
New-Jersey, United States	Office – multi-storey	Night set back	S	10-20%	-	(Rabl & Norford, 1991)
-	Commercial, high-rise, one office considered	Night set back and other	S	10-50%	-	(Andresen & Brandemuehl, 1992)
Sacramento, California, United States	Classroom in University	Night set back	E	100%	-	(Mahajan et al., 1993)
-	Laboratory Test Unit	Night set back	E	35%	-	(Andrews et al., 1993)
Test facility	Room in a large office building	Night set back and optimal control based on tariffs	E	41%	-	(Morris et al., 1994)
La Rochelle, France	Office, 3-storey	Night set back	E & S	0-50%	0-12%	(Blondeau et al., 1997)
Illinois, United States	Office – 3 storeys	Night set back	E & S	25%	-	(Keeney & Braun, 1997)
United Kingdom	Office – 3 storeys	Night ventilation	S	21-40%	-	(Kolokotroni & Aronis, 1999)
Athens, Greece	3 office buildings	Night ventilation	E & S	0-80%	-	(Geros et al., 1999)
Israel	Office – multi-storey	Night setback, intensive pre-cooling	S	1.3-27%	-	(Becker & Paciuk, 2002)

Iowa, United States	Office – 1 storey	Night set back, pre-cooling, optimal trajectory	S	31%	-	(Lee & Braun, 2008)
Madison, Wisconsin, United States	120 m ² house	Night set back	S	15%	-	(Peippo et al., 1991)
Helsinki, Finland				6%		
United States: Baltimore, Maryland Austin, Texas Phoenix, Arizona	Single storey, 204 m ² residential building	Night-setback	S	24-31% 17-19% 9-10%	-	(Cetin et al., 2016)
Sacramento, California, United States	Residential & Commercial	TOU-CPP	E	0-58%	-	(Herter, 2014)
California, United States	Commercial	Set-point set back	E & S	15-30%	-	(Yin et al., 2010)
Hawaii, Phoenix, San-Diego, Seattle	Office-high rise	Cost-driven optimal controller	S	-	6-18%	(Kintner-Meyer & Emery, 1995)
Hong-Kong, China	Residential, high rise	Night ventilation	S	0-38%	-	(Bojic & Yik, 2005)
Minneapolis, United States	Office – 3 storeys ASHRAE Low, Medium and Heavy Weight Assemblies	Night set back, optimal control	E	-	0- ~60%	(Henze et al., 2005)
United States (12 different zones)	195 m ² single storey house California State Energy Code Type 24 Prototype C House	TOU	S	0-50%	-	(Turner et al., 2015)
Sacramento, California United States	Residential, Single storey, 250 m ²	TOU, night ventilation	E & S	0-88%	0-21%	(Springer & Spiegel, 2013)
United States, Climate Zones 8-15	Residential, 164 m ² , 2-storey	Night set-back	E & S	0-30%	10-12%	(Walker et al., 2002)
Sacramento, California, United States	Residential, 250 m ² , 2-storey	Lower set point, constant	S	0-56%	-	(Anderson et al., 2006)
Pennsylvania, United States	Office – Simulation based	MPC	S	0-50%	-	(Nghiem, 2011)

Abbreviations:

E: Experimental; S: Simulation; TOU-CPP: Time of use critical peak pricing;

2.2 Forced-Air Activation

The principle is similar to embedded water pipes in concrete except that the conduits are larger and air passes through them. These cavities are then connected to a ventilation

system to condition the space (Park & Krarti, 2015). A predominant advantage of such systems is that not only does it act as a radiant exchange system but it can also supply fresh conditioned air to the environment, thus providing a much more comfortable environment (Shaw et al., 1994). It is important to note that in the case of pre-cast hollow core slabs, not all cavities can be used in conjunction with the HVAC system. The outermost passageways are usually reserved for passing mechanical and electrical systems (Faheem et al., 2016). Commercial applications of air activated thermal mass are usually pre-cast concrete components such as TermoDeck (TermoDeck, 2016).

Many studies are available on ventilated concrete slabs, but most report advantages in terms of thermal comfort and few demonstrate the peak shaving advantages of such a system (Corgnati & Kindinis, 2007). Table 2 lists the most recent studies involving forced-air activation of thermal mass for peak shaving and shifting. Barnaby et al. (1980) reported that hollow core concrete slabs could generate energy savings during peak periods of the order of 13-30%. But this study neglected the influence of thermal bridging from the perimeter of the slab. Another study was conducted where it was shown that air cavities in concrete for radiant ceilings could decrease chiller loads by up to 70% (Robert et al. (1980)). Zmeureanu et al. (1988) demonstrated that savings of 28.4 to 44.2 W/m² can be obtained using hollow core concrete slabs compared to conventional mechanical system ventilation which can completely offset office occupant loads or half the lighting loads. Ren and Wright (1998) developed a transient simulation model and concluded that approximating the slab as a lumped parameter model gave results in good agreement with experimental data. However, the heat transfer of the corner air paths had to be estimated to 50 times the heat transfer of straight duct runs for simulation results to match experimental results, which is questionable. It was later supported by Barton et al. (2002), through an extensive two-dimensional finite difference model, that the heat transfer of a concrete slab with air cavities is not dominated by the bends. The effectiveness of the pre-cast concrete components in shifting the peak load relies on the length of air passageway: longer air canals inside the component induce a larger phase shift because of the higher contact surface area available for heat transfer.

In terms of design, Park and Krarti (2015) conducted a parametric study on hollow core concrete slabs through simulation using a one-dimensional finite difference model, a two-dimensional finite difference model and a CFD model. Asymptotes are reached for the mass flow rate at around 2.5 kg/s and the effects of increasing the mass flow rate diminish rapidly from 1 kg/s. Increasing the depth of the slab considerably decreases the available heat flux from the slab despite the increase in thermal storage. The heat flux increases as a function of the contact surface between the concrete and the air ($n \cdot \pi \cdot D$); past 2 m² of contact area per 1 m² of horizontal slab area, there is negligible advantage to increasing the contact area.

Faheem et al. (2016) and Yu et al. (2015) investigated PCM additions to ventilated concrete slabs. It was concluded that the percentage of PCM should be optimized as a function of the airflow rate, thermal weight of the building and slab surface temperature. In their study, the buildings that best responded to these additions were thermally light buildings because the response due to the airflow of the slab was faster. More recent academic works with respect to hollow core concrete slabs include PCMs in the design in order to increase the storage capacity of such applications. Navarro et al. (2016) conducted an experiment in a 2.4 m x 2.4 m set up with such a system and achieved energy savings of the order of 0-55%. However, the difference between the original pre-fabricated slab and one with PCMs was not demonstrated. Furthermore, as the authors proclaim, the control strategy could have been better optimized as a considerable share of the energy consumed was for the fan.

Activating thermal mass in conjunction with the HVAC system was also studied by Patania et al. (2010) where a ventilated façade was equipped with thermally heavy materials on both sides of the intake air cavities. The geometry of the cavity as well as the fluid flow characteristics were studied to determine the most advantageous configuration. It was determined that ventilated facades are most useful when there is a large temperature difference between the temperature of the mass and the inlet air. Also, the amount of heat transfer tends to increase when the inlet velocity increases, but reaches an asymptote at around 2.5 m/s. Energy savings of up to 40% were obtained by preheating the inlet air to

the HVAC system using this approach. Corgnati et al. (2007) developed an analytical model for hollow core concrete slabs that showed good agreement with experimental data.

Evola et al. (2014) studied ventilated facades equipped with PCM wallboards and concluded that such assemblies enabled PCM wall boards to have a 30% higher heat flux compared to regular surface activation applications. Gracia et al. (2013) studied double skin facades equipped with PCM panels and registered energy savings of the order of 19-26%. The authors highlighted that better efficiencies could have been attained if the control would have been dependent on demand control rather than occupant comfort.

A new type of double skin façade was presented by Fallahi et al (2010) which works the same way as a Tromb wall except that the air between the glazing and the concrete wall is forced into motion. In their study, venetian blinds were replaced by thermal mass. They concluded that energy savings of 21-26% and 41-59% could be obtained in the summer and winter, respectively. This type of assembly limited solar gains in the summer through exterior air ventilation and increased solar gains in the winter, with both operations taking advantage of the thermal mass. This is particularly advantageous in locations where both winter and summer conditions are experienced. Note that the same assembly was tested with natural ventilation but no distinct advantage could be noticed with this configuration. When connecting thermal mass to the HVAC system, it is primarily important to locate the thermal mass between the exhaust of the HVAC system and the conditioned room. Such a design includes the least amount of installation costs, ensures the greatest temperature swing limitation potential and provides the most depth of charge/discharge of the thermal mass. Butala et al. (2010) investigated adding PCM units to HVAC lines just before room inlets. The focus of their work was directed towards the design of the inlet temperature and airflow rate for optimum storage potential, but HVAC energy savings or peak shaving opportunities was not discussed. A similar approach was adopted by Yanbing et al. (2003). In some cases, the energy stored by the PCM panels renders the supply air too hot (heating mode) or too cold (cooling mode) and therefore a central storage may be placed between the LHTES outlet and the room supply nozzles (El-sawi et al., 2013).

Recently, a new assembly has been studied that takes advantage of activating concrete thermal mass with air. This assembly proposes a steel deck laid out flat with concrete

poured on top. This has been studied, more recently, by Chen et al. (2010) (2013) and Ekrami et al. (2015) for residential applications. They have shown that this assembly can be used as active TES but that the temperature output is not high enough for space conditioning; hence it is proposed to couple this system with an air source heat pump. The main advantage of this system is the availability of the materials, the ease with which it can be integrated to an HVAC system. Note however, that the studies do not agree on the acceptable friction losses within the cavities. In their assembly, Chen et al. (2010) (2013) added wire mesh below the steel deck to form ridges in the cavities to increase turbulence while Ekrami et al. (2015) (2007) mentioned in their analysis that the cavity should be as smooth as possible.

Another application of forced-air activated thermal mass is chilled radiant ceilings. An example study of this principle was conducted by Chae et al. (2013) where a ceiling slab had air cavities. The cavities can be run in a closed loop with the HVAC system in order to render the ceiling slab entirely radiative or the air could be diverted to the room for ventilation. A peak shaving potential of 21.75% was obtained. Nonetheless, the goal of the study was merely to validate a model for the system, various operating scenarios are still to be analyzed by the authors.

An important advantage of forced-air activation over electrical or hydronic activation is that the system is not limited to addressing sensible loads. The air used for activation can be connected to a heat pump or an air-handling unit for dehumidification or humidification, depending on the needs. This is particularly important for buildings with a higher density of occupants or in areas where the climate is particularly humid. In cooling applications, having the air-handling unit before the thermal mass can reduce the water content of the air and therefore reduce the air dew point temperature. The thermal mass can therefore be cooled to a lower temperature.

Table 2 : Peak Shaving and Cost Saving Potential of Various Studies Exploring Forced-Air Thermal Mass Activation

Location of Project	Building Type	Control Type	Position of Mass	Method	Shaving Potential	Cost Saving Potential	Case Study
United States, Dry Climate	Commercial Building	Pre-cooling	Ceiling	S	13-30%	-	(Barnaby et al., 1980)

Montreal, Canada	Office Building	Pre-cooling	Ceiling	S	0-35%	-	(Zmeureanu & Fazio, 1988)
United Kingdom	Office Building	Pre-cooling	Ceiling	S	0-70%	-	(Russell & Surendran, 2001)
Montreal, Canada	Office, 450 m ²	Slab pre-cooling	Ventilated Ceiling Slab	S	28%	23%	(Chae & Strand, 2013)
EcoTera Project Eastman, Quebec, Canada	Residential, 2-storey, 234 m ²	Constant Flow	Floor	E & S	-	0-92%	(Chen, 2014) (Noguchi et al., 2008)
Puigverd de Lleida, Spain	Experimental, 5.76m ²	Night ventilation	Ceiling	E	-	0-20% (extreme conditions) 0-55%(mild conditions)	(Navarro et al., 2016)
Munich, Germany	University facade, 2.11 m ²	Various controls	Ventilated double skin facade	S	-	21-26% (summer) 41-59% (Winter)	(Fallahi et al., 2010)
Puigverd de Lleida, Spain	Experimental, 5.76 m ²	Night ventilation	Ventilated double skin facade	E	-	19-26%	(Gracia et al., 2013)

Abbreviations:

E: Experimental; S: Simulation

2.1.3 Hydronic Activation

Hydronic activation is the process of heating or cooling a thermal mass with pipes containing water or a mixture of water and additives. It has recently regained interest because of the possibility of integrating renewable energy sources (Li, et al, 2014); Zhu et al., 2014). Table 3 shows studies concerned with peak shaving and shifting using hydronically-activated thermal mass. There is a large variety of construction assemblies for hydronic TABS but common design configurations have a 4 K temperature difference between supply and return and a 15 kPa pressure difference across the piping loops (Henze et al., 2008). A small temperature difference between the slab and the room is achievable because of the large floor surface area; this entitles the heating/cooling systems to run much more efficiently and continuously. Hydraulically activated thermal mass is sometimes chosen over other space conditioning systems because of the additional floor space that is available due to the lack of bulky mechanical systems (Kim & Olesen, 2008).

Radiant floors/ceilings are not a new subject and their design is already well documented. Many standards are available for their design: ASHRAE fundamentals handbook (ASHRAE, 2005), ISO 11855 (ISO, 2012) (this replaces the former EN15377), and EN 1264 (CEN, 2008). But, their relevance in terms of cooling load calculations is challenged in recent scientific articles. For example, Feng et al. (2013) addressed the dynamic nature of the increased thermal mass associated with embedded pipe designs and the fact that it is not reflected in the calculation methods of the above standards. Numerous literature can be found on radiant systems including calculation methods (Feng et al., 2014), operative temperatures for comfort (Rhee & Kim, 2015), cooling capacities (Odyjas & Górká, 2013) and modelling (Koschütz & Dorer, 1999); (Zhu et al., 2014). But, a limited work can be found on peak shaving and shifting with building integrated thermal mass and its control.

Stetiu et al. (1999) analyzed the control of radiant systems as a function of the climate. When radiant systems are used for cooling applications, a critical factor to consider is condensation. In all cases, the relative humidity must be below 70%, cooling radiant systems are most effective in dry climates. Since the radiant systems can only address sensible loads, latent loads need to be addressed by an air-handling unit. The energy consumed for dehumidification often offsets the energy savings from radiant systems. Therefore, the performance of the system is highly dependent on the climate (Tian & Love, 2009). However, a combined system improves IAQ in comparison to only having radiant systems.

Lehmann et al. (2007) analyzed the control of hydronic radiant floors in an office with respect to occupation density as well as occupant behaviour. A critical parameter to control is the quantity of solar radiation in the room. Most times, when shading devices are manually operated, occupants control these as a function of illuminance, which has considerable effects on the comfort and performance of TABS (up to 20-30% increase in cooling demand).

Gwerder et al. (2008) developed a design procedure for water pipes lodged in concrete slabs as a means of conditioning an office building. Hydronic systems were identified as ineffective to counteract rapidly changing heat gains. The system must be modeled to

determine the maximum and minimum heat gains for which the TABS can maintain thermal comfort. Once this is identified, the occupancy type of the building can be analyzed for the probability of having heat gains that fall outside this predefined range and an air-handling unit can be sized in accordance. This is referred to as the Unknown-But-Bounded approach. A similar approach was also suggested by Ma et al. (2013). Saelens et al. (2011) studied TABS based on a stochastic approach to occupant behaviour and the probability of its occupation. They showed that it is more probable to create occupant discomfort if the user has control over the thermostat setting; uniform control settings should be determined based on average conditions of the most common occupation type in the space. Their focus was not on the shifting of the power consumption to unoccupied periods but rather continuous operation of the conditioning equipment at a smaller intensity. In that sense, the thermal mass is used as a damper, absorbing the heat gains in order to keep an acceptable occupant comfort level until the hydronic loops can cope with the loads. An example of a building that they studied had a maximum daily internal heat gain of 38 W/m^2 . With 8 hours of operation per day, the hydraulic loop could be designed for 37 W/m^2 , and 25 W/m^2 for 12 hours of operation. Several methods, from rough sizing (20-30 % error) to finite element modeling (6-10 % error), was proposed by them which could determine the optimal concrete thickness in order to achieve such performance standards. Depending on the application, the chiller/heat pump could be downsized by approximately 60-70 %.

Apart from radiant floors, the thermal mass in the envelope can also be activated with embedded water pipes. This approach shares the same advantages as pipe embedded ceilings or interior walls but it can also considerably reduce cooling loads in the summer (Zhu et al., 2014); Xie et al., 2015). Cvetkovik et al. (2015) analyzed numerically and experimentally the optimal location for radiant panels in a house. Their study included four types of panels (wall, floor, ceiling and a combined floor/ceiling panel) as well as three heat sources (boiler, geothermal well and a combination of geothermal well with PV panels). Their study involved estimation of CO₂ emission, price for heating and energy efficiency: it was concluded that the optimal location was the ceiling for cooling, floor for heating and/or a combination of both. As can be seen, literature is not unanimous on the relevance of wall thermal mass activation.

Some applications of chilled ceilings have shown to save energy and reduce peak electrical demand. The building's thermal mass is a damper in this kind of application, limiting the temperature swing of the room. The typical assembly is composed of water pipes in contact with a highly conductive material, like an aluminum or copper plate, to act as a diffuser. These applications are particularly effective in office buildings for increased occupant comfort. In addition, they are compact, have a lower time constant and reduce the required AHU size (Mumma, 2002). For example, Imanari et al. (1999) obtained 10-20% peak consumption decrease and Stetiu et al. (1999) obtained 27% peak reduction compared to all air systems, Jeong et al. (2003) obtained a 50% peak reduction and Moore (2008) obtained a 61% peak reduction in a climate acceptable for evaporative cooling. Chiang et al. (2012) compared radiant cooling ceilings to more modern mechanical ventilation systems and obtained an 8% total energy savings. Note that all these studies highlight the fact that hydronic cooling or heating can only address the sensible loads. Hao et al. (2007) studied a combined system comprised of a chilled ceiling and a mechanical ventilation system and still reported energy savings of the order of 8.2%. Similar results were found by Niu et al. (2002) and they mentioned the possibility of joining chilled ceilings with renewable energy sources and in line thermal storage. Odyjas et al. (2013) studied chilled floors and concluded that despite the low performance of the system for zone conditioning, its applicability is still relevant in building design as this approach can significantly reduce peak loads due to solar radiation (up to 150 W/m^2). Privara et al. (2011) determined that MPC coupled to a hydronic system could achieve 17-24% savings compared to conventional control for radiant ceilings. Bojic and Cvetkovic (2013; 2015) showed that the power savings could also be increased by the combination of radiant ceilings/floors with renewable energy sources like ground source heat pumps and solar collectors.

Reynders et al. (2013) analyzed the performance and comfort of a radiator in conjunction with a residential building's thermal mass using both conventional control and MPC. In both cases, the objective was to maximize the quantity of heat collected by a PV panel that generates electricity for a heat pump that conditions a water loop. The authors determined a control with no prediction performed better in terms of peak shaving (89.2% for a 4°C comfort band and 67.3% for a 2°C comfort band) as opposed to the predictive controller (79.1% for a 4°C comfort band and 59.9% for a 2°C comfort band). However,

the predictive controller managed to stay within the prescribed comfort band while the non-predictive controller did not, especially in mid seasons.

Storage tanks are another common application of activated thermal mass storage. The energy consumption for domestic hot water is directly associated with peak energy demand. Shifting its power consumption to off peak periods has a direct influence on the total grid's peak consumption. Shao et al. (2004) used the excess heat from a heat pump's condensing valve and evaporator in order to heat the domestic hot water at a later time. With this approach, excess heat from cooling the building is utilized. Usually, the COP of a hot water tank is 1.0 while the COP of a heat pump was shown to be 4.0 in this study, which generated 31.1 % annual energy efficiency. These tanks can also use PCMs as a storage medium such as in Hamada et al.'s (2005) study. A similar approach was adopted where storage tanks collected excess heat from heat pump cooling. To counteract the poor heat conduction of the PCMs, carbon fiber brushes were placed in between the cells and this reduced the cost of up to 75%. Another approach is to charge the hot water tank during off peak periods, which can be accomplished with the addition of PCMs within the tank. This was modeled by Nchelatebe et al. (2014-a) and the potential for peak shifting was also demonstrated (Bony & Citherlet, 2007); (Gracia et al., 2013); (Nchelatebe et al., 2014-b). Despite this, no study was found on the influence of shifting the domestic hot water tank electricity consumption to off peak periods on the total building energy consumption.

Table 3 : Peak Shaving and Cost Saving Potential of Various Studies Exploring Hydronic Thermal Mass Activation

Location of Project	Building Type	Control Type	Position of Mass	Method	Shaving Potential	Cost Saving Potential	Case Study
United States: Seattle (0-50% RH) Phoenix (0-50% RH) New-York (50-67% RH)	Office, Single storey, 700 m ²	Night pre-cooling	Building Thermal Mass, Hydronic Radiant Panel Ceiling + VAV	S	0-23% 0-37% 0-23%	0-23% 0-42% -	(Steti, 1999)
Tokyo, Japan (60% RH)	Office, multi-storey	Continuous Operation	Building Thermal Mass,	S	0-20%	6-10%	(Imanari et al., 1999)

			Hydronic Radiant Panel Ceiling + VAV				
United States	Office, single storey, 297.3 m ²	Continuous operation with 2 power stages	Building Thermal Mass, Hydronic Radiant Panel Ceiling + VAV	S	0-50%	0-42%	(Jeong et al., 2003)
Beijing, China	Residential	Continuous	Hot Water Tank	S	-	31.1%	(Shao et al., 2004)
Beirut, Lebanon	Simulation based office room, 7.5 m ²	Continuous Operation	TABS with Solar Collector	S	-	18-20%	(Ghali, 2007)
Swiss	Office – simulated	On/OFF	Floor	S	0-50%	-	(Lehmann et al., 2007)
Beijing, China	Office, single room	Continuous Operation	Building Thermal Mass, Hydronic Radiant Panel Ceiling + VAV + Desiccant Wheel	S	0-62%	8.2%	(Hao et al., 2007)
Denver, Colorado, United States	Office, 5-storey, simulated, 3125 m ²	Continuous Operation 2 power stages	TABS	S	61%	56-68%	(Moore, 2008)
Vancouver, BC, Canada (Zone 5C) Calgary, AB, Canada (Zone 7) Toronto, ON, Canada (Zone 6A) Helena, MT, US (Zone 6B) Portland, ME, US (Zone 5A) Salt Lake City, UT, US (Zone 5B)	One storey of a multi-zone multi-storey office building, 1540 m ²	Continuous operation with night shut down	Building Thermal Mass, Hydronic Radiant Panel Ceiling + VAV	S	-	29% 35% 21% 39% 16% 49%	(Tian & Love, 2009)
Bodegraven, Netherlands	Office building, 2054 m ²	Function of Current and Past Exterior Temperature	Ceiling	S	0-50%	-	(Rijksen et al., 2010)
Czech Technical University, Prague,	Multi-storey office building	Night pre-cooling MPC	Chilled Beams	E	-	15-28% 17-24%	(Privara et al., 2011)

Czechoslovakia							
United States	Multi-storey	Continuous Operation	Floor/ceiling	-	60-70%	-	(Olesen, 2012)
National Taiwan University	Single office room, ground floor of 9 storey building	Continuous Operation	Building Thermal Mass, Hydronic Radiant Panel Ceiling	E & S	-	8%	(Chiang et al., 2012)
Lebanon	Two office rooms, single storey	Continuous Operation	Radiant Floor, Heavy Building with Concrete Block Walls	S	26%	30%	(Kattan et al., 2012a)
Belgium	Single family house, 140 m ² , two-storey	Continuous Operation MPC	Building Thermal Mass, Radiators	S	0-89.2% 0-79.1%		(Reynders et al., 2013)
Seoul, Korea	Single room of a 2-storey house, 29 m ²	Continuous Operation	Radiant Floor and Ceiling with Packaged Air Conditioning Unit	S	22% (Heating) 73% (Cooling)	32% (Heating) 51% (Cooling)	(Park et al., 2014)
Experimental Room, MIT, United States	Typical office space	Conventional Control, MPC	Hydronic Radiant Panel Ceiling with DOAS and VAV	S	-	50%	(Zakula et al., 2015)

Abbreviations:

E: Experimental; S: Simulation; VAV: Variable air volume; TABS: Thermally activated building system; MPC: Model predictive control

2.1.4 Electrical Activation

Thermal mass is activated with electricity through heating cables, which are essentially long electrical resistances in the form of a wire. When using electric heating cables, the thermal mass can only be used for heating. Limited literature can be found on the application of electrical heating cables for the purpose of peak shaving. Of the literature available, an application that is seen is to install an electric heating mat below a thermally heavy layer made of either concrete or a PCM impregnated material. The thermal mass is used in this case as a damper to the intermittent operation of the heating elements. Several studies have acknowledged the potential of PCM panels for such applications (Li et al., 2009) (Cheng et al., 2015). Electric heating wires are most commonly seen in thermally light applications as a comfort item more than its potential for thermal storage. Nonetheless, there is a large potential for this kind of activation medium due to the

possibility of integrating various renewable energy sources like PV panels and wind turbine as demonstrated by Thieblemont et al. (2016). This has been demonstrated by various socio-economic investigations (Boßmann et al., 2015); (Patteeuw et al., 2015).

2.2. Thermal Performance and Control of Activated Thermal Mass

The most fundamental control strategies can be categorized as “Classical” strategies, based on heuristic control on a case-by-case method. Explicit by their naming, they include:

- 1) Chiller priority control,
- 2) Constant proportional control, and
- 3) Storage priority control.

In their simplest nature, the first two methods can be interpreted as energy efficient in the sense that all the load (and not more) is addressed by the equipment that is designed to be the right size since they instantaneously address the required load. However, in reality this is often not the case because of variable demands, non-linear part load performance of the equipment, and building thermal mass. They are still widely implemented because they are the easiest to design, operate and trouble shoot. The third strategy implies that the control prioritizes the use of the stored energy before any other form. An underlying problem with this approach is defining the required size of storage as well as the quantity of energy to store. This strategy requires some form of forecast of the load in order to store the correct amount of energy. The size of the storage dictates the time horizon of the load forecast length needed; the longer the length of the forecast, the higher the probability of having disturbances in the forecast (Krarti, Henze, & Dodier, 1997). This becomes one of the hardest challenges to overcome in the design of building integrated thermal mass. The term “optimal” control should be used with care as it is used extensively without any rigorous definition. In the context of building-integrated thermal mass, evaluating the performance of the system and the effectiveness of the control strategy is a tedious process because more often than not, it is a multi-objective type of optimisation.

Literature prior to the early 2000s focuses mainly on peak demand shaving and utility cost (Keeney & Braun, 1997); (Rabl & Norford, 1991); (Ruud et al., 1990); (West

& Braun, 1999). These studies focussed mostly on demonstrating the relevance of pre-cooling strategies for operation and management cost reduction in office buildings. Evaluation procedures were published in early 2000s presenting optimisation indicators related to thermal mass activation with respect to reducing utility costs (Braun et al., 2001). These optimisation schemes are most often divided into 2 parts: 1) occupant comfort penalty regime and 2) utility cost minimization regime. The result is a list of possible optimal solutions left to the discretion of the modeller. Or, combinations of the weighted parameters can be set up depending on the client needs. The environmental cost is often secondary to economic cost and therefore most optimisation objective functions that are seen in literature are economic cost based (Braun, 2003). As such, cost minimization is most effective in areas with on-on/off-peak tariffs rather than consistent electricity rates (Kintner-Meyer & Emery, 1995).

The most basic control strategy for the use of thermal mass is a night set back control. One of the possible reasons for this is that it is very easy to implement, as the only requirement is to modify the set point temperature of the zone thermostat. This strategy is applied by having a fixed set point temperature for the mechanical system during peak periods/occupied periods while the temperature is allowed to float during unoccupied periods (Henze et al., 2008). In the case of heating, when the room air temperature decreases, the energy from the thermal mass is discharged to the room. The opposite is true for cooling. Literature is unanimous on the fact that this control strategy is not the most energy efficient, but it is still much better than no thermal mass utilization at all. It is often the reference case for comparing other methods of optimising the control of thermal mass. This type of control can still be seen in recent literature, which can be explained by the fact that it can easily be implemented with current commercially available thermostats (Turner et al., 2015).

The set point strategy can be set in various ways depending on the desired objective.

- 1) A strategy for cost minimization should have the set point adjusted to the lower limit of the comfort range as soon as possible during the peak period. This increases the heat flux from the thermal mass to the room and therefore reduce the heating load on the mechanical equipment (Braun, 2003).

- 2) A strategy aimed at demand control should have the set point temperature at the upper limit of the comfort range at the beginning of the peak period. The set point should decrease at a rate that limits the heating load. If the required power reaches the prescribed limit, then the zone air temperature is permitted to float throughout the comfort range. An ideal scenario is one where the set point of the room is at the lower limit of the comfort range at the end of the demand-limiting period as to maximize the floating potential and therefore the demand-limiting potential of the control strategy.

Often times, strategies demonstrated as effective have fundamental assumptions that render the results questionable. For example, the COP and performance of the systems modelled are sometimes assumed to be proportional to the environment temperature. Assuming constant equipment performance is often seen in literature such as in the works of Krarti et al. (1995) and Henze et al. (1997) (2004) (2005). This could help the optimisation be conveniently separated into 2 parts:

- 1) Optimisation of the set point trajectories to minimize the cooling/heating load and,
- 2) Optimisation of the charging/discharging to address the loads and minimize the equipment energy consumption.

There is also another benefit to such models of equipment performance, which is that the performance curves become continuous. This is particularly interesting especially in the case of equipment with variable frequency drives because their performance can be discontinuous especially in low frequency ranges of up to 10 Hz. In this case the optimisation space is fully continuous and techniques such as the Quasi-Newton and Nelder Mead simplex can be used which are much faster (Henze et al., 2008). For discontinuous optimisation spaces, grid search and swarm particle optimisation are often used.

As demonstrated by Candanedo et al. (2015), a control that fails to accurately model the building and systems is most often prone to overshooting of temperature. In their study, they attempted different methods to gradually ramp the set point of the building for optimal

pre-cooling while limiting the demand and determined that the use of genetic algorithms is the most favourable and easiest to implement. They obtained a decrease in peak demand of 8% with this approach. They also suggested that it could be favourable to extend the transition period by an hour or two between the two set points in order to decrease the associated demand. By establishing a transition time of 3 hours, instead of 1, decreases the peak demand by up to 50%. They also investigated the relationship between the amount of thermal mass and the best set point trajectory for a demand limiting strategy.

An issue to consider when controlling various zones for peak shaving is the heat transfer between zones. This is particularly evident when various zones are conditioned with different control strategies. As demonstrated by Braun et al. (2002), it is particularly advantageous to consider the building as a unity in terms of control. Significant energy savings can be obtained by this approach and the control strategy is easier to implement. The optimal peak shaving potential for this study was 31% but when cumulating the potential of every zone, an average of 23% was obtained. The coupling between zones and the orientation of the zones with respect to the sun have a considerable impact on the zone thermal performance and the control system.

In regards to the time lag induced by the thermal mass, Henze et al. (2004) investigated the potential of a controller based on perfect predictions of weather and occupancy. It was shown that this lag time could be used to the advantage of the designer because offsets in the control strategy do not have an effect as instantaneous as all-air systems for example. As Rhee et al. (2015) mentioned it is often more advantageous in thermally heavy systems to have an ON/OFF type of control. In this case, the flow rate can be optimized base on the hydraulic resistance of the various loops and the chiller part load performance. The power delivered is dictated by the frequency of activation and the variability of the supply temperature is mitigated by the thermal inertia of the system. Many studies have demonstrated that the response time of thermally heavy systems are too high to consider offsetting instantaneous heat gains due to changing solar radiation from changing cloud cover or occupancy-related changes in internal heat gains (Rijksen et al., 2010). There are several methods to approach this:

- 1) Design the building/system to have less thermal storage, which will decrease the response time. However, this also reduces the damping effect of the thermal mass and its capability to shave peak consumption
- 2) Design the activated BITES to address only the base load of the building and have an air-handling unit to address the variable/random and latent loads. This is particularly useful in humid climates or for buildings with high internal latent loads. The thermal storage can be controlled based on past data (Rijksen et al., 2010) and exterior temperature (Gwerder et al., 2008). This approach is the easiest to design and operate but the potential of the thermal mass is limited.
- 3) Design the thermal storage with a control strategy that can predict the loads in advance. This requires forecasting weather and occupancy for various time horizons. But, it also allows access to a larger reservoir of thermal energy.

A sensitivity analysis was conducted by Liu et al. (2004) in order to determine the influence of various types of forecast uncertainties on an optimal controller. The result of the optimisation was used to determine the control of a chiller for every time step. Of the four types of uncertainties considered, all had better efficiencies (up to double) than the reference case with storage-priority control. It was concluded that it is better to over-estimate the storage required because the cost penalties for chiller operation during peak periods are higher than over charging the thermal storage during off-peak periods. This is particularly advantageous, considering uncertainties of weather predictions. In addition, most often tariffs from utilities are given on a daily basis, which means that there needs to be predictions of utility tariffs. Note that the time horizon of this study was up to 12 hours, but as shown by Krarti et al. (1999) the required time horizon can be much longer. Liu et al. (2004) also demonstrated that the building geometry and zoning barely affect the optimisation algorithm while an over-simplification of building construction, internal heat gain and system efficiency have large impacts on the algorithm.

A parametric analysis was conducted by Henze et a. (2005) in order to determine what are the influential factors for reducing the operation cost in the case of thermal mass

utilization with optimal control. One of their findings was that unless there is a considerable cost incentive to reducing energy consumption during peak periods, cost-driven optimal controllers would not fully utilize the pre-cooling potential. In addition, it is the areas with a larger load (either heating or cooling) that benefit most from TOU (time of use) based tariffs. In terms of comfort, massive buildings tend to have better comfort because the MRT (mean radiant temperature) is lower for cooling and higher for heating. This information, however, needs to be interpreted with care because an unbalanced controller can have susceptible overheating/overcooling introduced because of thermal mass. Also, it is sometimes impossible to determine simple relationships between the predictions of performance and real time control as demonstrated by Henze et al. (2010).

Another popular approach to control is model predictive control (MPC). A model of the system is used in order to forecast the behavior of the building which is then optimized to determine the best sequence of actions. The first action of this sequence is often the only one applied. At a former time step, the entire model is re-optimized for a new action operating sequence (Cole et al., 2014). MPC have been extensively used in combination to active and activated thermal mass (Ma et al., 2012); (J. Ma et al., 2012); (Hajiah & Krarti, 2012b); (Hajiah & Krarti, 2012a). But, the downside of this approach is that extensive dynamic building models are too computationally expensive for real time optimisation and simplified models need to be developed (Yu et al., 2015). The topic engages much interest in scientific papers, but a realistic and cost effective approach is yet to be applied (Zakula et al., 2014).

To overcome the shortcomings of optimal control, reinforcement learning was introduced in the control of building integrated thermal mass. Its first apparition was with pre-cooling of a heavy mass office building (Liu & Henze, 2004). The basis of reinforcement learning is to have real time assessment data of the building and its components in order for the optimisation algorithm to learn and correct deviations between the building model and the actual building. The building model, which characterizes the work space of the reinforcement learning algorithm, is defined by a two-dimensional space where one dimension represents the various actions of the controller while the other dimension represents the various state variables of the system. The size of this area is what

defines the relative speed at which the learning algorithm computes the learning processes. In all cases, reinforcement learning can obtain an optimum solution for an imposed system, but the computation time is far too heavy for realistic and practical application for real time controlling. A later study conducted by Liu and Henze (2006) showed that reinforcement based learning algorithms with no prior knowledge of the system is not a practical solution to thermal energy storage management. They obtained less favourable results than model-predictive control (MPC) but better results than classical controls. This conclusion is mainly due to the computation time required for the learning processes.

The control of buildings can also be applied from the utility company's standpoint, which inquires that buildings be not considered as standalone environments but be part of a larger community. An indirect application of this is the time of use (TOU) tariff system in which customers are encouraged to change behaviour regarding the conditioning of their home by having energy price rates that are more advantageous in off-peak periods. The application of such an approach is not new. Experiments were conducted as early as the 1980s (Caves & Christensen, 1980) but in the advent of energy efficiency measures, global warming issues and the control of greenhouse gas emissions, such an approach regained popularity. There has been extensive work conducted by Woo et al. (2001) (2003) and Bushnell et al. (2004) and Herter et al. (2014), to name a few. The most recent application and findings is that maximum peak shaving can be obtained by the time of use with critical peak events (TOU-CPP) in which 58% peak shaving can be obtained. Intelligent thermostats enable utility to customer communication by displaying when critical peak consumption periods are happening with a 24-hour warning. Customers have the choice of adapting to save on their electricity bills or not. This approach gives the highest peak shaving and highest customer appreciation rate.

2.3. Barriers to Application

Braun et al. (2002) demonstrated the potential savings from using a buildings thermal mass. The lack of guidelines for the development and application was one of their conclusions because research up to this point failed to relate to most of the building types; most focused on high-rise office buildings.

This remark was further supported by Henze et al. (2008) a few years later despite the extensive research realized up to this point. This reality was attributed to the vast quantity of parameters to take into consideration and to optimize to produce a reliable and convenient control strategy: utility rate structure, building type, location of building, climate, and mechanical equipment in place, to name just a few. The number of possible combinations of all these parameters is very large and there is a lack of knowledge as to what combinations are most beneficial for specific optimisation objectives.

In fall 2010, a report by the U.S. Department of Energy concerning energy storage systems and their application in the commercial sector (Kintner-Meyer et al., 2010) depicted that the effectiveness of energy storage solutions had been demonstrated by various R&D programs but that there lacked term business models for its application. In addition, many R&D studies considered the building as a dependent system, responsible for managing its loads and supply independently. But, what might seem cost ineffective for the building owner might become of importance at the community scale such as grid load stability. The need for designing in a holistic manner becomes even more evident when thermal mass storage is applied extensively for load managing. An example of how this can be applied was introduced by Yin et al. (2015) in their final project report for controlling thermal energy storage in commercial buildings where actual utility tariffs rates were used instead of fictional ones. From this, the actual potential of the system can be measured rather than the maximum potential.

From a sustainability standpoint, the inclusion of thermal mass into buildings needs to be questioned. From a viewpoint focussed on energy consumption due to the operation of the building, this literature review has demonstrated that there can be significant ameliorations to the management of the energy consumption and that the demand can be better controlled during peak periods with effective use of thermal mass. However, from a more general viewpoint, such as a life cycle analysis of all materials required for such a technology, the benefits of a thermally heavy building in terms of energy consumption are not better than thermally light buildings, simply because the production of concrete is much more energy intensive than wood for example. This was investigated by Dadoo et al. (2012) and compared with many such investigations. The addition of thermal mass to a

building design solely for energy management and energy efficiency is questionable from an environmental standpoint. On the other hand, taking advantage of the thermal mass that is already used for structural reasons can help reduce the environmental footprint of buildings.

In terms of control, available literature points towards systems that have forecasting abilities for real time optimisation of a building's conditioning events. This is essential if substantial fractions of the load must be supplied by the stored thermal energy. However, excessive storage increases the thermal losses to the environment from having readily available thermal energy and can render the entire predictive process counterproductive in terms of energy efficiency. The performance of the model predictive control and reinforcement learning is highly dependent on the quality of the weather forecast and the ability of the building model to represent the physics of heat transfer with a reasonable accuracy, which depends on factors like climate, assemblies, workmanship during construction, operation & management, mechanical systems, etc. (Zakula et al., 2014). There is a predominant lack of demonstration and simulation tools, which would enable such a simplified model to be developed and implemented. The two most utilized energy simulation software packages, EnergyPlus and TRNSYS, do not have host easy-to-use plugins/packages at the moment.

The climate of the project is one of the most crucial factors in determining the effectiveness of the thermal storage solutions. Two of the means of activation presented in this literature can solely be used for sensible heating and cooling. When taking into account the energy consumption related to addressing latent loads, it can be more economical and efficient to install an air-handling unit that addresses both sensible and latent loads. The types of climates that are most favorable for sensible heating and cooling are dry climates. In addition, the maximum heat flux that can be obtained from the thermal mass is to be taken into account, especially if the loads are high. Typical hydronic floors and ceilings have an installed power of 50-60 W/m² while electric heating floors can go up to 120 W/m².

2.4. Summary

Space conditioning of buildings has been shown to be a large energy consumer, and it could have a significant influence on the total energy consumption. Several solutions

have been proposed in literature: 1) increase the distribution grid capacity, 2) improve even more the energy efficiency of buildings and 3) shift the peak power consumption to another period of the day, thus stabilizing the demand. Shifting peak power consumption is believed to be the most economically friendly approach on a short-term basis. This review has focused on up to date studies related to activated thermal storage for peak shaving and shifting.

When analysing the recent studies, one can see that most are in either a hot or mild climate. Very little research has been conducted on cold climates. Often, when thermal mass is activated, heat is extracted through coupling of the concrete floor with the room air and therefore the heat extraction rate is dependent on the convective and radiative heat transfer rate between the thermal mass and the interior air. The heat transfer is often too little to address all space conditioning loads in very cold or very hot climates. A lot of literature can be found regarding peak shaving with surface activation as well as hydronic activation and air activation but mostly for cooling applications. Only two recent studies could be found on electrically activated thermal mass, of which the input power was approximated by a uniform heat flux. Both studies had PCM's activated using electrical heating mats.

In all experiments and simulations addressed by the presented literature, the occupant comfort limited the charging/discharging depth of the thermal mass. Decoupling the thermal mass from the room air could be worth investigating in order to limit room air temperature swing. Also, the limited load forecasting abilities restricted extensive storage in advance without substantial thermal losses from the energy reservoir. A lot of research work is being conducted on predictive modelling. Simple night-set back control strategies have shown to offer good performances in terms of peak shaving and are easily applicable with off the shelf products. They are also very easy to implement and trouble shoot. Predictive control has shown to be more efficient than night set back strategies (order of 10-25%) but require extensive implementation effort.

CHAPTER 3: METHODOLOGY

This study is aimed at demonstrating the peak shave potential form using the basement floor concrete slab as a means of thermal storage. This is done by using a combination of field measurement, numerical work and simulation.

This project is separated into three phases:

1. To monitor a house equipped with a heated floor in the basement,
2. To develop a thermal model calibrated and validated on the data set obtained from the monitoring campaign, and
3. To determine the peak shave potential of the proposed approach using the developed thermal model.

3.1 Monitoring Campaign

3.1.1 Description of the Building

The house selected for the monitoring campaign is one where electric heating cables are already installed in the basement slab. Figure 2 shows the front and back view of the house, which is approximately 10 years old. It is located near Quebec City in the province of Quebec, Canada. The residence was constructed following the highest energy efficiency standard of Quebec, which entitles the owner to pass the NovoClimat certification (Québec, 2017). This approbation prescribes assemblies, workmanship as well as building infiltration. For a complete set of drawings of the house, please refer to Appendix C and F.

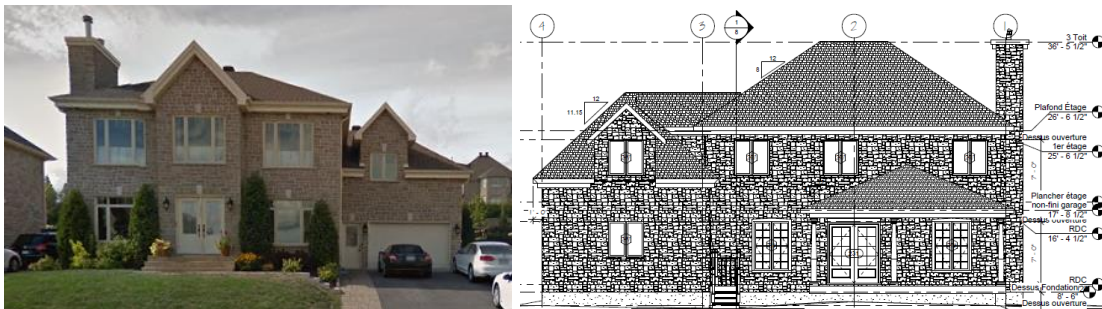


Figure 2 : Front View (Left) and Back View (Right) of the House.

The building is a two-storey plus basement, (which is liveable) with each storey totalizing 144 m² of liveable space. The exterior walls are made of 39 mm x 140 mm wood

studs every 406 mm insulated with mineral wool. The walls are sheathed with asphalt-impregnated fiberboard and faced with a 90 mm brick with a 25 mm air space for moisture removal. The interior side is faced with 12 mm aluminum covered extruded polystyrene panels with an air space and 12 mm gypsum panels. The roof trusses are insulated with 250 mm of mineral wool with a similar interior finish. The foundation walls are made of 250 mm of concrete. The interior assembly includes 50 mm aluminum covered expanded polystyrene panels with an airspace and a 12mm gypsum panel. The basement slab is made of a 150 mm concrete pad with a 50 mm extruded polystyrene panel underlayment on a sand bed. Floor finish covers vary throughout the house.

There are three types of heating systems in this residence:

- Buried Floor Heating System (BFHS): electrical heating wires are lodged in the concrete. They are installed on the bottom of the concrete slab. This type of system is installed throughout the basement and as well as in the garage slab.
- Surface Floor Heating System (SFHS): electrical heating wires are installed in a 0.6 cm layer of ceramic adhesive directly below the floor cover. This system is meant uniquely as occupant comfort and offers no mentionable thermal mass. This type of system is installed on the ground floor kitchen and bathroom area as well as in the second-floor bathrooms.
- Convective Heating System (CHS): an electrical heating unit that is placed at a certain distance from the wall and the floor, which promotes air movement through the heating device and within the room. This type of system is installed in some rooms in the basement and ground floor as well as throughout the second floor.

Other systems installed include a 280 L electric hot water tank. Due to the NovoClimat certification of the house, a heat exchanger is installed for moisture removal and indoor air quality. Bathrooms of every storey are connected to the exhaust duct. The fresh air duct supplies the basement family room. More technical information concerning the monitored house is available in Appendix B, C, D, E and F.

3.1.2 Selection of Parameters

The parameters chosen in this measuring campaign are a compromise between the simulation accuracy, cost of instrumentation and occupant intrusiveness. A major challenge behind this measurement campaign is that the building was occupied. Parameters that can be studied wirelessly through web-enabled systems are prioritized to limit the research project’s intrusiveness on the occupant’s personal life. This criterion also limits the number of parameters that can be monitored and how they could be monitored. The following table presents the selected list of parameters for the monitoring, which took place between January 23rd, 2017 and May 19th, 2017.

Table 4 Parameters Monitored during the Campaign.

Parameter	Equipment Used	Description
Weather Data	Weather station	Obtained through Environment Canada, interval of 1 hour
Total Building Electricity Consumption	Web enabled building electricity meter	The total building electricity consumption was obtained at an interval of 15 minutes from the electricity utility company.
Air Infiltration	Blower Door Test Apparatus	Depressurization test using ASTM-E1827 test protocol’s two-point method
Heating System Power Consumption	Web-enabled thermostat	Data available at interval of 5 minutes.
Zone Air Temperature and Floor Surface Temperature	Web enable thermostat	Data available at interval of 5 minutes.
	Thermocouple	Data available at interval of 1 minute.
DHW Power Consumption	Web enabled in line switch	Data available at interval of 5 minutes.
Air exchanger Energy Balance	Custom equipment	Data available at interval of 5 minutes.

Please refer to the Appendix B section for installed equipment details as well as installation specifications.

3.1.3 Data Quality Validation

Whenever possible, more than one type of sensors is used to measure a parameter. Thermocouples are installed during the last month of the monitoring campaign to monitor both room air temperatures and floor surface temperatures in rooms where floors are electrically heated. Temperature data recorded by the thermocouples are then compared to thermostat data. Detailed explanations of the monitoring installation accompanied with pictures are available in the Appendix B. The thermocouples are calibrated in an environmental chamber to ± 0.1 °C prior to installation.

3.2 Model Development

The following section presents an overview of the methodology to produce a reliable thermal model to be used as a tool to evaluate peak shifting and shaving. The model developed is based on the heat balance method where a set of heat and mass balance equations describe every room of the building, which are each represented by a single node. For detailed technical specifications of the model, please refer to the Appendix D.

3.2.1 Modelling Software Description

TRNSYS is a building software used to simulate highly transient systems through a graphical interface. An extensive library of components and systems is available to the modeller. Input and output parameters are linked to represent the relationship of these components. Hourly calculations can be done for simulation durations of years if needed. The modeller also has to his disposal access to the script behind the graphical representation of the system for added freedom and therefore new components can be created and added to the library. Each component/system in TRNSYS is referred to as a “type” and the labelling of types is done with a number. For example, *type56* in TRNSYS is the component that represents a multi-zone building. The thermal mass of all materials of a building is taken into consideration (Schmidt et al. 2000, Fort 1999).

A clear advantage of using TRNSYS as a modelling approach is the ability to model using a graphical interface and linking already pre-set components makes developing a model much faster (Saelens et al., 2011). Another advantage of using TRNSYS is the ease with which the model can be integrated with schedules, occupancy, appliances and various mechanical systems (Lehmann et al., 2007).

In its inherent nature, this tool can be considered as a prognostic law-driven model meaning that it can be used to predict the behaviour of a system given a set of well-defined laws that govern the system (mass balance, energy balance, heat transfers and conductivity, etc). This approach requires a significant amount of time to develop but its main advantage is that it can predict a system’s behaviour even when given previously unobserved conditions (Coakley et al., 2014).

3.2.2 Approaches to Produce Reliable Model Input

A large quantity of data is required to develop a model of a building able to predict hourly electricity consumptions. This section presents the steps that are taken to guarantee the quality of the model input files.

3.2.2.1 Audit

An audit refers to a tour of the building and a visual inspection of the layout as well as the installed systems (Coakley et al., 2014). In this project, construction drawings were available from the architect. Nonetheless, it was important to validate that the building was constructed according to plan and that the materials modeled be representative of the reality. This step involves a thorough inspection of the building to document its geometry, installed systems, orientation, etc. A detailed building description is presented in Appendix F.

3.2.2.2 High Resolution Data

The data acquisition equipment used in this study enables recording at sub hourly intervals. The web-enabled systems record data at a five-minute time step, thermocouples at a minute time step and the building energy meter record data at an interval of 15 minutes. This data is then averaged to the simulation time step of 5 minutes. In the case of a loss of internet connection, missing blocks of data is adjusted by interpolating linearly values before and after the Internet connection malfunction.

3.2.2.3 Data Manipulation

The format of the data sets from the various types of sensors does not match the required input file format of the modelling software. MATLAB was used to adapt the data to adapt the data to the required format. Using a script to achieve this tedious and repetitive process limits the possibility of human induced error. Two processes used this type of data manipulation:

3.2.2.3.1 Geometry Input File

During the building audit, all rooms are sub-divided into volumes and surfaces, where every element is characterized by its dimensions and constituting assembly. A single

excel file containing all the data is created and peer reviewed. With this approach, every room can be color-coded and organised in a user-friendly manner, which limits possible errors.

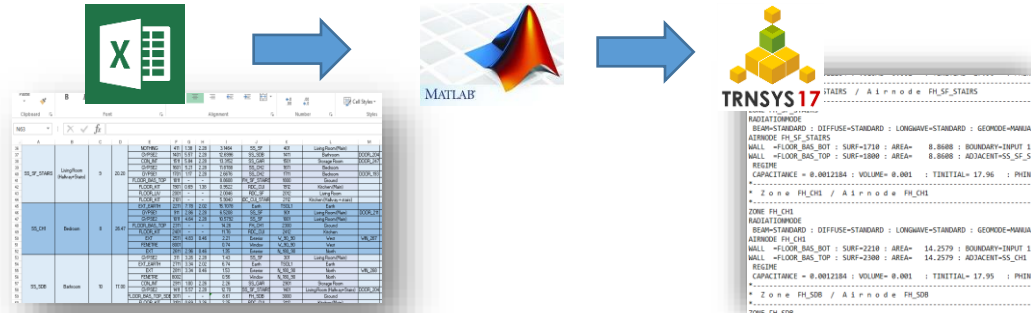


Figure 3: Workflow for Geometry File Creation

The TRNBuild module in TRNSYS requires a specific text file format. The transition is done using a MATLAB script, as presented by Figure 3.

3.2.2.3.1 Building System Input Files

Data pertaining to the recorded temperatures and energy consumptions are in a variety of different file formats and time scales due to the various software platforms used for data recording. However, input files for TRNSYS require single text files for the simulation period, per system. Therefore, reports are concatenated in an excel file and then compiled in the proper text format using MATLAB. Figure 4 shows this workflow graphically.

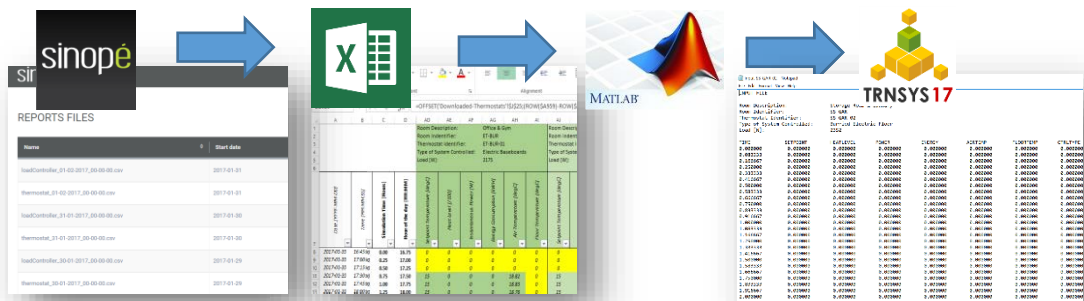


Figure 4 : Sample Workflow for TRNSYS Input File Creation

3.2.3 Model Validation

Many models have been developed where the performance was evaluated simply by percent differences between model outputs and experimental data (Coakley et al., 2014). This approach is blindfolded to errors cancelling out each other. Overestimated outputs during the simulation can cancel out underestimated outputs and result in a non-representative performance and lead to a misinterpretation of the performance of the model. A model deemed calibrated is not unique because there are numerous models of a building that can achieve the same criteria of performance. This is essentially because performance indicators are based on total building energy consumption. For this reason, the validation methodology mentioned in this section does not rely solely on validating the total building energy consumption, as suggested by ASHRAE (2005). The following sections detail the thermal model validation procedure.

3.2.3.1 Energy Losses

To validate the heat transfer mechanisms, the recorded power consumption of every heating system of the building is used as an input into the building model. Therefore, the model at this stage is subject to the same heating intensity as the actual building. The simulated and experimental average building and storey temperatures, on a mass basis, are then compared. The heat transfer to the ground and through the building envelope in the model is considered validated if the resulting air temperatures show the same behaviors as the actual building.

In addition, since the purpose of this project is to study the thermal storage potential of the house, it is mandatory that the temperature profile of the basement slab in the model behave like the experimental temperature profiles. To do this, floor surface temperatures of the model are compared to the floor surface temperatures recorded by the installed thermocouples.

3.2.3.2 Thermal Time Constant

The building room air temperatures are increased to 25°C until steady state conditions are met. Then, all heating systems are powered off to observe the rate of building air temperature decrease. Because the building is occupied during all tests, the lower limit of the air set point temperature cannot be any lower than 18°C. The same conditions are

replicated with the thermal model to compare its thermal behavior with the actual building thermal behavior.

The following formula can be used to describe the air temperature as a function of time:

$$T(t) = (T_i - T_{ext})e^{-t/\tau} + T_{ext}$$

where $T(t)$ is the air temperature at time t , T_i is the initial air temperature, T_{ext} is the exterior air temperature and τ is the thermal time constant. The thermal time constant is then determined using the following formula:

$$\tau = \frac{-t}{\ln\left(\frac{T(t) - T_{ext}}{T_i - T_{ext}}\right)}$$

This building has more thermal mass in the basement than the ground floor and second storey. Therefore, the thermal constant is calculated for the entire building and the individual storeys. This approach allows a better comparison between the thermal model and the actual building.

3.2.3.3 Building Energy Consumption

The building energy consumption performance of the thermal model is evaluated using ASHRAE Guideline 14 (ASHRAE, 2002) which states that for an hourly based model:

- The normalized mean bias error (NMBE) should be below 15% and;
- The coefficient of variance of the root mean squared error (CVRMSE) should be below 30%.

The above comparison is done for the total building energy consumption and for every individual storey. Analyzing the individual storey energy consumption is not a requirement as per ASHRAE guidelines but it is still important to take it into consideration to demonstrate that the thermal inertia of the building model is representative of the actual building, given that the thermal inertia of the storeys is very different from one another.

3.3 Peak Shave Potential

This section presents the methodology used to determine the peak shave potential of the proposed system. There are two peak periods that need to be addressed: a morning peak lasting from 6:00 a.m. to 10:00 a.m. and an evening peak lasting from 4:00 p.m. to 10:00 p.m. An optimal system is required to reduce the building electrical consumption during both peak periods and there can only be charging at night between the evening peak and the morning peak.

Considering this, there are three distinct scenarios that can be investigated:

- To determine the maximum peak shave potential given the configuration currently installed in the building;
- To determine if there exists an optimal thermal storage configuration for maximum peak shave potential other than what is installed in the monitored building;
- To optimize the thermal storage configuration for maximum peak shave potential of buildings with varying footprints.

These scenarios are detailed in the following sections. The results of these scenarios will demonstrate that there exists potential for peak shaving related to space heating for buildings in a northern climate. In addition, design parameters, such as required control schedules, concrete thickness and insulation thickness, will be identified as a function of the size of a building.

3.3.1 Description of the Thermal Storage System

The National Building Code of Canada (NBCC, 2005) states that basement concrete slabs require to be insulated with at least 50 mm of rigid insulation. In addition, the concrete slab needs to be at least 102 mm thick for structural integrity. The assembly studied in this project is a derivative of NBCC. It is composed of, from the ground up, insulation overlaid with concrete and a floor cover as presented by Figure 5. The electric heating cables are positioned at the bottom of the concrete slab.

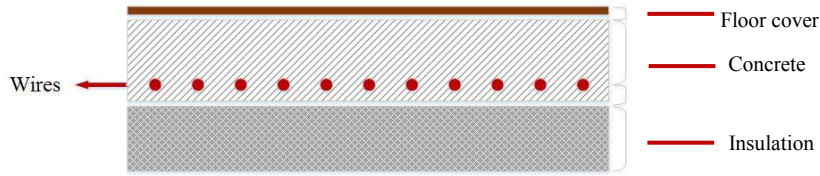


Figure 5 : Thermal Storage Assembly

Residential buildings typically have thermal mass located in the basement and all above ground assemblies contain little thermal mass. In addition, most buildings do not have a central HVAC system and therefore there is little air movement between rooms and storeys. This has an impact on this study because heat stored in the thermal mass of the basement cannot be used to heat above storeys. Therefore, this study only considers storing heat in the slab concrete to shift the peak consumption of the basement rooms. All other rooms of the building are subject to normal operating conditions.

3.3.2 Description of the Control Strategy

The electric heating system is controlled using commercially available residential thermostats, which have the ability of being pre-programmed with a daily air temperature setpoint schedule. Therefore, the charging and discharging of the thermal storage are done by increasing or decreasing the air set point temperature. For all simulations, the air set point temperature when there is no charging is 21°C. Two parameters are required to be defined with respect to the charging in the control strategy. The first one is the required air set point temperature during the charging period. An air temperature setpoint too low will result in not enough energy stored and an air temperature setpoint too high will increase the energy losses to the ground and create temperature overshoot in the room. The second parameter is the time required to charge the system. The higher the thermal capacity of the system, the longer the required time to charge. A charging time too short will result in not enough energy stored and a charging temperature too long will result in increased energy losses to the ground without creating any additional peak shave. Figure 6 is a visual representation of the control strategy where dT is the increase in air set point temperature during the charging period and t_c is the charging duration.

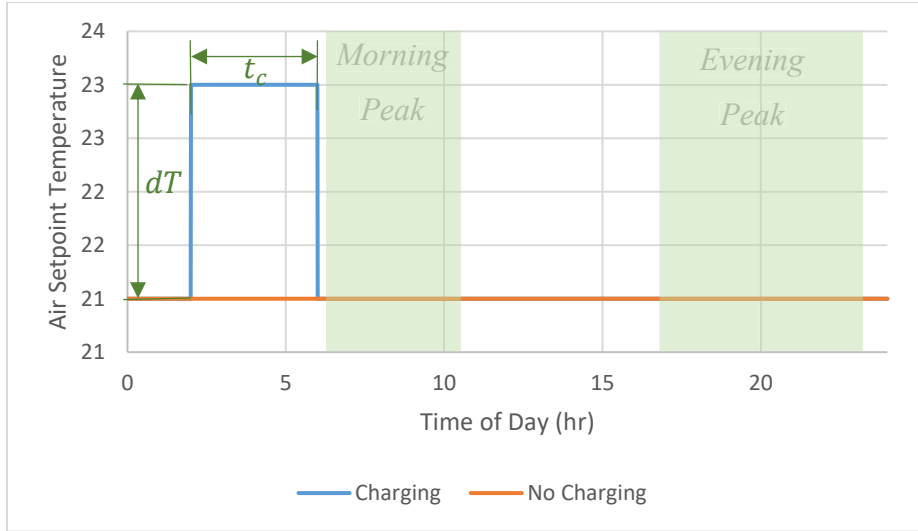


Figure 6 : Implemented Control Strategy with Arbitrary Charging Set Point Temperature

The control strategy presented above is rudimentary, but it corresponds to capabilities of off-the-shelf thermostats. Thus, these devices do not have the capability of adapting themselves to the varying heating demand as a function of the outdoor temperature. Since the objective is to find a solution giving maximum peak potential, the charging air set point temperature and duration are optimized for the coldest days of the winter season. All simulations are run from February to May to capture not only maximum peak shave potential but also to observe the influence of outdoor temperature swing during spring days on the performance of the system.

3.3.3 Performance Evaluation

The performance of the system is analyzed using the following set of criteria.

3.3.3.1 Peak Shave

The most important performance indicator in this project is the peak shave potential of the system. This parameter is calculated using the following formulae:

$$PS = \frac{\sum_{n=1}^N (P_{s,n} - P_{r,n})}{N}$$

where PS is the average peak shave in kW, $P_{s,n}$ is the building power consumption of the scenario at time n , $P_{r,n}$ is the reference building power consumption at time n and N is the

number of time steps in the peak period. The peak shave potential is calculated for both the morning peak and the evening peak.

3.3.3.2 Charge Depth

The charge depth is used to assess if the system is fully charged before the start of the morning period. Any system that cannot reach full charging depth before the morning peak period is not taken as a valuable solution. The charging depth is defined using the following formula:

$$CD = \frac{T - T_s}{dT}$$

where CD is the charge depth as a percentage, T is the average basement air temperature before the morning peak period, T_s is the air set point temperature (21°C) and dT is the increase in air setpoint temperature during the charging period.

3.3.3.3 Charging Time

This parameter is calculated for two reasons. The first one is to determine if the system can be fully charged during the night. The evening peak period ends at 10:00 p.m. and the morning peak only starts at 6:00 a.m. the following morning. Therefore, there are 8 hours available for the system to be charged. Any system that takes more than 8 hours to be charged will not be considered as a viable solution.

The other reason this parameter is calculated is to limit the energy losses to the ground. Having the concrete at a higher temperature than normal operating conditions increases the heat flux to the ground. The control strategy should be developed to reach maximum charging capacity right before the morning peak.

3.3.3.4 Discharging Time

The discharge time is calculated to determine the total time during which the slab can discharge heat to the basement. The time between the start of the morning peak and the end of the evening peak corresponds to 16 hours. Therefore, any system that will be considered a valuable solution will need to dissipate energy to the rooms for a minimum of 16 hours. This parameter is determined by comparing the total building power consumption of the simulation to a reference power consumption profile. The discharge

time is then defined as the time during which the storage system can keep the total building power consumption below the reference total building power consumption.

3.3.3.5 Maximum Air Temperature

This parameter is calculated to determine if there is considerable air temperature overshoot as a result of charging the thermal mass. The electric heating cables are located below a certain thickness of concrete and the control from the thermostat is based on the room air. This is the working principle of most radiant floor systems. In this context there is a lag between the activation of the wires and the room temperature response, which increases as a function of the slab thickness. This can induce some thermal discomfort in the event that the resulting temperature swing is too large. This can also produce higher energy losses if there is excessive temperature overshoot. Therefore, the maximum air temperature is taken into consideration to prevent this.

3.3.3.6 Increase in Energy Consumption

The anticipated increase in energy consumption due to thermal storage in the basement slab is expressed as a percentage. The daily energy consumption of the system is compared to the reference building as a function of outdoor temperature.

3.3.4 Reference Scenario

To evaluate the peak shaving potential of the system, a reference power consumption profile needs to be defined. This profile is the result of operating the building with the room air temperature setpoint of 21°C. In addition, the basis for comparison needs to be representative of the current construction methods for basement slabs in a northern climate. This corresponds to CMHC (2010) requirements in terms of slab construction (i.e. 51 mm on insulation with 102 mm of concrete) with baseboard heating in all rooms of the building.

It is important to note that the basement slab and heating system setup is different from what is currently installed in the house. The basement slab of the monitored building has 51 mm of insulation and 152 mm of concrete. The thickness of insulation in the reference building is kept at 51 mm because it corresponds to minimum requirements as per CMHC. However, the thickness of concrete is reduced to 102 mm. Also, the basement

heating systems are replaced by electric baseboards. The air set point temperature is set to 21°C for all rooms of the building. The same weather file as model validation is used.

3.3.5 Peak Shave Potential of Current Configuration

This section aims to investigate if the current configuration of the building can be used for peak shaving purposes and if so, what should be the control schedule implemented in the thermostats. The monitored building already has an electric heating floor installed, and the assembly is composed of 51 mm of insulation and 152 mm of concrete with a floor cover.

There are two steps required to determine the optimal control schedule. The first one involves running successive simulations with varying air setpoint temperatures during the available charging period (from 10:00 p.m. to 6:00 a.m.). This is to determine the required charging time as a function of the control schedule. The air setpoint temperature during the charging phase is varied between 22°C to 24°C in increments of 0.5°C.

A simulation is run with the optimal parameter and its associated required charging time to determine the peak shave potential of the system as well as the resulting increase in total daily energy consumption.

3.3.6 Optimal System Configuration for the Monitored Building

This section aims to investigate if the electric heating floor system installed in the monitored building has the optimal assembly configuration. In terms of insulation, the current configuration conforms to CMHC minimum requirements (51 mm). However, adding insulation beneath the concrete could reduce energy losses to the ground and thus allow a higher proportion of the thermal energy to be directed towards the basement rooms. In terms of concrete, the current configuration has 152 mm of concrete, which is higher than CMHC requirements. To determine the optimal thermal storage capacity, a range of concrete thicknesses is assessed, ranging from CMHC minimum requirements to 203 mm. For each configuration, the range of air setpoint temperatures of basement rooms during charging is varied between 22°C and 24°C in increments of 0.5°C. The following table summarizes the parameters investigated and their associated range of values.

Table 5 : Parameters Investigated and their Associated Range

Parameter	Range	Notes
Air set point temperature	22-24°C	Simulations in increments 0.5°C.
Thickness of Concrete	51, 102, and 152 mm	Concrete is specified in increments of 51 mm.
Thickness of Insulation	51 and 102 mm	Insulation is available in increments of 51 mm

For each simulation, the performance indicators are tabulated. The optimal system configuration is selected on the basis that the discharge time should be above 16 hours (to address both morning and evening peaks) and that a charging depth of 100% should be achieved before the morning peak. Of the system configurations meeting these two criteria, the configuration which requires the lowest required charging time is selected.

3.3.7 Optimal System Configuration for Buildings of Various Footprints

This section aims to investigate the potential for peak shave of buildings with various footprints. The thermal model developed is based on a building of 144 m². According to Statistics Canada, the average footprint of new constructions in the year 2015 was 159 m². Similarly, houses built prior to 1960 had an average footprint of 111 m² and at the end of the 20th century, the average footprint of homes had reached approximately 136 m² (Natural Resources Canada, 2017). Thus, there is a variety of residential building sizes to which the developed system could be applied. The performance of the system as a function of building size needs to be examined.

The developed thermal model is used to analyze the performance of the thermal storage system as a function of building size. To do so, the dimensions of the rooms in the model are changed. The building size is modified by increasing or decreasing the horizontal surface area of the rooms while maintain the same building width to length ratio. The storey heights are kept the same, independent of the room overall dimensions. The windows are scaled accordingly while the doors are kept at a uniform size.

There are 4 different building sizes that are investigated: 80, 120, 160 and 200 m². For each building size, the procedure discussed in section 3.5.6 is applied to determine the optimal insulation and concrete thicknesses. In addition, the associated charging time, charging air temperature setpoint of basement rooms, discharging time and maximum room air temperature are also determined to select the optimal system configuration as a function of building size. Simulations are then run with the optimal configuration for each size to

determine the associated increase in total daily energy consumption and peak shave potential.

CHAPTER 4: RESULTS

4.1 Monitored Data Quality Validation

The air temperature data set is validated by comparing the data collected by the web-enabled thermostats with the data collected by the installed thermocouples. Table 6 shows the difference between the two data sets as a function of building storey.

Table 6 : Temperature Difference between Thermostat and Thermocouple Readings (°C)

Measurement	Basement	Ground Floor	2nd Floor	Building
Room Air Temperature	0.548	0.552	0.362	0.487
Floor Temperature	3.359	0.710	0.140	1.403

The temperature differences between the two sets, despite that they are very small, can be attributed to the fact that the thermostats and the thermocouples do not record temperatures in the same way. The thermostats measure the mean radiant temperature whereas the thermocouples only measure the air temperature close to the thermostat. Thus, the thermostat data set is used for model validation because the recorded temperatures are a better representation of the room air conditions. It is important to note that the floor temperature probes of the basement and ground floor thermostats are installed in the slab at the heating cable level whereas the thermocouples are installed on the top of the floor cover, which explains the floor temperature differences.

Figure 7 shows temperature profiles of typical rooms conditioned with electric heating floors. The left graph corresponds to a room with the heating wires buried into 15 cm of concrete making it a very massive assembly. This corresponds to most of the electric heating cable installations in the house. For the room air, the two temperature profiles coincide very well with each other. The right graph shows a room where the electric heating wires are installed on the surface of the floor just below the floor cover. This configuration has negligible thermal mass and the intent of this system is mostly for occupant comfort. This type of assembly is used in the kitchen as well as the two bathrooms on the second floor. The readings are particularly sensitive to temperature probe location because the heating wires are so close to the surface, which makes it very hard to monitor. This explains the difference between the two temperature profiles. The graphs presented in

Figure 7 are from individual rooms but are representative of the collection of rooms having the same heating system installed.

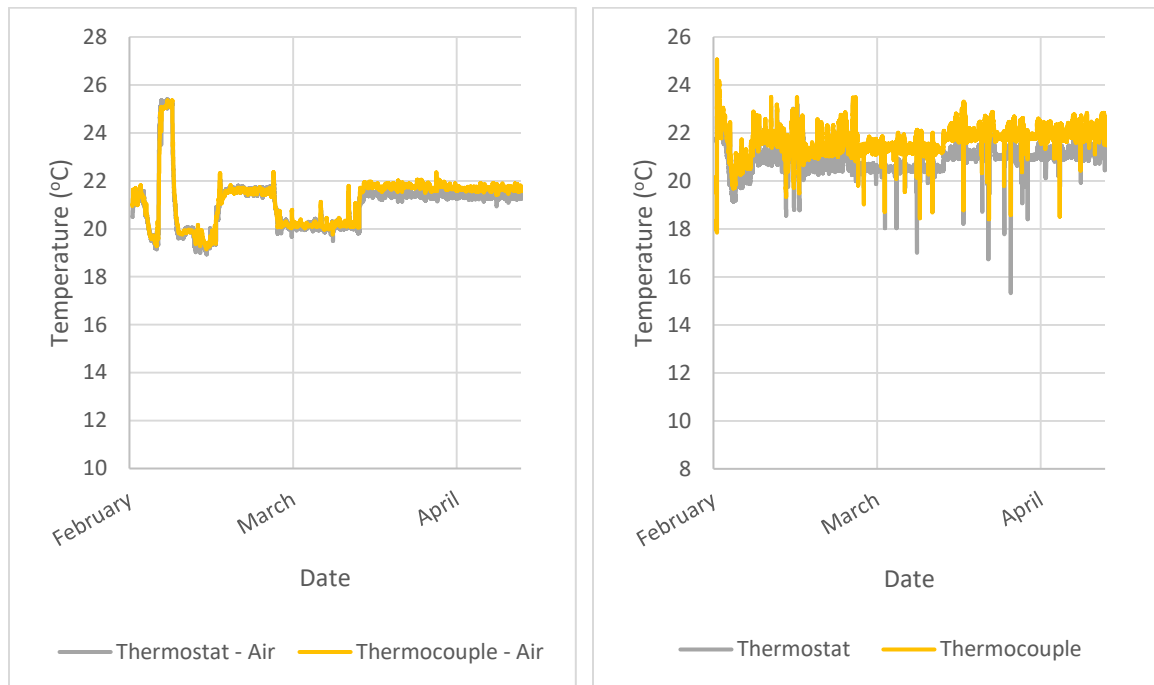


Figure 7 : Temperature Profiles of Rooms Heated with an Electric Heating Floor: Basement Living Room (Left) and Ground Floor Kitchen (Right)

For almost all the rooms in the house conditioned with baseboards the air temperature from both monitoring systems coincided. Figure 8 shows air temperatures of two of these rooms. The left graph shows the basement family room. The two temperature profiles coincide well, even with a fast temperature ascent. The right graph shows the only room for which the monitoring equipment did not function properly. This corresponds to the ground floor living room. The air temperature collected using the thermostat had some small discrepancies when the electric baseboard was turned on during the first few weeks of the monitoring campaign. The reason for this difference is that the thermocouple and the thermostat were installed too close to the electrical baseboard and therefore the temperature measurements were influenced by the updraft of hot air from the heating equipment. This can be observed by comparing the room air temperatures profile to the power consumption profile of the baseboard. Except for the ground floor living room, all air temperature data sets can be considered valid because the recorded data set from both types of instruments coincide.

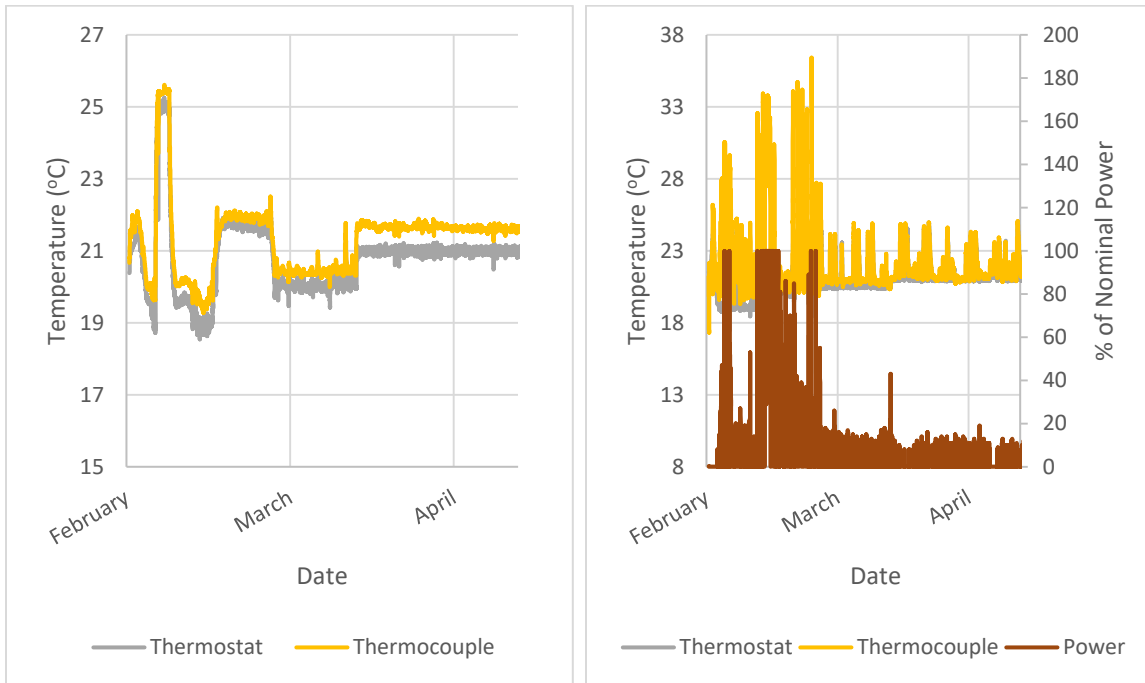


Figure 8 : Temperature Profiles of Rooms Heated by Baseboards: Basement Family Room (Left) and Ground Floor Family Room (Right).

4.2 Model Validation

4.2.1 Energy Losses

The temperature profile resulting from inputting the recorded power consumption of the heating systems in the thermal model is shown by Figure 9. The simulated average building temperature is close to the actual recorded average building temperature, which indicates that there is good agreement between the model and measured data. During this simulation period, two events were scheduled to impose extreme conditions to the building. The first one happened on February 3rd. The entire building was heated to 25°C and then cooled. The model gave similar behaviors given the same power consumption input: the model average building temperature increased to 27.15°C while the actual recorded peak temperature was 25.09°C. Another event happened on March 4th, where only the basement was increased to 25°C: in this case, the model average building temperature was 23.03°C while the actual recorded average building temperature was 22.68°C.

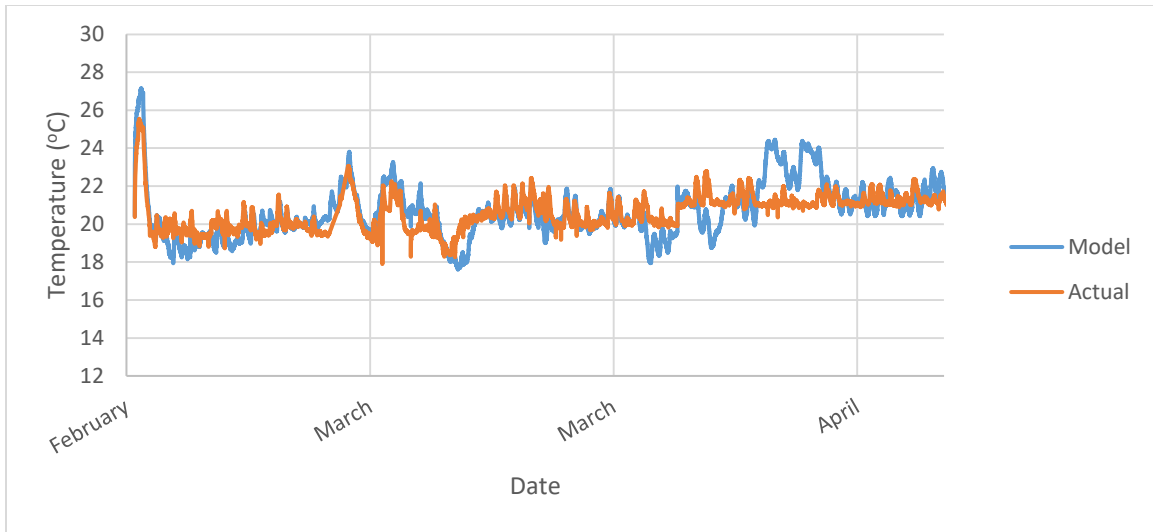


Figure 9 : Volume Weighted Average Building Temperature

The performance indices MBE and CVRMSE were also used to characterize the performance of the model. Table 7 shows the summary of these indices for the whole building and for individual storeys. The following table shows that there is very good agreement between the thermal model and the actual building.

Table 7: Model Performance from Temperature Profile Comparison

	Performance Indicator	Model Accuracy
Building	NMBE	0.33%
	CVRMSE	4.70%
Basement	NMBE	0.85%
	CVRMSE	5.60%
Ground Floor	NMBE	0.68%
	CVRMSE	2.51%
2nd Floor	NMBE	0.54
	CVRMSE	9.76%

The energy losses to the ground in the thermal model are validated by comparing the basement slab surface temperature to the recorded basement slab surface temperature. The two temperature profiles are presented in the following graph. The basement surface slab temperature was only recorded with thermocouples starting on February 27th. Fortunately, one of the charging events, where the basement was heated to 25°C and then cooled, was recorded by the thermocouples. Based on the following graph, the basement

slab temperature is well represented by the model even during charging and discharging of the stored energy.

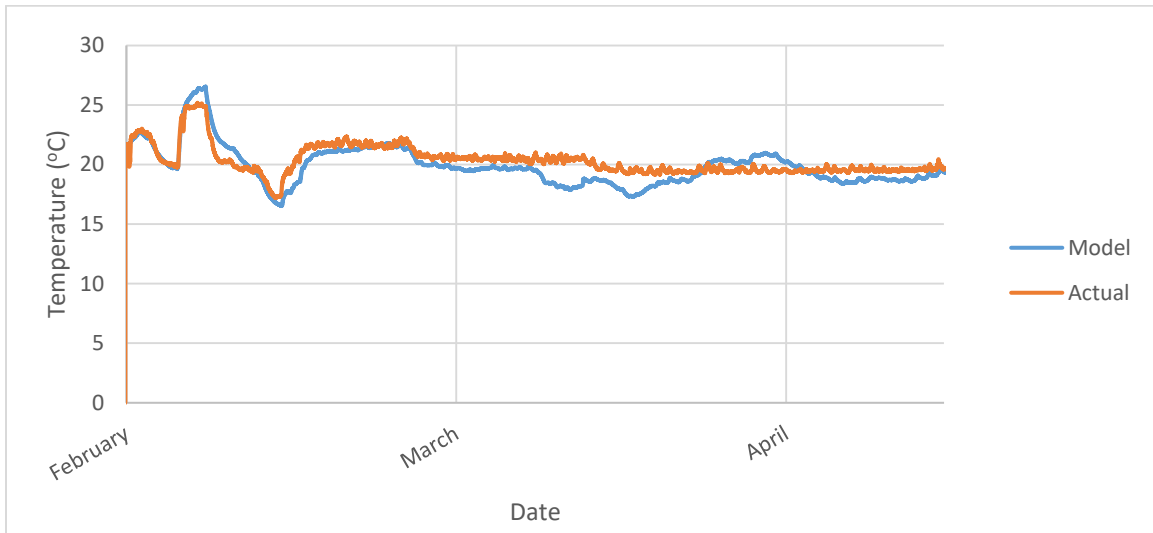


Figure 10 : Average Basement Slab Surface Temperature

The discrepancies between model output and recorded data can be attributed to the fact that furniture was not modelled with TRNSYS. In many basement rooms, a large proportion of the room floor surface area is covered by furniture, especially in bedrooms. This influences the quantity of heat dissipated to the room.

4.2.2 Thermal Time Constant

This section presents results of the test conducted to estimate the thermal time constant. This is to validate the dynamics of the thermal model and show that heat diffusion from the thermal mass is well represented. The average outdoor temperature during the test is -10.03°C. The air setpoint temperatures of all the thermostats of the building were raised to 25°C for a period of 2 days. This enabled steady state conditions to be met. The air set point temperature was then set to 18°C to allow the building to cool. It took 18.75 hours before any heating device was activated by a thermostat. The actual and modelled thermal time constants are presented in the following table.

Table 8 : Building Actual Versus Simulated Thermal Time Constant

Storey	Actual Air Temperatures [°C]	Model Air Temperatures [°C]	Time Constant [h]

	@ t=0 [h]	@ t=18.75 [h]	@ t=0 [h]	@ t=18.75 [h]	Actual	Model
Basement	24.98	20.32	25.12	21.02	131.98	151.18
Ground Floor	25.32	20.25	25.51	19.90	121.23	109.14
2nd Floor	25.07	18.43	28.93	19.93	89.45	71.18
Building	25.12	19.67	26.52	20.28	111.29	100.16

The results show that the thermal response of the model is very similar to the actual building. In addition, the thermal behavior of each storey is very close to the actual building. Therefore, the different thermal inertia of the storeys is well represented in the thermal model. This study emphasises thermal storage in the basement; but it is important that the model agree with the actual building for each storey.

4.2.3 Building Energy Consumption

The same set point temperatures were applied to the thermal model as the actual building to compare the model total energy consumption to the actual recorded total consumption. Table 9 shows the summary of the NMBE and CVRMSE performance indices for the total building energy consumption. The calculated indices are below the ASHRAE Guideline 14 requirements for an hourly model. Therefore, the model can be considered valid. In addition, the same performance indices were calculated for all storeys of the building and they too are below the ASHRAE Guideline 14 requirements. This shows that the behavior of individual storeys in the model is representative of the individual storeys of the actual building. The second floor contains considerably less thermal mass and has a large percentage of wall area which is windows. Therefore, it reacts much faster to outdoor stimuli like varying outdoor temperature and solar radiation. Nonetheless, its behavior is well represented in the thermal model. The same can be said of the basement despite that it contains much more thermal inertia than all above storeys.

Table 9 : Model Performance

	Performance Indicator	Model	ASHRAE Requirement
Building	NMBE	1.10%	15%
	CVRMSE	24.20%	30%
Basement	NMBE	3.38%	-
	CVRMSE	28.84%	-
Ground Floor	NMBE	11.80%	-
	CVRMSE	28.24%	-
2 nd Floor	NMBE	3.28	-
	CVRMSE	28.80%	-

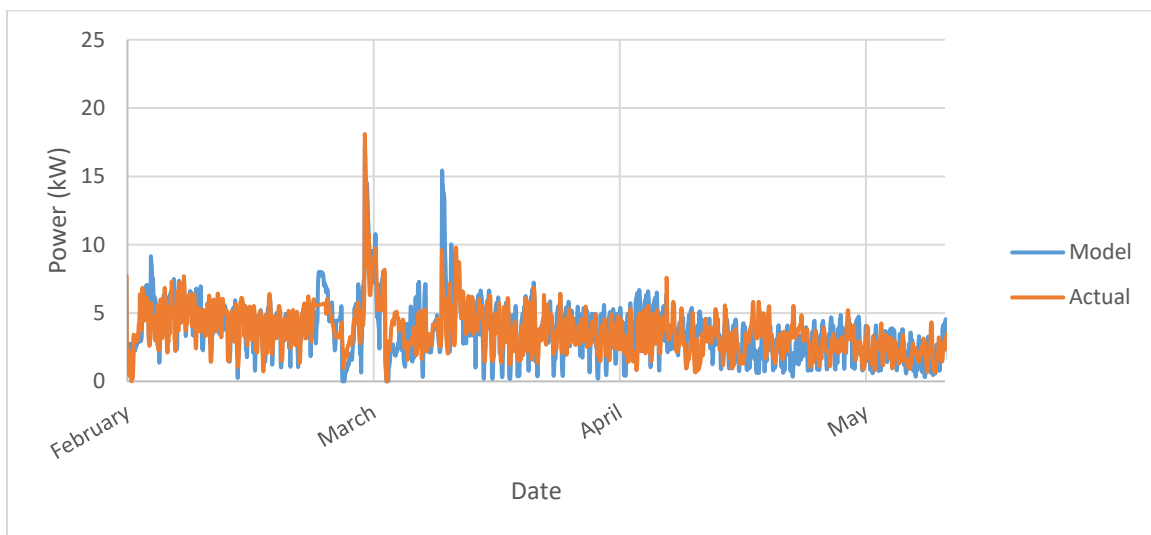


Figure 11 : Simulated versus Actual Building Electrical Consumption for Space Heating

From the above graph, there is a minor difference between the power consumption of the model versus the actual recorded power consumption, although the thermal model respects ASHRAE guidelines in terms of hourly power consumption. This can be explained by the fact that the air temperature inside the thermal model is assumed to be represented by a single node of energy balance. In that regards, the natural buoyancy effects of the air within the room created by heating equipment or drafts from windows is not considered in the model. The simulated rooms are one-dimensional and the heating equipment has an instantaneous influence on the room air. The simulated air temperature has a much faster response to the input energy from a heating system than the actual room.

Differences between the model and the actual building also arise from the assumptions behind the convective heat transfer coefficient. In the model, the relative difference in temperature between the surface and the air as well as the orientation of the heat flux are taken into consideration but not the existence and the layout of furniture in the rooms. This has a considerable influence on the discharging of the thermal mass. The basement bedrooms, for instance, have a bed and side tables, which account for more than 50% of the room surface area. Other examples include the family rooms, which have a billiard table, couches, multimedia furniture as well as coffee tables or the laundry room, which also serves as a storage room.

Another aspect that can explain the differences between the model predictions and the measured data is the fact that the building was occupied during the monitoring campaign conducted. The hardest parameter to validate in thermal modelling is occupancy-related behaviors because they can be stochastic. In this study, there was no tracking or record of the occupant presence or activity. However, it was known that the occupants worked long hours during the week and rested in their cottage house over the weekends. Their influence was therefore only perceivable on weekday mornings, evenings and occasional weekends. In addition, the house is very large, and the family is only composed of three individuals. Their appliance/lighting use is therefore very small compared to the space available. The garage was used as the main entrance of the house and no cars were ever parked inside. Therefore, the influence of cold winter air from opening doors is only limited to the garage side door.

Last but not least, some behaviors of the occupants could not be avoided despite their detrimental influence on the quality of the data recorded. As an example, the thermostat air set point temperatures were adjusted to have a common temperature setting throughout the building. This is to limit inter-storey air movement from buoyancy. Yet it did not take long before the occupants would change this set point to accommodate their momentaneous comfort needs. On the other hand, other occupant behaviours had a positive influence on the validation of the model. For instance, the family never activated the heat exchanger installed in the house because it was not part of their habits. Thus, it was never integrated to the model.

4.3 Peak Shave Potential

4.3.1 Reference Power Consumption

This section presents the power consumption used as a reference to evaluate the peak shave potential of the scenarios discussed in the following sections. Figure 12 shows the daily electricity demand of the building as a function of outdoor temperature. The two data sets shown on the graph correspond to the resulting electricity demand of the same building but with two different heating systems installed in the basement: one has electrical heating cables in the floor concrete slab and the other has electrical baseboards. The baseboard-only building has a lower electricity demand for any outdoor air condition. This is because rooms with heated floors have higher energy losses to the ground.

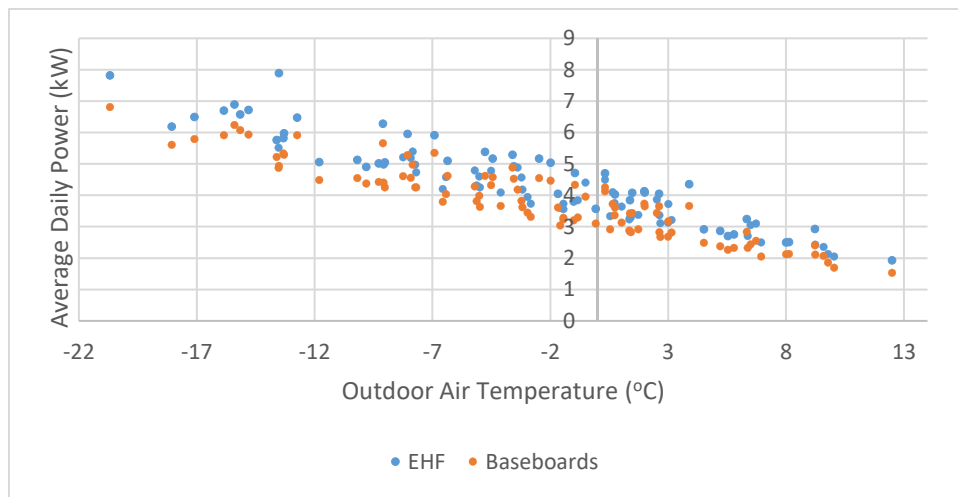


Figure 12 : Daily Building Electricity Demand as a Function of Outdoor Temperature

The above graph shows how the electricity demand of the building changes as a function of outdoor temperature. The energy consumption of the building at an outdoor temperature of -20°C is almost double the energy consumption of the building when the outdoor air temperature is at 10°C . This indicates that there is a larger potential for peak shave when the outdoor temperature is cold. On the other hand, if the outdoor air temperature for a given day is 10°C , then the daily electricity demand is expected to vary between 1.68 kW to 1.86 kW. In this case, the peak shave is limited to this value.

For any outdoor air temperature, the electricity demand cannot be represented by a single value but by a range of values. For example, at a temperature of -5°C , one can expect the electricity demand to vary between 3.62 kW and 4.61 kW. This can be attributed

to the influence of the thermal mass of the building. The electricity demand for a particular day is dependent on the weather conditions of the day before.

4.3.2 Peak Shave Potential of Current Configuration

The model is run using air setpoint temperatures during the charging period varying from 22°C and 24°C for the basement rooms. All other rooms have an air set point temperature of 21°C. The performance results of these simulations are presented in Table 10. For air set point temperatures up to 23°C, a charging depth of 100% is achieved. For setpoints above 23°C, full charging capacity cannot be achieved in the time available between the evening peak and the morning peak of the following day. Therefore, it is not advantageous to use air set point temperatures higher than 23°C. The time required to charge varies between 3.94 hours to 6.75 hours for air setpoint temperatures of 22°C to 23°C. For an additional degree Celsius, 2.81 hours of charging time are required. For all simulations, the maximum air temperature in the room is never more than 0.36°C above the air set point temperature. This shows that the system is sufficiently controllable to prevent excessive air temperature overshoot, which could create occupant discomfort. Based on the results of the following table, the optimal charging air set point temperature is 23°C because the system can be fully charged in the time allowed and it offers more discharge time compared to air setpoint temperatures that are lower. The selection is highlighted in yellow in the table.

Table 10 : Charging and Discharging Time as a Function of Air Setpoint Temperature Design Charging Period

Air Setpoint Temperature During Charging Period (°C)	Charge Depth Achieved	Time Required to Charge (hr)	Discharge Time Achieved (hr)	Maximum Temperature (°C)
22	100%	3.94	8.08	22.36
22.5	100%	5.15	11.11	22.84
23	100%	6.75	13.36	23.23
23.5	99%	8+	15.18	23.62
24	94%	8+	15.95	23.99

A simulation was run where the air set point temperature during the charging phase was set to 23°C and the charging duration was set to 6.75 hours. The resulting peak shave for both the morning peak and the evening peak are presented in the following figure.

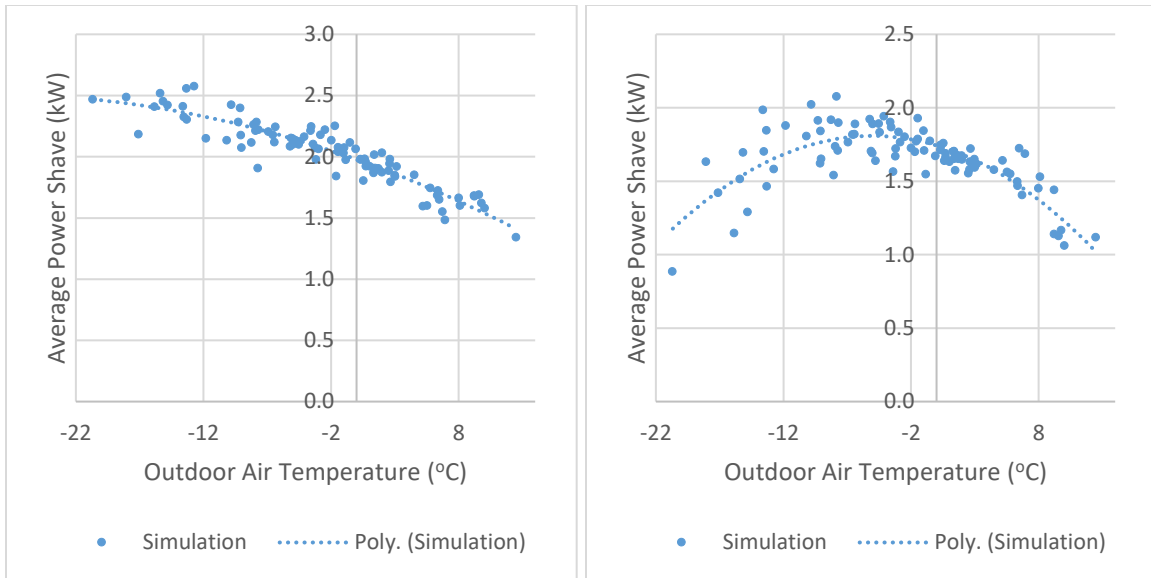


Figure 13 : Average Peak Potential as a Function of Outdoor Air Temperature for the Morning Peak (left) and the Evening Peak (right)

The above graphs show the simulated peak shave potential of the system for both the morning peak and the evening peak. The morning peak graph indicates that the peak shave increases as the outdoor temperature decreases. This is because the reference power consumption also increases when the outdoor temperature decreases. The peak shave can be compared to the reference power consumption to determine the percentage of the total building consumption that is reduced. As an example, for an outdoor temperature of -18°C , the reference power consumption is approximately 5.6 kW whereas it can be reduced to 2.49 kW with a thermal storage strategy. The daily increase in energy consumption is 18.22 kWh due to the implementation of this control in comparison to the reference building.

For the evening peak period, the peak shave potential increases when the outdoor temperature decreases but only down to approximately -6°C . Below this outdoor air temperature, the peak shave potential decreases. This is an indication that at low outdoor air temperatures, there is not a sufficient amount of energy stored to address both the morning peak and the evening peak, considering that there is only a single charging period at night that needs to address both peaks.

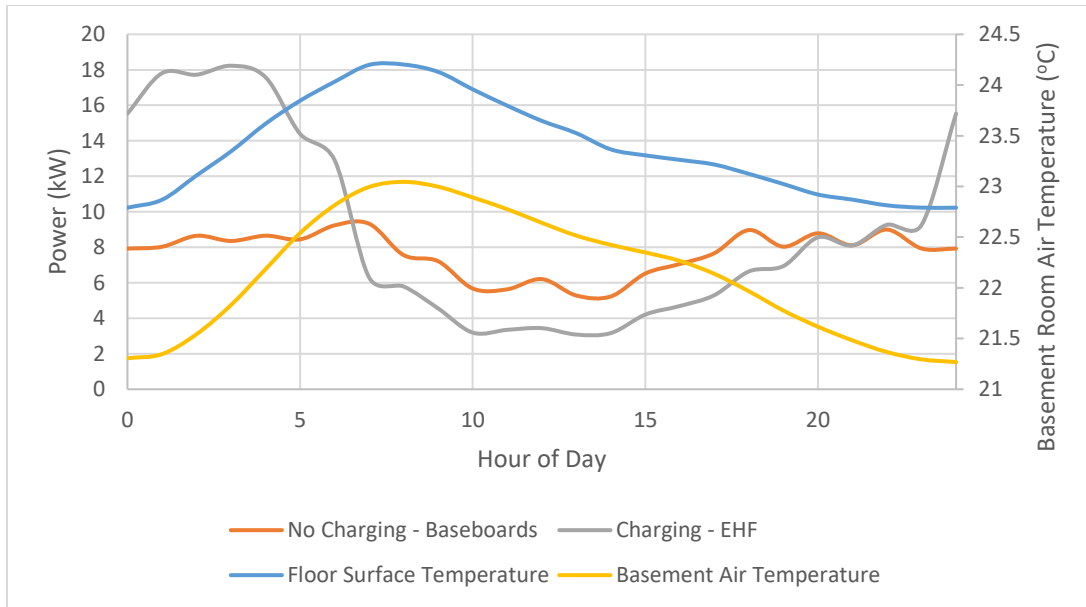


Figure 14 : Average Daily Energy Consumption Profile of the Three Coldest Days of Simulation Period

The daily electricity consumption profile is determined from taking the average hourly power consumption of the three coldest days of the simulation period, which corresponds to an average outdoor air temperature of -18.6°C . The profile shows that the energy consumption of the building increases dramatically at night during the charging phase and decreases rapidly at the beginning of the morning peak. The electricity consumption of the scenario with charging is below the reference power consumption up to approximately 8:00 PM, which is before the end of the evening peak period. Nonetheless, the system is effective in lowering the total building electricity consumption for most of the day, even though the outdoor air temperature is very low. In addition, despite the cold outdoor air temperatures, which increase the building space heating load, the basement slab heat flux to the air is high enough to allow the basement room air temperatures to the desired 23°C .

4.3.3 Optimal System Configuration for Monitored Building

An optimal selection of parameters for this system needs to guarantee discharging times of more than 16 hours and be able to address both the morning and evening peaks. In addition to varying the air setpoint temperature during the charging period between 22°C and 24°C , the thickness of insulation and concrete are also varied. The results of the charging depth and required time to charge are presented in Table 11 while the discharging time and maximum room air temperature are presented in

Table 12.

All simulations with 102 mm of concrete did not obtain the required discharging time. Therefore, the storage capacity of minimum CMHC requirements in terms of basement slab concrete thickness does not have a sufficient storage capacity. Of the simulations with a discharging time sufficiently large and a charging depth of 100%, the required time to charge is the parameter used to select the optimal system configuration. Therefore, the optimal system configuration has an air setpoint temperature during the charging period of 23°C with 102 mm of insulation and 152 mm of concrete. This selection requires 5.3 hours to be fully charged before the morning peak. This selection resembles the current installation of the monitored building with the exception that an additional 51 mm of insulation is required. Thus 5.3 hours of charging are required instead of 6.75 hours and a longer discharge time can be expected.

Table 11 : Charing Depth and Charging Time Required as a Function of Air Setpoint Temperature During Charging, Insulation Thickness and Concrete Thickness

Air Setpoint Temperature During Charing Period (°C)	Insulation Thickness (m)	Charge Depth Achieved			Time Required to Charge (hr)		
		Concrete Thickness (m)					
		0.102	0.152	0.203	0.102	0.152	0.203
22	0.051	100%	100%	100%	2.99	3.94	5.56
	0.102	100%	100%	100%	2.63	3.62	5.49
22.5	0.051	100%	100%	100%	3.39	5.15	7.20
	0.102	100%	100%	100%	2.99	4.48	6.17
23	0.051	100%	100%	97%	4.36	6.75	8+
	0.102	100%	100%	100%	3.82	5.30	6.69
23.5	0.051	100%	99%	91%	5.62	8+	8+
	0.102	100%	100%	98%	4.74	5.93	8+
24	0.051	100%	94%	84%	6.92	8+	8+
	0.102	100%	100%	97%	5.56	6.59	8+

Table 12 : Discharge Time and Maximum Air Temperature as a Function of Air Setpoint Temperature During Charging, Insulation Thickness and Concrete Thickness

Air Setpoint Temperature During Charing Period (°C)	Insulation Thickness (m)	Discharge Time Achieved (hr)			Maximum Air Temperature (°C)		
		Concrete Thickness (m)					
		0.102	0.152	0.203	0.102	0.152	0.203
22	0.051	4.84	8.08	11.35	22.38	22.36	22.38
	0.102	7.22	11.36	14.70	22.51	22.51	22.46
22.5	0.051	6.99	11.11	14.75	22.86	22.84	22.80
	0.102	10.04	14.16	16+	22.96	22.99	22.92
23	0.051	9.27	13.36	16+	23.29	23.23	23.18
	0.102	11.52	16+	16+	23.39	23.41	23.35
23.5	0.051	10.85	15.18	16+	23.70	23.62	23.56
	0.102	13.56	16+	16+	23.85	23.84	23.78
24	0.051	12.33	15.95	16+	24.13	23.99	23.86
	0.102	15.56	16+	16+	24.29	24.26	24.18

A simulation was run with the optimal selection the peak shave potential is presented in Figure 15. The morning peak shave of this assembly has a magnitude that is very similar to the peak shave achieved with the current installation of the building. However, with the added insulation, the system can now address much better the evening peak. In addition, because the energy losses to the ground are reduce, a smaller charging time is required, and the total energy increase is reduced to a 4.98 kWh per day. When the outdoor air temperature is at approximately -13°C, the daily energy consumption of the electric heating floor is very similar to the reference building, even though the floor is heated. However, for colder and hotter outdoor air temperatures, the electric heating floor system consumes more energy than the reference baseboard system, especially for outdoor air temperatures above 0°C.

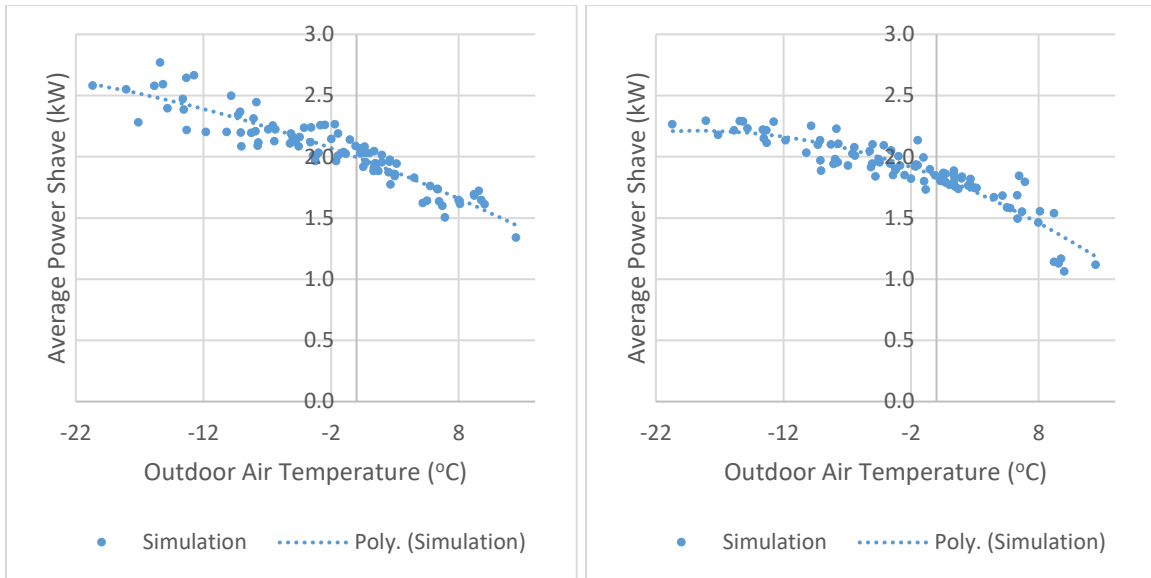


Figure 15 : Average Peak Potential as a Function of Outdoor Air Temperature for the Morning Peak (left) and the Evening Peak (right) of Optimal System Configuration

The daily consumption profile, obtained by averaging the profile of the three coldest days, is presented in Figure 16. As a means of comparison, the daily profile of the reference building, the current configuration with charging and the optimal configuration with charging are shown. In both simulations with charging, the power consumption during the morning peak is the same. However, the optimal assembly shows a smaller charging period during the night. In addition, the power consumption of the optimal assembly stays below the reference power consumption for the entire duration of the evening peak.

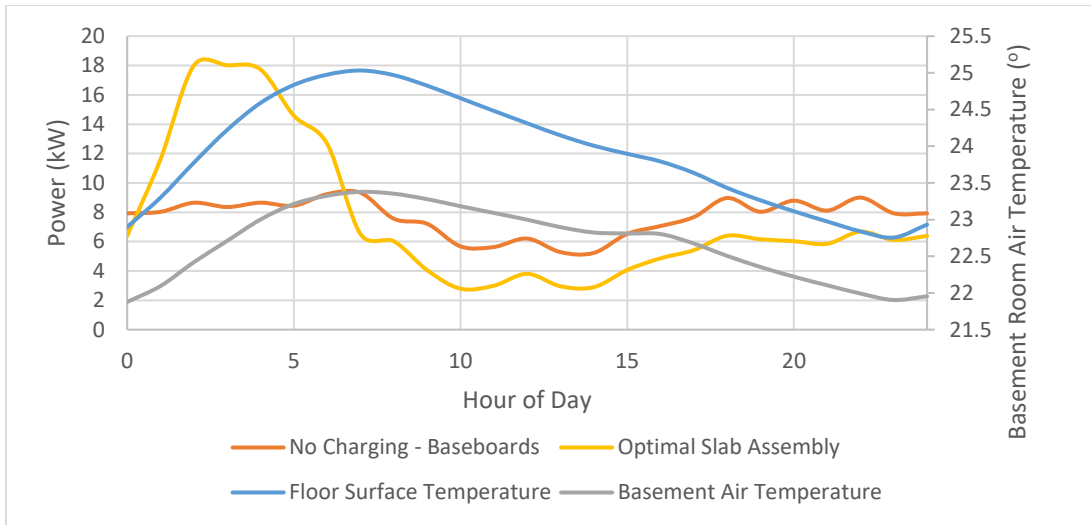


Figure 16 : Average Daily Energy Consumption Profile of the Three Coldest Days of Simulation Period

4.3.4 Optimal System Configuration for Buildings of Various Footprints

For every building size, simulations are run varying the air temperature setpoint during charging, thickness of insulation as well as concrete thickness. The results of the simulations are available in the Appendix A. For every simulation, the required charging time, charging depth, discharging time and maximum temperature are determined. Similar to the previous sections, the selection of the optimal configuration is based first on whether or not the system can provide sufficient discharging time to address both the morning peak and the evening peak and if the system can be fully charged within the 8 hours available to charge. The optimal configuration is then based on the assembly that requires the least amount of charging time. The optimal slab configuration for all building sizes ranging from 80 m² to 200 m² is the same and is composed of 102 mm of insulation covered by 152 mm of concrete and uses 23°C as a charging air temperature setpoint. The performance of this system configuration as a function of building size is shown in the following table.

Table 13: Discharge Time and Maximum Air Temperature as a Function of Air Setpoint Temperature During Charging, Insulation Thickness and Concrete Thickness

Building Size (m ²)	Charging Depth	Required Time for Concrete to be Thermally Fully Charged (hr)	Discharge Time (hr)	Maximum Temperature (°C)
80	100%	6.00	16+	23.18
120	100%	5.51	16+	23.31
160	100%	5.05	16+	23.44
200	100%	4.66	16+	23.49

In all cases, the thickness of insulation and concrete are determined to have a complete charging depth and a discharging time of over 16 hours. The “+” symbol next to the values of the discharging time column indicates that a discharging time of over 16 hours is achieved with the system.

The required charging times shown in the table above indicate that as the building size decreases, the required charging time increases. This is because the ratio of the exterior envelope surface area to the volume of the building increases as the footprint decreases. The heat loss to the environment is proportional to the exterior wall surface area whereas the space heating available power for space heating is proportional to the footprint of the building. Therefore, less time is required to reach the charging air setpoint temperature for large buildings than for smaller buildings.

In all cases, the maximum air temperature is very close to the maximum air temperature setpoint of 23°C, which indicates that there is little temperature overshoot in the room. The resulting temperature swing from charging the basement slab is therefore very close to the desired imposed 2°C difference in air temperature setpoints between the charging and discharging period.

For all the building sizes, the system offers a peak shave potential for both the morning and evening peak as presented by Figure 17 and Figure 18. This holds true even for cold outdoor temperatures. However, the evening peak shave potential reaches its maximum value for when the outdoor air temperature falls below approximately -15°C. The selected system configuration is therefore not well suited for extreme outdoor air temperatures. Another selection of configuration would be required for better performances in colder outdoor air temperatures. Also, the peak shave potential per meter square is higher for smaller buildings because the space heating load per meter square is proportional to the

ratio of exterior envelope surface area to building volume. The associated increase in daily energy consumption is 3.68 kWh, 4.49 kWh, 5.3 kWh and 6.11 kWh for buildings of 80 m², 120 m², 160 m² and 200 m².

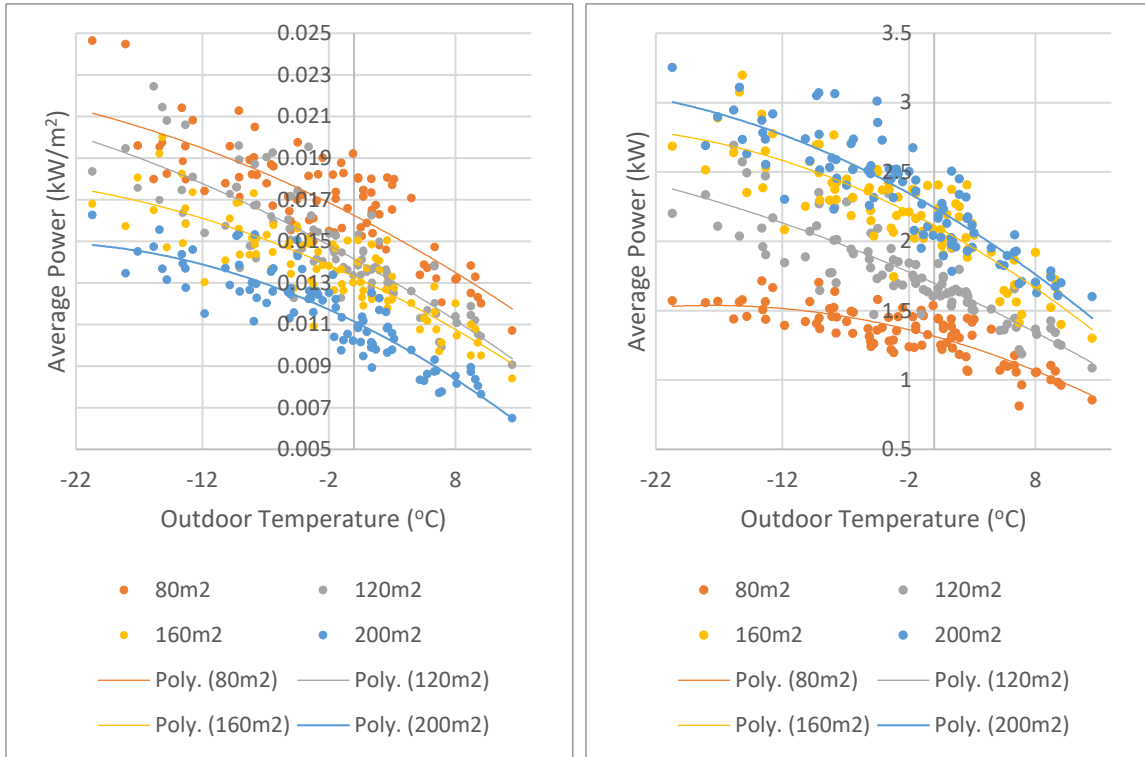


Figure 17 : Average Peak Potential as a Function of Outdoor Air Temperature for the Morning Peak of Optimal System Configuration for Buildings of 80, 120, 160 and 200 m² Footprints

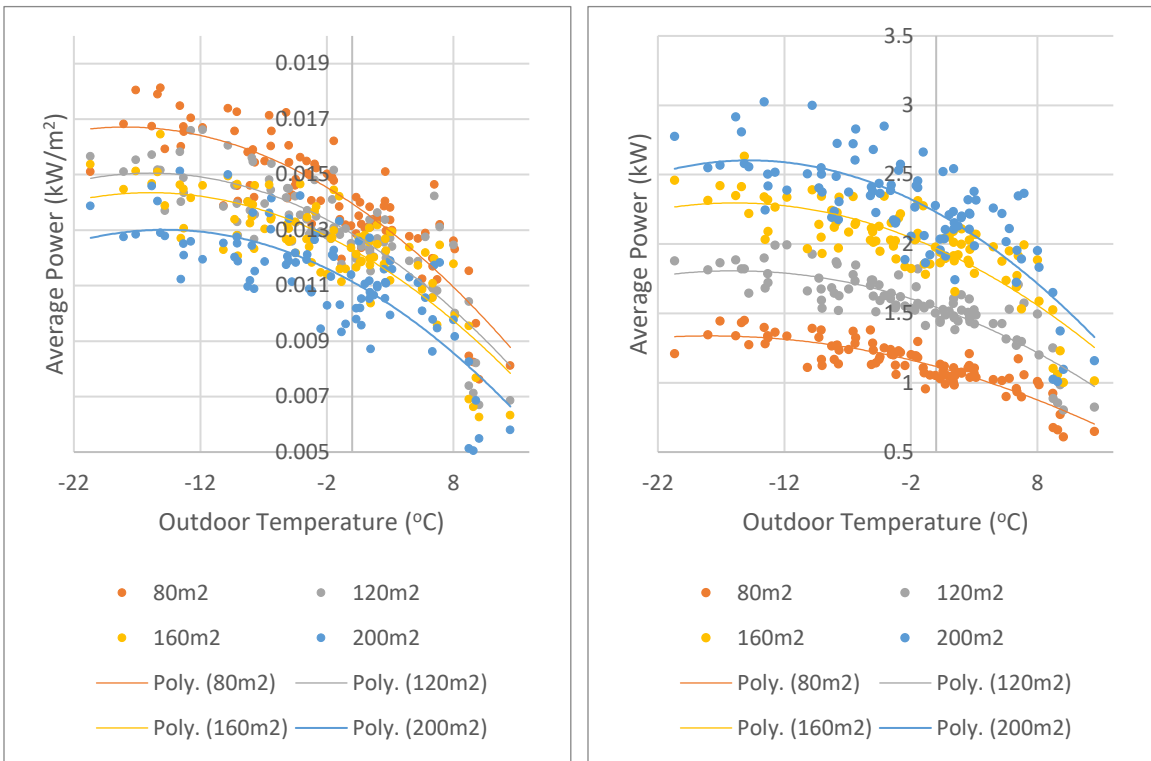


Figure 18 : Average Peak Potential as a Function of Outdoor Air Temperature for the Evening Peak of Optimal System Configuration for Buildings of 80, 120, 160 and 200 m² Footprints

CHAPTER 5: CONCLUSION

This thesis has demonstrated that an electrically activated thermal storage system can be used for peak shaving of a residential building in a northern climate. Within the context of this project, peak periods were defined as 6:00 a.m. to 10:00 a.m. and 4:00 p.m. to 10:00 p.m. A residential building with its basement equipped with electrically heated floors in the basement was monitored. The recorded data quality was validated and used to develop a thermal model with TRNSYS. The thermal model was used as a tool to investigate various system configurations and control. The objective of the system was to shift the basement power consumption to off peak period. It was shown, from a scenario analysis, that a charging time window from 10:00 p.m. to 6:00 a.m. is enough and that both the morning and evening peak could be shifted given an appropriate system configuration.

The existing configuration installed in the home can be used for peak shaving given a charging air set point temperature for the basement rooms 2°C higher than normal operating temperatures for a duration of 6.75 hours. With this assembly and control, the basement power consumption could entirely be shifted for the morning peak period but not shave entirely for the evening peak. By increasing the thickness of insulation to 102 mm and keeping the same air set point temperature control, this issue can be resolved. It should be noted that the reference power consumption is based on air set point temperatures of 21°C and that the performance of the system is sensitive to the selected air set point temperature.

On a general basis, total building space heating power consumption can be shaved by shifting the basement power consumption using thermal storage in the basement floor concrete slab, for buildings with a footprint of 80 to 200 m². The optimal assembly for the basement floor is composed of 102 mm of extruded polystyrene insulation followed by 152 mm of concrete. The electric heating cables are positioned at the bottom of the concrete layer. This assembly can be controlled with the air set point temperature. The basement rooms' air setpoint temperature during charging needs to be 2°C higher than the air setpoint temperature during normal operating conditions. The required charging time for building footprint of 80, 120 160 and 200 m² corresponds to 6.00, 5.51, 5.05 and 4.66 hours respectively. In all cases, the increase in energy consumption due to this system is

negligible for outdoor air temperatures of approximately -13°C but can become significant as the outdoor air temperature increases, especially for warm weather like in the spring or fall seasons.

The literature review has identified that one of the barriers to the application of peak shaving strategies is the lack of clear guidelines for its integration to buildings and that R&D applications included mostly high-rise buildings. The results of this thesis have identified design guidelines for the integration of the proposed system in a residential building, both in terms of its construction and its control. This is true for buildings sharing the same width to depth ratio as the monitored building. The system proposed within this study is based on commercially available products, which further facilitates its application.

Another key point identified by the literature review is that many R&D studies have developed building peak shave systems that are independent from the grid, managing their own loads. There needs to be an incentive to design such thermal storage systems to be able to control them in a holistic manner. The solution presented in this thesis can be used to address this. Web-enabled thermostats were used to record data and control the monitored building. These same devices could be used to implement strategies over entire neighborhoods. The control strategy developed calls for an increase of 2°C above the normal operating air set point temperature during the charging phase. The thermal storage strategy is easily applicable across a multitude of buildings because it can be applied independent of the reference air set-point temperature. This becomes a considerable advantage for utility companies that seek stability on the grid.

From an environmental standpoint, literature has pointed to the fact that thermal energy storage allows for better management of the energy use. Despite this, some materials, like concrete, require a considerable amount of energy to create and produce a large quantity of GHG gases in the process. Taking this into account, the solution presented in this thesis takes advantage of the already existing concrete used for the basement floor slab as a means of storing heat, which reduces the required additional concrete. Only an additional 51 mm of concrete would be required to shift the basement power consumption during morning and evening peak periods.

There are several limitations to the work presented that could be complemented by future works. The first aspect is to consider the use of mechanical ventilation to distribute energy stored to all storeys of the building. Only peak shifting of the basement power consumption was considered because the monitored building did not contain any central ventilation system. However, all above ground assemblies have much higher heat losses than the basement and therefore could benefit from being conditioned with stored thermal energy. Another aspect that could be further developed is the use of predictive controllers to better manage the quantity of energy stored. The presented solution was evaluated with a focus of peak shaving performance. However, this study has shown that as soon as the outdoor temperature becomes higher, there is a considerable increase in daily energy consumption. This could be resolved by taking weather forecasts into consideration to better optimize the stored thermal energy. A detailed cost analysis has not been completed for the proposed thermal storage system because only focus was directed towards evaluating its performance for a cold climate. Now that demonstrating the thermal storage system's performance with respect to demand management, an analysis of the economics of the project as a function of different utility tariffs is worth completing.

BIBLIOGRAPHY

- Akeiber, H., Nejat, P., Zaimi, M., Majid, A., Wahid, M. A., Jomehzadeh, F., ... Ahmad, S. (2016). A review on phase change material (PCM) for sustainable passive cooling in building envelopes. *Renewable and Sustainable Energy Reviews*, *60*, 1470–1497. <https://doi.org/10.1016/j.rser.2016.03.036>
- Al-Sanea, S. A., Zedan, M. F., & Al-Hussain, S. N. (2012). Effect of thermal mass on performance of insulated building walls and the concept of energy savings potential. *Applied Energy*, *89*(1), 430–442. <https://doi.org/10.1016/j.apenergy.2011.08.009>
- Alqallaf, H. J., & Alawadhi, E. M. (2013). Concrete roof with cylindrical holes containing PCM to reduce the heat gain. *Energy & Buildings*, *61*, 73–80. <https://doi.org/10.1016/j.enbuild.2013.01.041>
- Anderson, R., Christensen, C., & Renewable, N. (2006). Program design analysis using BEopt (building energy optimization) software: Defining a technology pathway leading to new homes with zero peak cooling demand. *American Council for an Energy-Efficient Economy (ACEEE)*, 2-23-2–35.
- Andresen, I., & Brandemuehl, M. J. (1992). Heat storage in building thermal mass: A parametric study. *ASHRAE Transactions*, *98*(1).
- Andrews, J. W., M., P., & Strasser, J. (1993). Laboratory testing of control strategies to reduce peak air-conditioning loads. *ASHRAE Transactions*.
- ASHRAE. (2002). *Guideline 14-2002: measurement of energy and demand savings*. Atlanta, GA.
- ASHRAE. (2005). *ASHRAE Handbook - Fundamentals*. Atlanta: American Society of Heating, Refrigerating and Air-Conditioning Engineers.
- Aste, N., Caputo, P., Buzzetti, M., & Fattore, M. (2016). Energy efficiency in buildings: What drives the investments? The case of Lombardy Region. *Sustainable Cities and Society*, *20*, 27–37. <https://doi.org/10.1016/j.scs.2015.09.003>

- Awbi, H. B., & Hatton, A. (1999). Natural convection from heated room surfaces. *Energy and Buildings*, 30(3), 233–244.
- Barnaby, C. D., Nall, D. H., & Dean, E. D. (1980). Structural mass cooling in a commercial building using hollow core concrete plank. In *Proceedings of the National Solar Conference*. Amherst, MA.
- Barton, P., Beggs, C. B., & Sleigh, P. a. (2002). A theoretical study of the thermal performance of the TermoDeck hollow core slab system. *Applied Thermal Engineering*, 22, 1485–1499. [https://doi.org/10.1016/S1359-4311\(02\)00059-5](https://doi.org/10.1016/S1359-4311(02)00059-5)
- Bastani, A., Haghghat, F., & Kozinski, J. (2015). Designing building envelope with PCM wallboards : Design tool development. *Renewable and Sustainable Energy Reviews*, 31(2014), 554–562. <https://doi.org/10.1016/j.rser.2013.12.031>
- Becker, R., & Paciuk, M. (2002). Inter-related effects of cooling strategies and building features on energy performance of office buildings. *Energy and Buildings*, 34, 25–31.
- Blocken, B., Defraeye, T., Derome, D., & Carmeliet, J. (2009). High-resolution CFD simulations for forced convective heat transfer coefficients at the facade of a low-rise building. *Building and Environment*, 44(12), 2396–2412. <https://doi.org/10.1016/j.buildenv.2009.04.004>
- Blondeau, P., Spérandio, M., & Allard, F. (1997). Night ventilation for building cooling in summer. *Solar*, 61(5), 327–335.
- Bojić, M., Cvetković, D., Marjanović, V., Blagojević, M., & Djordjević, Z. (2013). Performances of low temperature radiant heating systems. *Energy and Buildings*, 61, 233–238.
- Bojic, M., & Yik, F. (2005). Cooling energy evaluation for high-rise residential buildings in Hong Kong. *Energy and Buildings*, 37, 345–351. <https://doi.org/10.1016/j.enbuild.2004.07.003>
- Bony, J., & Citherlet, S. (2007). Numerical model and experimental validation of heat storage with phase change materials. *Energy and Buildings*, 39, 1065–1072. <https://doi.org/10.1016/j.enbuild.2006.10.017>

- Boßmann, T., Elsland, R., Klingler, A.-L., Catenazzi, G., & Jakob, M. (2015). Assessing the optimal use of electric heating systems for integrating renewable energy sources. *Energy Procedia*, 83, 130–139. <https://doi.org/10.1016/j.egypro.2015.12.203>
- Braun, J. (2003). Load control using building thermal mass. *Transactions of the ASME*, 125(August), 292. <https://doi.org/10.1115/1.1592184>
- Braun, J. E., Lawrence, T. M., Klassen, C. J., & House, J. M. (2002). Demonstration of load S shifting and peak load reduction with control of building thermal mass. In *ACEEE Buildings - Summer Study on Energy Efficiency in Buildings*.
- Braun, J. E., Montgomery, K. W., & Chaturvedi, N. (2001). Evaluating the performance of building thermal mass control strategies. *HVAC&R Research*, 7(4), 403–428.
- BS EN 1254-5. (2008). Heating and cooling surfaces embedded in floors, ceilings and walls - Determination of the thermal output.
- Building Products of Canada Corp. (2016). Enermax. Retrieved November 23, 2016, from <http://bpcan.com/en-CA/products/insulation-and-structural-boards/composite-insulation-panels/enermax-east/>
- Bushnell, J. (2004). California ' s electricity crisis : a market apart ? *Energy Policy*, 32, 1045–1052. <https://doi.org/10.1016/j.enpol.2003.11.003>
- Candanedo, J. A., Dehkordi, V. R., Saberi-derakhtenjani, A., & Athienitis, A. K. (2015). Near-optimal transition between temperature setpoints for peak load reduction in small buildings. *Energy & Buildings*, 87, 123–133. <https://doi.org/10.1016/j.enbuild.2014.11.021>
- Caves, D. W., & Christensen, L. R. (1980). Econometric analysis of residential time-of-use electricity pricing experiments. *Journal of Economics*, 14(14), 287–306.
- CEN. (2008). Water based surface embedded heating and cooling systems. European Committee for Standardization.
- Çengel, Y. A., & Ghajar, A. J. (2011). *Heat and Mass Transfer: Fundamentals & Applications* (4th ed.). New-York: McGraw Hill.

- Cetin, K. S., Manuel, L., & Novoselac, A. (2016). Effect of technology-enabled time-of-use energy pricing on thermal comfort and energy use in mechanically-conditioned residential buildings in cooling dominated climates. *Building and Environment*, *96*, 118–130. <https://doi.org/10.1016/j.buildenv.2015.11.012>
- Chae, Y. T., & Strand, R. K. (2013). Modeling ventilated slab systems using a hollow core slab : Implementation in a whole building energy simulation program &. *Energy & Buildings*, *57*, 165–175. <https://doi.org/10.1016/j.enbuild.2012.10.036>
- Chen, Y. (2014). Design and operation methodology for active building-integrated thermal energy storage systems. *Energy and Buildings*, *84*, 575–585.
- Chen, Y., Athienitis, A. K., & Galal, K. E. (2013). Frequency domain and finite difference modeling of ventilated concrete slabs and comparison with field measurements: Part 2. Application. *International Journal of Heat and Mass Transfer*, *66*, 957–966. <https://doi.org/10.1016/j.ijheatmasstransfer.2013.07.086>
- Chen, Y., Galal, K., & Athienitis, A. K. (2010). Modeling, design and thermal performance of a BIPV/T system thermally coupled with a ventilated concrete slab in a low energy solar house: Part 2, ventilated concrete slab. *Solar Energy*, *84*(11), 1908–1919. <https://doi.org/10.1016/j.solener.2010.06.012>
- Cheng, W., Xie, B., Zhang, R., Xu, Z., & Xia, Y. (2015). Effect of thermal conductivities of shape stabilized PCM on under-floor heating system. *Applied Energy*, *144*, 10–18. <https://doi.org/10.1016/j.apenergy.2015.01.055>
- Chiang, W., Wang, C., & Huang, J. (2012). Evaluation of cooling ceiling and mechanical ventilation systems on thermal comfort using CFD study in an office for subtropical region. *Building and Environment*, *48*, 113–127. <https://doi.org/10.1016/j.buildenv.2011.09.002>
- CMHC. (2010). *Canadian Wood-frame House Construction*.
- Coakley, D., Raftery, P., & Keane, M. (2014). A review of methods to match building energy simulation models to measured data. *Renewable and Sustainable Energy Reviews*, *37*, 123–141. <https://doi.org/10.1016/j.rser.2014.05.007>

- Cole, W. J., Powell, K. M., Hale, E. T., & Edgar, T. F. (2014). Reduced-order residential home modeling for model predictive control. *Energy & Buildings*, 74, 69–77. <https://doi.org/10.1016/j.enbuild.2014.01.033>
- Corgnati, S. P., & Kindinis, A. (2007). Thermal mass activation by hollow core slab coupled with night ventilation to reduce summer cooling loads. *Building and Environment*, 42(9), 3285–3297. <https://doi.org/10.1016/j.buildenv.2006.08.018>
- Croome, D. J., & Robert, B. M. (1980). *Air Conditioning and Ventilation of Buildings*. Pergamon Press, Oxford, 2.
- Cvetkovic, D., & Bojic, L. (2015). Decreasing energy use and influence to environment by radiant panel heating using different energy sources. *Applied Energy*, 138, 404–413. <https://doi.org/10.1016/j.apenergy.2014.10.063>
- Defraeye, T., Blocken, B., & Carmeliet, J. (2010). CFD analysis of convective heat transfer at the surfaces of a cube immersed in a turbulent boundary layer. *International Journal of Heat and Mass Transfer*, 53(1–3), 297–308. <https://doi.org/10.1016/j.ijheatmasstransfer.2009.09.029>
- Defraeye, T., Blocken, B., & Carmeliet, J. (2011). Convective heat transfer coefficients for exterior building surfaces: Existing correlations and CFD modelling. *Energy Conversion and Management*, 52(1), 512–522. <https://doi.org/10.1016/j.enconman.2010.07.026>
- Dodoo, A., Gustavsson, L., & Sathre, R. (2012). Effect of thermal mass on life cycle primary energy balances of a concrete- and a wood-frame building. *Applied Energy*, 92, 462–472. <https://doi.org/10.1016/j.apenergy.2011.11.017>
- Dow Building Solutions. (2017). Floormate 200.
- Ekrami, N., Kamel, R. S., & Fung, A. S. (2007). Effectiveness of a Ventilated Concrete Slab on an Air Source Heat Pump Performance in Cold Climate.
- Ekrami, N., Kamel, R. S., Garat, A., Amirirad, A., & Fung, A. S. (2015). Applications of active hollow core slabs and insulated concrete foam walls as thermal storage in cold climate residential buildings. *Energy Procedia*, 78, 459–464.

<https://doi.org/10.1016/j.egypro.2015.11.698>

- El-sawi, A., Haghghat, F., & Akbari, H. (2013). Centralized latent heat thermal energy storage system : Model development and validation. *Energy & Buildings*, *65*, 260–271. <https://doi.org/10.1016/j.enbuild.2013.05.027>
- Emmel, M. G., Abadie, M. O., & Mendes, N. (2007). New external convective heat transfer coefficient correlations for isolated low-rise buildings. *Energy and Buildings*, *39*(3), 335–342. <https://doi.org/10.1016/j.enbuild.2006.08.001>
- ENEA. (2015). *Italian Energy Efficiency Annual Report 2015 Executive Summary*.
- Entrop, A. G., Brouwers, H. J. H., & Reinders, A. H. M. E. (2011). Experimental research on the use of micro-encapsulated Phase Change Materials to store solar energy in concrete floors and to save energy in Dutch houses. *Solar Energy*, *85*(5), 1007–1020. <https://doi.org/10.1016/j.solener.2011.02.017>
- Evola, G., Marletta, L., & Sicurella, F. (2014). Simulation of a ventilated cavity to enhance the effectiveness of PCM wallboards for summer thermal comfort in buildings. *Energy & Buildings*, *70*, 480–489. <https://doi.org/10.1016/j.enbuild.2013.11.089>
- Faheem, A., Ranzi, G., Fiorito, F., & Lei, C. (2016). A numerical study on the thermal performance of night ventilated hollow core slabs cast with micro-encapsulated PCM concrete. *Energy & Buildings*, *127*, 892–906. <https://doi.org/10.1016/j.enbuild.2016.06.014>
- Fallahi, A., Haghghat, F., & Elsadi, H. (2010). Energy performance assessment of double-skin facade with thermal mass. *Energy & Buildings*, *42*(9), 1499–1509. <https://doi.org/10.1016/j.enbuild.2010.03.020>
- Feng, J. D., Bauman, F., & Schiavon, S. (2014). Experimental comparison of zone cooling load between radiant and air systems. *Energy & Buildings*, *84*, 152–159. <https://doi.org/10.1016/j.enbuild.2014.07.080>
- Feng, J. D., Schiavon, S., & Bauman, F. (2013). Cooling load differences between radiant and air systems. *Energy & Buildings*, *65*, 310–321. <https://doi.org/10.1016/j.enbuild.2013.06.009>

- Feustel, H. E., Stetiu, C., Feustel, H. E., & Stetiu, C. (1997). *Thermal Performance of Phase Change Wallboard for Residential Cooling Application Thermal Performance of Phase Change Wallboard for Residential Cooling Application*.
- Gan, G., Riffat, S. B., & Chong, C. S. A. (2007). A novel rainwater – ground source heat pump – Measurement and simulation, 27, 430–441. <https://doi.org/10.1016/j.applthermaleng.2006.07.011>
- Geros, V., Santamouris, M., Tsangrasoulis, A., & Guarracino, G. (1999). Experimental evaluation of night ventilation phenomena. *Energy and Buildings*, 29, 141–154.
- Ghali, K. (2007). Economic viability of under floor heating system: A case study in Beirut climate. In *International Conference on Renewable Energies & Power Quality*. Sevilla, Spain.
- Gracia, A. De, Navarro, L., Castell, A., Ruiz-pardo, Á., Álvarez, S., & Cabeza, L. F. (2013). Experimental study of a ventilated facade with PCM during winter period. *Energy & Buildings*, 58, 324–332. <https://doi.org/10.1016/j.enbuild.2012.10.026>
- Gwerder, M., Lehmann, B., Tödtli, J., Dorer, V., & Renggli, F. (2008). Control of thermally-activated building systems (TABS). *Applied Energy*, 85(7), 565–581.
- Haghighat, F., Inard, C., Bastani, A., Stathopoulos, N., El Mankibi, M., & Moreau, A. (2013). *Applying Energy Storage in Building of the Future Best Practice for Architects and Engineers Edited*.
- Hajiah, A., & Krarti, M. (2012a). Optimal control of building storage systems using both ice storage and thermal mass – Part I: Simulation environment. *Energy Conversion and Management*, 64, 499–508.
- Hajiah, A., & Krarti, M. (2012b). Optimal controls of building storage systems using both ice storage and thermal mass – Part II: Parametric analysis. *Energy Conversion and Management*, 64, 509–515.
- Hamada, Y., & Fukai, J. (2005). Latent heat thermal energy storage tanks for space heating of buildings : Comparison between calculations and experiments. *Energy Conversion and Management*, 46, 3221–3235. <https://doi.org/10.1016/j.enconman.2005.03.009>

- Hao, X., Zhang, G., Chen, Y., Zou, S., & Moschandreas, D. J. (2007). A combined system of chilled ceiling , displacement ventilation and desiccant dehumidification. *Building and Environment*, *42*, 3298–3308. <https://doi.org/10.1016/j.buildenv.2006.08.020>
- Henze, G. P., Brandemuehl, M. J., Florita, A. R., Felsmann, C., & Cheng, H. (2010). Advances in near-optimal control of passive building thermal storage. *Journal of Solar Energy Engineering*, *132*(021009).
- Henze, G. P., Felsmann, C., Florita, A. R., Brandemuehl, M. J., Cheng, H., & Waters, C. E. (2008). Optimization of building thermal mass control in the presence of energy and demand charges. *ASHRAE Transactions*, *114*(2), 75–84.
- Henze, G. P., Felsmann, C., Kalz, D. E., & Herkel, S. (2008). Primary energy and comfort performance of ventilation assisted thermo-active building systems in continental climates. *Energy and Buildings*, *40*, 99–111. <https://doi.org/10.1016/j.enbuild.2007.01.014>
- Henze, G. P., Felsmann, C., & Knabe, G. (2004). Evaluation of optimal control for active and passive building thermal storage. *International Journal of Thermal Sciences*, *43*, 173–183. <https://doi.org/10.1016/j.ijthermalsci.2003.06.001>
- Henze, G. P., Zhou, G., & Krarti, M. (2005). Parametric analysis of active and passive building thermal storage utilization. *Journal of Solar Energy Engineering*, *127*, 37–46. <https://doi.org/10.1115/1.1824110>
- Herter, K. (2014). *SMUD 's Residential Summer Solutions Study*. Sacramento, California.
- Hutcheon, N. B., & Handegord, G. O. (1983). *Building Science for a Cold Climate*. Toronto: John Wiley & Sons.
- Imanari, T., Omori, T., & Bogaki, K. (1999). Thermal comfort and energy consumption of the radiant ceiling panel system . Comparison with the conventional all-air system. *Energy and Buildings*, *30*, 167–175.
- Ismail, K. A. R., & Henriquez, J. R. (2001). Thermally effective windows with moving phase change material curtains. *Applied Thermal Engineering*, *21*, 1909–1923.

- ISO. (2012). ISO-11855: Building environment design - Design, dimensioning, installation and control of embedded radiant heating and cooling systems. International Organization for Standardization.
- Jeong, J., Mumma, S. A., & Bahnfleth, W. P. (2003). Energy conservation benefits of a dedicated outdoor air system with parallel sensible cooling by ceiling radiant panels. *ASHRAE Transactions*, *109*(2), 627–636.
- Jiao, F., & Xu, P. (2015). Simulation and feasibility analysis of PCM based passive cooling technique in residential house. *Procedia Engineering*, *121*, 1969–1976. <https://doi.org/10.1016/j.proeng.2015.09.189>
- Kalz, D. E., Wienold, J., Fischer, M., & Cali, D. (2010). Novel heating and cooling concept employing rainwater cisterns and thermo-active building systems for a residential building. *Applied Energy*, *87*(2), 650–660. <https://doi.org/10.1016/j.apenergy.2009.06.002>
- Kattan, P., Ghali, K., & Al-Hindi, M. (2012). Modeling of under-floor heating systems: A compromise between accuracy and complexity. *HVAC and R Research*, *18*(February 2015), 468–480. <https://doi.org/10.1080/10789669.2012.649881>
- Keeney, K. R., & Braun, J. E. (1997). Application of building precooling to reduce peak cooling requirements. *ASHRAE*, *103*(1), 463–469.
- Kenizarin, M., & Mahkamov, K. (2016). Passive thermal control in residential buildings using phase change materials. *Renewable and Sustainable Energy Reviews*, *55*, 371–398. <https://doi.org/10.1016/j.rser.2015.10.128>
- Kim, K. W., & Olesen, B. W. (2008). Radiant heating and cooling systems. *US Patent 8,256,690*, (March). Retrieved from <http://www.google.com/patents/US8256690>
- Kintner-Meyer, M., & Emery, A. F. (1995). Optimal control of an HVAC system using cold storage and building thermal capacitance. *Energy and Buildings*, *23*, 19–31.
- Kintner-Meyer, M., Subbarao, K., Prakash, K. N., Bandyopadhyay, G., Finley, C., Koritarov, V. S., ... Florita, A. R. (2010). *The Role of Energy Storage in Commercial Building A Preliminary Report*.

- Klein, S. A., Duffie, J. A., Mitchell, J. C., Kummer, J. P., Thornton, J. W., Bradley, D. E., ... Kummert, M. (2014). *TRNSYS 17 Volume 4: Mathematical Reference*.
- Kolokotroni, M., & Aronis, A. (1999). Cooling-energy reduction in air-conditioned offices by using night ventilation. *Applied Energy*, *63*, 241–253.
- Koschenz, M., & Dorer, V. (1999). Interaction of an air system with concrete core conditioning. *Energy and Buildings*, *30*(October 1996), 139–145. [https://doi.org/10.1016/S0378-7788\(98\)00081-4](https://doi.org/10.1016/S0378-7788(98)00081-4)
- Krarti, M., Brandemuehl, M. J., & Henze, G. P. (1995). *Final Project Report for ASHRAE 809-RP: Evaluation of Optimal Control for Ice Storage Systems"*.
- Krarti, M., Henze, G. P., & Bell, D. (1999). Planning horizon for a predictive optimal controller for thermal energy storage systems. *ASHRAE Transactions*, *105*(1).
- Krarti, M., Henze, G. P., & Dodier, R. H. (1997). Development of a predictive optimal controller for thermal energy storage systems. *HVAC&R Research*, *3*(3), 233–264.
- Kylili, A., & Fokaides, P. A. (2015). European smart cities: The role of zero energy buildings. *Sustainable Cities and Society*, *15*, 86–95. <https://doi.org/10.1016/j.scs.2014.12.003>
- Lanoue, R. (2014). *Maîtriser notre avenir énergétique*.
- Lee, K. H., & Braun, J. E. (2006). An experimental evaluation of demand limiting using building thermal mass in a small commercial building. *ASHRAE Transactions*, *112*(21), 558–571.
- Lee, K. H., & Braun, J. E. (2008). A data-driven method for determining zone temperature trajectories that minimize peak electrical demand. *ASHRAE Transactions*, *114*(2), 65–74.
- Lehmann, B., Dorer, V., & Koschenz, M. (2007). Application range of thermally activated building systems tabs. *Energy and Buildings*, *39*(5), 593–598. <https://doi.org/10.1016/j.enbuild.2006.09.009>
- Li, A., Xu, X., & Gao, J. (2014). Analysis of frequency thermal characteristics of pipe-

embedded concrete radiant floors based on FDFD method. *Energy Procedia*, 61(0), 1339–1342. <https://doi.org/http://dx.doi.org/10.1016/j.egypro.2014.12.122>

Li, J., Xue, P., He, H., Ding, W., & Han, J. (2009). Preparation and application effects of a novel form-stable phase change material as the thermal storage layer of an electric floor heating system. *Energy and Buildings*, 41(8), 871–880.

Liu, S., & Henze, G. P. (2004). Impact of modeling accuracy on predictive optimal control of active and passive building thermal storage inventory. *ASHRAE Transactions*, 4683.

Liu, S., & Henze, G. P. (2004). Investigation of reinforcement learning for building thermal mass control. In *IBPSA-USA National Conference Boulder* (pp. 1–11).

Liu, S., & Henze, G. P. (2006). Experimental analysis of simulated reinforcement learning control for active and passive building thermal storage inventory Part 1 . Theoretical foundation. *Energy and Buildings*, 38, 142–147. <https://doi.org/10.1016/j.enbuild.2005.06.002>

Liu, Y., & Harris, D. J. (2007). Full-scale measurements of convective coefficient on external surface of a low-rise building in sheltered conditions. *Building and Environment*, 42(7), 2718–2736. <https://doi.org/10.1016/j.buildenv.2006.07.013>

Liu, Y., Wang, D., & Liu, J. (2012). Study on heat transfer process for in-slab heating floor. *Building and Environment*, 54, 77–85. <https://doi.org/10.1016/j.buildenv.2012.02.007>

Lyon, E. G., & Saldanha, C. M. (2016). Integrating whole building air leakage test data into EnergyPlus infiltration models. In *Building performance Modeling Conference* (pp. 393–398). Salt Lake City, UT: ASHRAE and IBPSA-USA.

Ma, J., Qin, J., Salsbury, T., & Xu, P. (2012). Demand reduction in building energy systems based on economic model predictive control. *Chemical Engineering Science*, 67(1), 92–100. <https://doi.org/10.1016/j.ces.2011.07.052>

Ma, P., Wang, L.-S., & Guo, N. (2013). Modeling of TABS-based thermally manageable buildings in Simulink. *Applied Energy*, 104, 791–800.

<https://doi.org/10.1016/j.apenergy.2012.12.006>

- Ma, P., Wang, L.-S., & Guo, N. (2015). Energy storage and heat extraction – From thermally activated building systems (TABS) to thermally homeostatic buildings. *Renewable and Sustainable Energy Reviews*, 45, 677–685. <https://doi.org/10.1016/j.rser.2015.02.017>
- Ma, Y., Borrelli, F., Hancey, B., Coffey, B., Bengea, S., & Haves, P. (2012). Model predictive control for the operation of building cooling systems. *IEEE Transactions on Control Systems Technology*, 20(3), 796–803.
- Macgregor, R. K., & Emery, A. F. (1969). Free convection through vertical plane layers - Moderate and high Prandtl number fluids. *ASME Journal of Heat Transfer*, 91, 391–401.
- Mahajan, S., Newcomb, C., Bluck, S., & Ehteshamzadeh, R. (1993). *Optimizing the Use of Energy Management and Control Systems to Reduce Peak Load and Energy Consumption in Non-residential Buildings*.
- Min, T. C., Schutrum, L. F., Parmelee, G. V., & Vouris, J. D. (1956). Natural Convection and Radiation in a Panel-Heated Room. *ASHRAE Transactions*, 62(1), 337–358.
- Montazeri, H., Blocken, B., Derome, D., Carmeliet, J., & Hensen, J. L. M. (2015). CFD analysis of forced convective heat transfer coefficients at windward building facades: Influence of building geometry. *Journal of Wind Engineering and Industrial Aerodynamics*, 146, 102–116. <https://doi.org/10.1016/j.jweia.2015.07.007>
- Moore, T. (2008). Potential and limitations for hydronic radiant slabs using waterside free cooling and dedicated outside air systems. In *Third National Conference of IBPSA-USA* (pp. 148–155). Berkeley, California.
- Morris, F. B., Braun, J. E., & Treado, S. J. (1994). Experimental and simulated performance of optimal control of building thermal storage. *ASHRAE Transactions*, 100(1), 403–414.
- Mumma, S. A. (2002). Chilled ceilings in parallel with dedicated outdoor air systems : Addressing the concerns of condensation , capacity , and cost. *ASHRAE Transactions*,

108(2), 120–231.

Natural Resources Canada. (2011). Energy efficiency trends in Canada: 1990 to 2009, (December).

Natural Resources Canada. (2017). Residential housing stock and floor space. Retrieved from <http://oee.nrcan.gc.ca/corporate/statistics/neud/dpa/showTable.cfm?type=HB§or=res&juris=00&rn=11&page=0>

Navarro, L., Gracia, A. De, Castell, A., & Cabeza, L. F. (2016). Experimental evaluation of a concrete core slab with phase change materials for cooling purposes. *Energy & Buildings*, 116, 411–419. <https://doi.org/10.1016/j.enbuild.2016.01.026>

NBCC. (2005). National Building Code of Canada.

Nchelatebe, D., Vouillamoz, P., Haghghat, F., El-mankibi, M., Moreau, A., & Daoud, A. (2014). Impact of phase change materials types and positioning on hot water tank thermal performance : Using measured water demand profile. *Applied Thermal Engineering*, 67(1–2), 460–468. <https://doi.org/10.1016/j.applthermaleng.2014.03.051>

Nchelatebe, D., Vouillamoz, P., Haghghat, F., El, M., Moreau, A., & Desai, K. (2014). Phase change materials in hot water tank for shifting peak power demand. *Solar Energy*, 107, 628–635. <https://doi.org/10.1016/j.solener.2014.05.034>

Nemry, F., Uihlein, A., Colodel, C. M., Wetzal, C., Braune, A., Wittstock, B., ... Frech, Y. (2010). Options to reduce the environmental impacts of residential buildings in the European Union—Potential and costs. *Energy and Buildings*, 42(7), 976–984. <https://doi.org/10.1016/j.enbuild.2010.01.009>

Nghiem, T. X. (2011). *Green Scheduling of Control Systems for Peak Demand Reduction*. University of Pennsylvania.

Niu, J. L., Zhang, L. Z., & Zuo, H. G. (2002). Energy savings potential of chilled-ceiling combined with desiccant cooling in hot and humid climates. *Energy and Buildings*,

34, 487–495.

- Noguchi, M., Athienitis, A. K., Delisle, V., Ayoub, J., & Berneche, B. (2008). Net-zero energy homes of the future: A case study of the ÉcoTerra house in Canada. *Renewable Energy*, (Fig 1), 877–882. Retrieved from http://cetc-ctec.nrcan-nrcan.gc.ca/fichier.php/codectec/En/2008-112/2008-112_OP-J_411-PVTZEH_EcoTerra.pdf
- Odyjas, A., & Górká, A. (2013). Simulations of floor cooling system capacity. *Applied Thermal Engineering*, 51(1–2), 84–90. <https://doi.org/10.1016/j.applthermaleng.2012.08.029>
- Olesen, B. W. (2001). Cooling and heating of buildings by activating their thermal mass with embedded hydronic pipe systems. *Ashrae-Cibse Dublin*, 19.
- Olesen, B. W. (2012). Thermo active building systems: Using building mass to heat and cool. *ASHRAE Journal*, 54(2), 44–52.
- Olesen, B. W., & Pittarello, E. (2007). The cooling capacity of the Thermo Active Building System combined with acoustic ceiling. *Iristor.Vub.Ac.Be*, 1–8. Retrieved from <ftp://iristor.vub.ac.be/patio/ARCH/pub/fdescamp/bruface/literature/tabs/TabsWithAcousticCeiling.pdf>
- Olsen, P. K., Lambertsen, H., Hummelshøj, R., Bøhm, B., Christiansen, C. H., Svendsen, S., ... Worm, J. (2008). A new low-temperature district heating system for low-energy buildings. *Proc. of the 11th International Symposium on District Heating and Cooling*, 1–8.
- Park, B., & Krarti, M. (2015). Development of a simulation analysis environment for ventilated slab systems. *Applied Thermal Engineering*, 87, 66–78. <https://doi.org/10.1016/j.applthermaleng.2015.04.065>
- Park, S. H., Chung, W. J., Yeo, M. S., & Kim, K. W. (2014). Evaluation of the thermal performance of a Thermally Activated Building System (TABS) according to the thermal load in a residential building. *Energy and Buildings*, 73, 69–82. <https://doi.org/10.1016/j.enbuild.2014.01.008>

- Patania, F., Gagliano, A., Nocera, F., Ferlito, A., & Galesi, A. (2010). Thermofluid-dynamic analysis of ventilated facades. *Energy and Buildings*, *42*(7), 1148–1155. <https://doi.org/10.1016/j.enbuild.2010.02.006>
- Patteeuw, D., Bruninx, K., Arteconi, A., Delarue, E., D'haeseleer, W., & Helsen, L. (2015). Integrated modeling of active demand response with electric heating systems coupled to thermal energy storage systems. *Applied Energy*, *151*, 306–319. <https://doi.org/10.1016/j.apenergy.2015.04.014>
- Peippo, K., Kauranen, P., & Lund, P. D. (1991). A multicomponent PCM wall optimized for passive solar heating. *Energy and Buildings*, *17*, 259–270.
- Prívará, S., Široký, J., Ferkl, L., & Cigler, J. (2011). Model predictive control of a building heating system: The first experience. *Energy and Buildings*, *43*(2–3), 564–572.
- Québec, T. É. (2017). Novoclimat 2.0. Retrieved June 18, 2017, from <http://www.transitionenergetique.gouv.qc.ca/clientele-affaires/construction-residentielle/novoclimat-20/#.WUaQTGjys2w>
- Rabl, A., & Norford, L. K. (1991). Peak load reduction by preconditioning buildings at night. *International Journal of Energy Resources*, *15*, 781–798.
- Raithby, G. D., & Hollands, K. G. T. (1975). A general method of obtaining approximate solutions to laminar and turbulent free convection problems. *Advances in Heat Transfer*, *11*, 265–315. [https://doi.org/10.1016/S0065-2717\(08\)70076-5](https://doi.org/10.1016/S0065-2717(08)70076-5)
- Ren, M. J., & Wright, J. a. (1998). Slab thermal storage system. *Building and Environment*, *1323*(97), 43–52.
- Reynders, G., Nuytten, T., & Saelens, D. (2013). Potential of structural thermal mass for demand-side management in dwellings. *Building and Environment*, *64*, 187–199. <https://doi.org/10.1016/j.buildenv.2013.03.010>
- Rhee, K.-N., & Kim, K. W. (2015). A 50 year review of basic and applied research in radiant heating and cooling systems for the built environment. *Building and Environment*, *91*, 166–190. <https://doi.org/10.1016/j.buildenv.2015.03.040>

- Rijksen, D. O., Wisse, C. J., & Schijndel, A. W. M. Van. (2010). Reducing peak requirements for cooling by using thermally activated building systems. *Energy and Buildings*, *42*, 298–304. <https://doi.org/10.1016/j.enbuild.2009.09.007>
- Roucoul, J. M., Douzane, O., & Langlet, T. (1999). Incorporation of thermal inertia in the aim of installing a natural nighttime ventilation system in buildings. *Energy and Buildings*, *29*(2), 129–133.
- Ruddell, B. L., Salamanca, F., & Mahalov, A. (2014). Reducing a semiarid city's peak electrical demand using distributed cold thermal energy storage. *Applied Energy*, *134*, 35–44. <https://doi.org/10.1016/j.apenergy.2014.07.096>
- Ruparathna, R., Hewage, K., & Sadiq, R. (2016). Improving the energy efficiency of the existing building stock: A critical review of commercial and institutional buildings. *Renewable and Sustainable Energy Reviews*, *53*, 1032–1045. <https://doi.org/10.1016/j.rser.2015.09.084>
- Russell, M. B., & Surendran, P. N. (2001). Influence of active heat sinks on fabric thermal storage in building mass. *Applied Energy*, *70*, 17–33.
- Ruud, M. D., Mitchell, J. W., & Klein, S. A. (1990). Use of building thermal mass to offset cooling loads. *ASHRAE Transactions*, *96*(2), 820–829.
- Saelens, D., Parys, W., & Baetens, R. (2011). Energy and comfort performance of thermally activated building systems including occupant behavior. *Building and Environment*, *46*(4), 835–848. <https://doi.org/10.1016/j.buildenv.2010.10.012>
- Shao, S., Shi, W., Li, X., & Ma, J. (2004). A new inverter heat pump operated all year round with domestic hot water. *Energy Conversion and Management*, *45*, 2255–2268. <https://doi.org/10.1016/j.enconman.2003.10.013>
- Sharples, S. (1984). Full-scale measurements of convective energy losses from exterior building surfaces. *Building and Environment*, *19*(1), 31–39. [https://doi.org/10.1016/0360-1323\(84\)90011-8](https://doi.org/10.1016/0360-1323(84)90011-8)
- Shaw, C. Y. (1980). Wind and temperature induced pressure differentials and an equivalent pressure difference model for predicting air infiltration in schools. *ASHRAE*

Transactions, 86(1), 268–279.

Shaw, M. R., Treadaway, K. W., & Willis, S. T. P. (1994). Effective use of building mass. *Renewable Energy*, 5, 1028–1034.

Sheetrock, U. (2017). USG Sheetrock Brand Ultralight Panel.

Shin, M. S., Rhee, K. N., Ryu, S. R., Yeo, M. S., & Kim, K. W. (2015). *Design of radiant floor heating panel in view of floor surface temperatures*. *Building and Environment*. Elsevier Ltd. <https://doi.org/10.1016/j.buildenv.2015.05.006>

Springer, D., & Spiegel, L. (2013). *Final Project Report Smud Off - Peak Over - Cooling Project*. Davis, California.

Stetiu, C. (1999). Energy and peak power savings potential of radiant cooling systems in US commercial buildings. *Energy and Buildings*, 30, 127–138.

Stetiu, C., & Feustel, H. E. (1996). Phase change wallboard as an alternative to compressor cooling in californian residences? In *ACEE Summer Study for Energy Efficient Building*. California, USA.

Stovall, T. K., & Tomlinson, J. J. (1995). What are the potential benefits of including latent storage in common wallboard? *Journal of Solar Engineering*, 117(4), 318–325.

Stritih, U., & Butala, V. (2010). Experimental investigation of energy saving in buildings with PCM cold storage. *International Journal of Refrigeration*, 33(8), 1676–1683. <https://doi.org/10.1016/j.ijrefrig.2010.07.017>

Tenwolde, A., & Carll, C. (1992). Effect of cavity ventilation on moisture in walls and roofs. In *Thermal Performance of the Exterior Envelope of Buildings* (pp. 555–562). Clearwater Beach, Florida: American Society of Heating, Refrigerating and Air-Conditioning Engineers.

TermoDeck. (2016). Home. Retrieved from <http://www.termodeck.com/termodeck.html>

Thieblemont, H., Haghghat, F., & Moreau, A. (2016). Thermal Energy Storage for Building Load Management: Application to Electrically Heated Floor. *Applied Sciences*, 6(7), 194. <https://doi.org/10.3390/app6070194>

- Thieblemont, H., Haghghat, F., Moreau, A., Bastani, A., & Kuznik, F. (2016). Alternative method to integrate electrically heated floor in TRNSYS: Load management. In *CLIMA 2016 - proceedings of the 12th REHVA World Congress*.
- Tian, Z., & Love, J. A. (2009). Application of radiant cooling in defferent climates: Assessment of office buildings through simulations. In *Eleventh International IBPSA Conference* (pp. 2220–2227). Glasgow, Scotland.
- Tomlinson, J. J., & Heberle, D. O. (1990). Analysis of wallboard containing a phase change material. In *Energy Conversion Engineering Conference*.
- Turner, W. J. N., Walker, I. S., & Roux, J. (2015). Peak load reductions: Electric load shifting with mechanical pre-cooling of residential buildings with low thermal mass. *Energy*, 82, 1057–1067. <https://doi.org/10.1016/j.energy.2015.02.011>
- U.S. Energy Information Administration. (2009). Residential Energy Consumption Survey (RECS). Retrieved December 31, 2015, from <http://www.eia.gov/consumption/residential/data/2009/?src=Consumption> Residential Energy Consumption Survey (RECS)-b3
- Upshaw, C. R., Rhodes, J. D., & Webber, M. E. (2015). Modeling peak load reduction and energy consumption enabled by an integrated thermal energy and water storage system for residential air conditioning systems in Austin, Texas. *Energy and Buildings*, 97(0), 21–32. <https://doi.org/http://dx.doi.org/10.1016/j.enbuild.2015.03.050>
- Walker, I. S., Degenetais, G., & Seigel, J. A. (2002). *Simulations of sizing and comfort improvements for residential forced-air heating and cooling systems*. Berkeley, California.
- West, J., & Braun, J. E. (1999). Modeling partial charging and discharging of area-constrained ice storage tanks. *HVAC&R Research*, 5(3), 209–228.
- Woo, C. (2001). What went wrong in California ' s electricity market ? *Energy*, 26, 747–758.
- Woo, C., Lloyd, D., & Tishler, A. (2003). Electricity market reform failures : UK , Norway

- , Alberta and California. *Energy Policy*, 31, 1103–1115.
- Xie, J., Xu, X., Li, A., & Zhu, Q. (2015). Experimental validation of frequency-domain finite-difference model of active pipe-embedded building envelope in time domain by using Fourier series analysis. *Energy and Buildings*, 99, 177–188. <https://doi.org/10.1016/j.enbuild.2015.04.043>
- Xu, P., Haves, P., Piette, M. A., & Berkeley, L. (2004). Peak demand reduction from pre-cooling with zone temperature reset in an office building. In *ACEEE Summer Study on Energy Efficiency in Buildings* (pp. 376–386).
- Xu, X., Zhang, Y., Lin, K., Di, H., & Yang, R. (2005). Modeling and simulation on the thermal performance of shape-stabilized phase change material floor used in passive solar buildings, 37, 1084–1091. <https://doi.org/10.1016/j.enbuild.2004.12.016>
- Yanbing, K., Yi, J., & Yinping, Z. (2003). Modeling and experimental study on an innovative passive cooling system — NVP system. *Energy and Buildings*, 35, 417–425.
- Yazdanian, M., & Klems, J. H. (1993). Measurement of the exterior convective film coefficient for windows in low-rise buildings. *ASHRAE Transactions*, 100.
- Yin, R., Black, D., Piette, M. A., & Schiess, K. (2015). *Control of Thermal Energy Storage in Commercial Buildings for California Utility Tariffs and Demand Response*.
- Yin, R., Xu, P., Piette, M. A., & Kiliccote, S. (2010). Study on Auto-DR and pre-cooling of commercial buildings with thermal mass in California. *Energy and Buildings*, 42(7), 967–975. <https://doi.org/10.1016/j.enbuild.2010.01.008>
- Yu, J., Yang, J., & Xiong, C. (2015). Study of dynamic thermal performance of hollow block ventilated wall. *Renewable Energy*, 84, 145–151. <https://doi.org/10.1016/j.renene.2015.07.020>
- Yu, Z. (Jerry), Huang, G., Haghghat, F., Li, H., & Zhang, G. (2015). Control strategies for integration of thermal energy storage into buildings: State-of-the-art review. *Energy and Buildings*, 106, 203–215.

- Zakula, T., Armstrong, P., & Norford, L. K. (2015). Advanced cooling technology with thermally activated building surfaces and model predictive control. *Energy & Buildings*, *86*, 640–650. <https://doi.org/10.1016/j.enbuild.2014.10.054>
- Zakula, T., Armstrong, P. R., & Norford, L. K. (2014). Modeling environment for model predictive control of buildings. *Energy & Buildings*, *85*, 549–559. <https://doi.org/10.1016/j.enbuild.2014.09.039>
- Zhang, L., Liu, X.-H., & Jiang, Y. (2012). Simplified calculation for cooling/heating capacity, surface temperature distribution of radiant floor. *Energy and Buildings*, *55*, 397–404. <https://doi.org/10.1016/j.enbuild.2012.08.026>
- Zhu, Q., Xu, X., Wang, J., & Xiao, F. (2014). Development of dynamic simplified thermal models of active pipe-embedded building envelopes using genetic algorithm. *International Journal of Thermal Sciences*, *76*, 258–272. <https://doi.org/10.1016/j.ijthermalsci.2013.09.008>
- Zmeureanu, R., & Fazio, P. (1988). Thermal performance of a hollow core concrete floor system for passive cooling. *Building and Environment*, *23*(3), 243–252.

APPENDIX A – Optimal System Configuration Selection

This appendix presents the results of the simulation to obtain the optimal system configuration as a function of building size. For all tables, the optimal configuration is highlighted by a yellow box.

A.1 Building with an 80 m² Footprint

Table 14 : Charging Depth and Charging Time Required as a Function of Air Setpoint Temperature during Charging, Insulation Thickness and Concrete Thickness for an 80 m² Building

Air Setpoint Temperature During Charing Period (°C)	Insulation Thickness (m)	Charge Depth Achieved			Time Required to Charge (hr)		
		Concrete Thickness (m)					
		0.102	0.152	0.203	0.102	0.152	0.203
22	0.051	100%	100%	100%	3.49	4.58	6.28
	0.102	100%	100%	100%	2.71	3.87	5.42
22.5	0.051	100%	100%	88%	4.29	5.98	8+
	0.102	100%	100%	99%	3.34	4.91	8+
23	0.051	99%	94%	75%	5.70	8+	8+
	0.102	100%	100%	100%	4.26	6.00	6.71
23.5	0.051	97%	83%	65%	6.64	8+	8+
	0.102	100%	100%	90%	5.40	7.40	8+
24	0.051	92%	72%	54%	8+	8+	8+
	0.102	100%	92%	82%	7.73	8+	8+

Table 15 : Discharge Time and Maximum Air Temperature as a Function of Air Setpoint Temperature during Charging, Insulation Thickness and Concrete Thickness for an 80 m² Building

Air Setpoint Temperature During Charing Period (°C)	Insulation Thickness (m)	Discharge Time Achieved (hr)			Maximum Air Temperature (°C)		
		Concrete Thickness (m)					
		0.102	0.152	0.203	0.102	0.152	0.203
22	0.051	3.75	6.99	10.18	22.15	22.17	22.18
	0.102	6.71	10.51	13.14	22.39	22.33	22.32
22.5	0.051	5.81	10.09	13.05	22.63	22.61	22.58
	0.102	9.47	12.84	16+	22.84	22.79	22.74
23	0.051	8.25	12.04	16+	23.06	22.99	22.88
	0.102	11.05	16+	16+	23.26	23.18	23.15
23.5	0.051	9.98	13.70	16+	23.46	23.30	23.07
	0.102	12.58	16+	16+	23.67	23.57	23.53
24	0.051	11.14	14.44	16+	23.80	23.47	23.08
	0.102	14.07	16+	16+	24.06	23.94	23.83

A.2 Building with a 120 m² Footprint

Table 16 : Charing Depth and Charging Time Required as a Function of Air Setpoint Temperature during Charging, Insulation Thickness and Concrete Thickness for a 120 m² Building

Air Setpoint Temperature During Charing Period (°C)	Insulation Thickness (m)	Charge Depth Achieved			Time Required to Charge (hr)		
		Concrete Thickness (m)					
		0.102	0.152	0.203	0.102	0.152	0.203
22	0.051	100%	100%	100%	3.06	4.29	6.03
	0.102	100%	100%	100%	2.81	3.81	5.57
22.5	0.051	100%	100%	100%	3.74	5.55	7.58
	0.102	100%	100%	100%	3.18	4.81	6.46
23	0.051	100%	100%	93%	4.76	7.06	8+
	0.102	100%	100%	100%	4.02	5.51	7.02
23.5	0.051	100%	97%	86%	6.19	8+	8+
	0.102	100%	100%	100%	5.03	6.32	7.43
24	0.051	100%	90%	79%	7.59	8+	8+
	0.102	100%	100%	96%	5.97	7.07	8+

Table 17 : Discharge Time and Maximum Air Temperature as a Function of Air Setpoint Temperature during Charging, Insulation Thickness and Concrete Thickness for a 120 m² Building

Air Setpoint Temperature During Charing Period (°C)	Insulation Thickness (m)	Discharge Time Achieved (hr)			Maximum Air Temperature (°C)		
		Concrete Thickness (m)					
		0.102	0.152	0.203	0.102	0.152	0.203
22	0.051	4.59	7.77	11.06	22.35	22.32	22.33
	0.102	7.02	11.19	14.25	22.51	22.48	22.44
22.5	0.051	6.92	10.91	14.34	22.81	22.79	22.75
	0.102	9.88	14.05	16+	22.94	22.96	22.87
23	0.051	9.14	13.02	16+	23.24	23.18	23.13
	0.102	11.41	16+	16+	23.38	23.39	23.32
23.5	0.051	10.71	14.89	16+	23.66	23.55	23.48
	0.102	13.32	16+	16+	23.83	23.80	23.73
24	0.051	11.94	15.82	16+	24.06	23.91	23.78
	0.102	15.39	16+	16+	24.25	24.20	24.12

A.3 Building with a 160 m² Footprint

Table 18 : Charging Depth and Charging Time Required as a Function of Air Setpoint Temperature during Charging, Insulation Thickness and Concrete Thickness for a 160 m² Building

Air Setpoint Temperature During Charing Period (°C)	Insulation Thickness (m)	Charge Depth Achieved			Time Required to Charge (hr)		
		Concrete Thickness (m)					
		0.102	0.152	0.203	0.102	0.152	0.203
22	0.051	100%	100%	100%	2.94	3.84	5.44
	0.102	100%	100%	100%	2.56	3.50	5.37
22.5	0.051	100%	100%	100%	3.26	5.00	6.99
	0.102	100%	100%	100%	2.96	4.36	6.06
23	0.051	100%	100%	98%	4.26	6.50	8+
	0.102	100%	100%	100%	3.70	5.05	6.56
23.5	0.051	100%	100%	93%	5.35	7.66	8+
	0.102	100%	100%	99%	4.62	5.65	6.87
24	0.051	100%	96%	86%	6.77	8+	8+
	0.102	100%	100%	97%	5.35	6.40	8+

Table 19 : Discharge Time and Maximum Air Temperature as a Function of Air Setpoint Temperature during Charging, Insulation Thickness and Concrete Thickness for a 160 m² Building

Air Setpoint Temperature During Charing Period (°C)	Insulation Thickness (m)	Discharge Time Achieved (hr)			Maximum Air Temperature (°C)		
		Concrete Thickness (m)					
		0.102	0.152	0.203	0.102	0.152	0.203
22	0.051	4.82	8.27	11.47	22.40	22.38	22.39
	0.102	6.95	11.31	14.84	22.53	22.52	22.47
22.5	0.051	7.10	11.09	14.86	22.87	22.86	22.82
	0.102	10.11	14.39	16+	22.98	23.00	22.93
23	0.051	9.26	13.52	16+	23.30	23.27	23.21
	0.102	11.65	16+	16+	23.41	23.44	23.37
23.5	0.051	10.89	15.26	16+	23.73	23.64	23.58
	0.102	13.43	16+	16+	23.86	23.87	23.80
24	0.051	12.33	15.99	16+	24.14	24.02	23.91
	0.102	15.67	16+	16+	24.30	24.29	24.22

A.4 Building with a 200 m² Footprint

Table 20 : Charing Depth and Charging Time Required as a Function of Air Setpoint Temperature during Charging, Insulation Thickness and Concrete Thickness for a 200 m² Building

Air Setpoint Temperature During Charing Period (°C)	Insulation Thickness (m)	Charge Depth Achieved			Time Required to Charge (hr)		
		Concrete Thickness (m)					
		0.102	0.152	0.203	0.102	0.152	0.203
22	0.051	100%	100%	100%	2.68	3.69	5.34
	0.102	100%	100%	100%	2.43	3.28	5.06
22.5	0.051	100%	100%	100%	3.12	4.62	6.44
	0.102	100%	100%	100%	2.72	4.16	5.62
23	0.051	100%	100%	100%	4.03	6.00	7.35
	0.102	100%	100%	100%	3.45	4.66	6.18
23.5	0.051	100%	100%	97%	5.05	7.00	8+
	0.102	100%	100%	99%	4.17	5.14	6.62
24	0.051	100%	99%	92%	6.13	8+	8+
	0.102	100%	100%	98%	4.81	5.70	8+

Table 21 : Discharge Time and Maximum Air Temperature as a Function of Air Setpoint Temperature during Charging, Insulation Thickness and Concrete Thickness for a 200 m² Building

Air Setpoint Temperature During Charing Period (°C)	Insulation Thickness (m)	Discharge Time Achieved (hr)			Maximum Air Temperature (°C)		
		Concrete Thickness (m)					
		0.102	0.152	0.203	0.102	0.152	0.203
22	0.051	4.88	9.18	12.11	22.45	22.43	22.43
	0.102	6.81	11.43	15.05	22.55	22.57	22.51
22.5	0.051	7.27	11.23	15.04	22.90	22.90	22.88
	0.102	10.35	14.35	16+	23.02	23.05	22.98
23	0.051	9.57	13.61	16+	23.33	23.32	23.28
	0.102	11.90	16+	16+	23.47	23.49	23.42
23.5	0.051	10.86	15.48	16+	23.76	23.72	23.68
	0.102	13.71	16+	16+	23.93	23.93	23.85
24	0.051	12.46	16.00	16+	24.19	24.11	24.04
	0.102	15.86	16+	16+	24.35	24.35	24.29

APPENDIX B – Monitoring Equipment Installation

This appendix presents the monitoring equipment used in this study. This section is meant to document and comment on the location and adjustment of the monitoring equipment. Any specifications that could influence the results and their validity are discussed here. For ease of analysis, the following color code was used for the image call-outs: red for web-enabled products, blue for thermocouples and green for any orientation aid.

B.1 SS-CH1 (Basement Bedroom 1)

There is a close proximity between the bedroom thermostat and the doorway to the family room. The air temperature read from both the thermostat and the thermocouple is influenced by the temperature of both rooms. The door is kept open to mimic normal operating conditions.

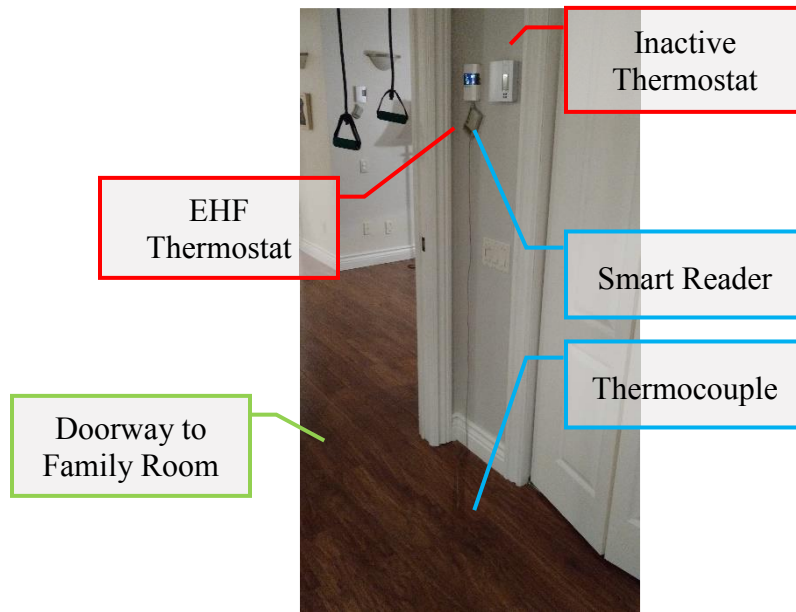


Figure 19 : SS_CH1 Thermostat and Smart Reader Install. Thermostat ID: SS-CH1-01

B.2 SS-SF (Basement Family Room)

There is a close proximity of the SS-SF-02 baseboard to the thermostat as presented in the left picture. In order to avoid having the baseboard upward air draft influence the air reading of the thermostat, the set point of both baseboards were set as to avoid them being activated. This corresponds to a lower activation response time of the heating system. But, the occupants of the house do not use this room very often. The only time that the baseboards are activated during the study is when fast charging times are required such as the three organized events. The SS-SF-01 thermostat is installed on an exterior wall. This is usually not suggested because the thermostat metal casing is in the wall which is usually a few degrees colder than the room. This will influence the results.

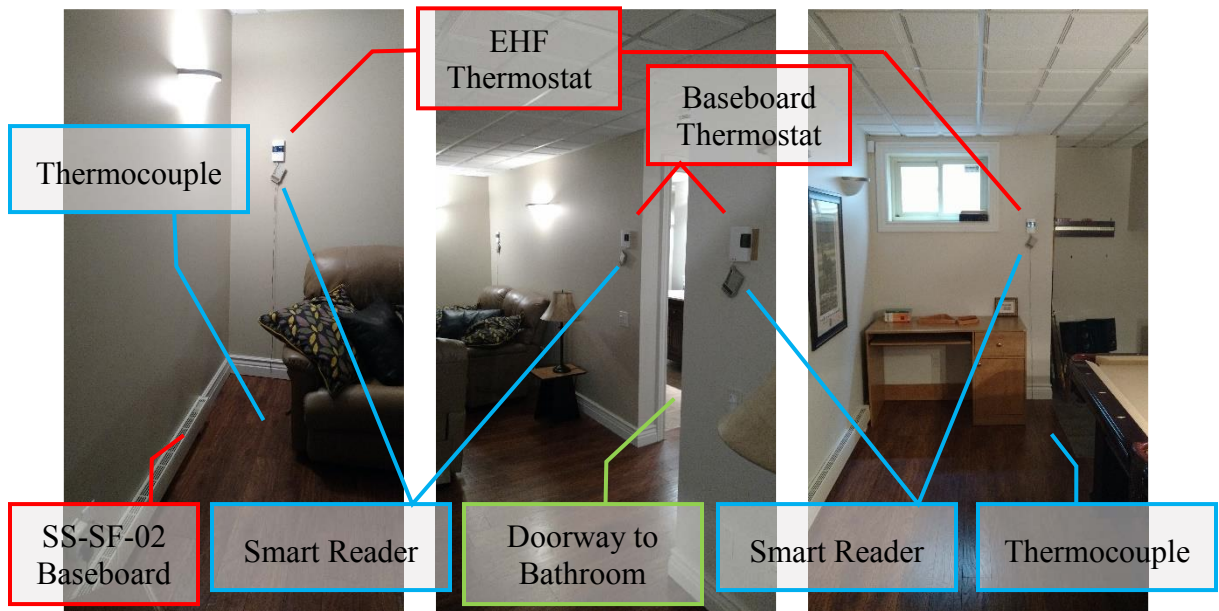


Figure 20 : SS-SF Thermostat and Smart Reader Install. Thermostat ID: SS-SF-04 (Left), SS-SF-04, SS-SF-03 and SS-SF-02 (Middle), SS-SF-01 (Right).

B.3 SS-SDB (Basement Bathroom)

The thermostat is located on an exterior wall. The air temperature is therefore slightly higher than what the thermostat reads.

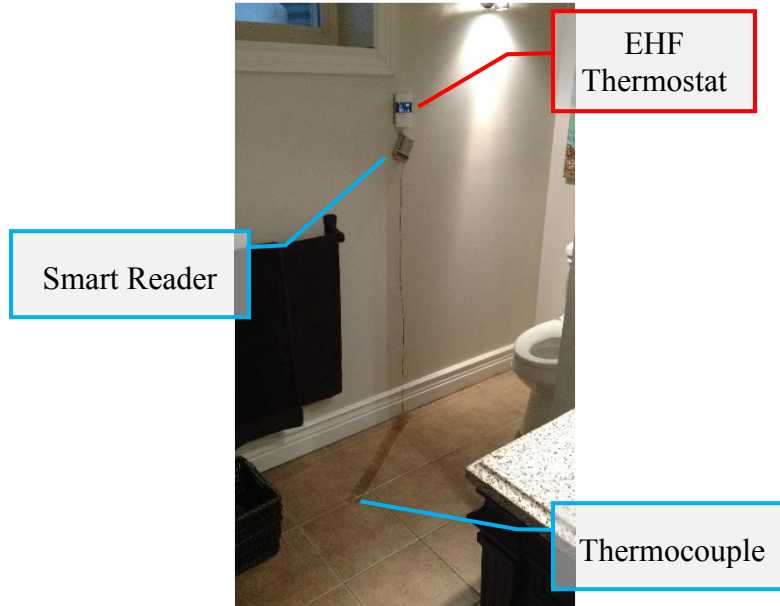


Figure 21 : SS-SDB Thermostat and Smart Reader Install. Thermostat ID: SS-SDB-01

B.4 SS-CH2 (Basement Bedroom 2)

In this room both thermostats are located very close to the doorway. The adjacent room is the hallway and staircase area of the basement which has no heating equipment. The air temperature of this volume of air is usually a few degrees lower than adjacent rooms.

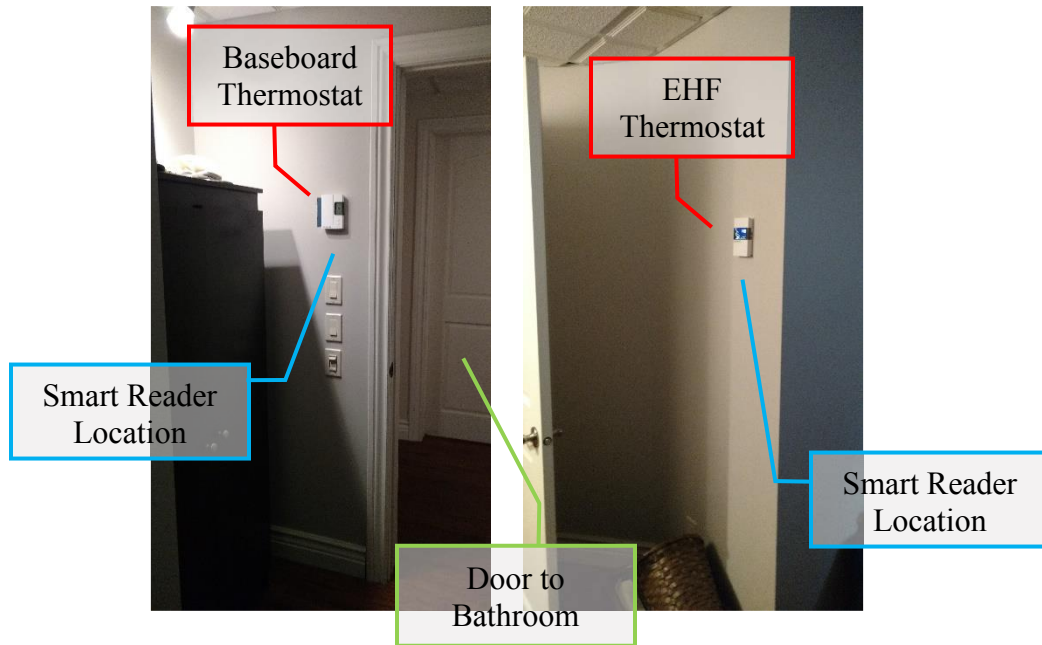


Figure 22 : SS-CH2 Thermostat Installation. Thermostat ID: SS-CH2-01 (left) and SS-CH2-02 (Right).

B.5 SS-GAR (Basement Storage and Laundry Room)

The two EHF thermostats on the left picture are positioned directly over one another. These thermostat models can generate some heat because of the frequency emulator within the device. They are designed with slots on the bottom and top to be air cooled. But, the heat generated by the bottom thermostat influences the reading of the top thermostat. Therefore, only the temperature of the bottom thermostat is used for model validation. Also, both EHF thermostats are installed on an exterior wall. However, they are mounted on surface electrical boxes, which are installed over the gypsum panels. Therefore, their location does not affect the temperature reading.

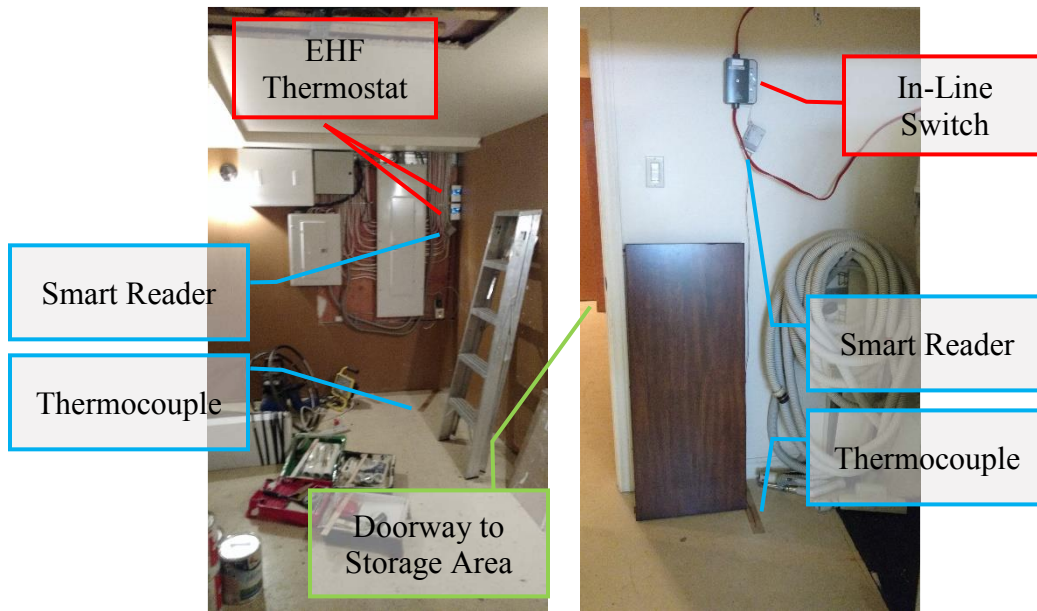


Figure 23 : Thermostat and Smart Reader Install. Thermostat ID: SS-GAR-01 and SS-GAR-02 (Left) and Sinope In-Line Web Enabled Electrical Switch (Right).

B.6 RDC-SF (Ground Floor Family Room and Dining Area)

This room had no heating equipment before the monitoring campaign. It was installed at the owner's request during the first house visit. A single thermostat controls two convective baseboards installed on exterior walls. The location of the thermostat is very close to the heating systems.

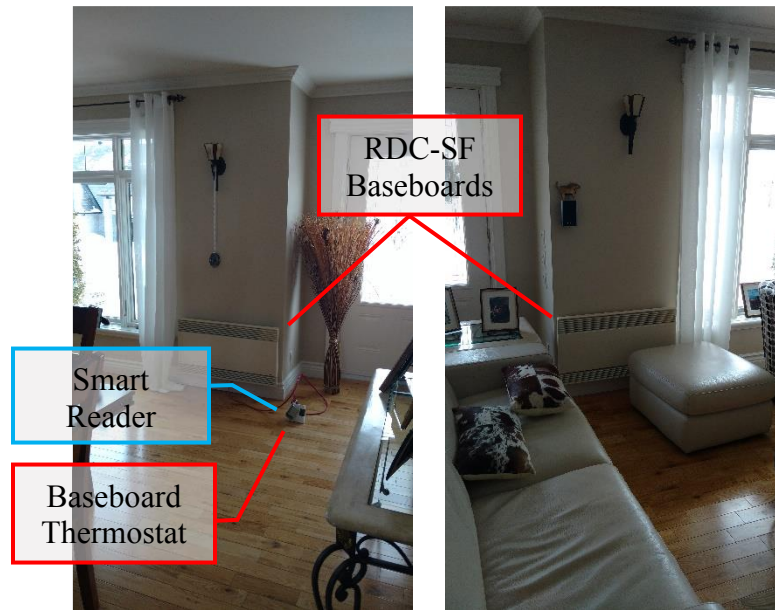


Figure 24 : Thermostat and Smart Reader Install (Left) and 2nd Baseboard (Right). Thermostat ID: RDC-SF-01.

B.7 RDC-CUI (Ground Floor Kitchen, Dining Area, Mudroom)

The surface of this room is heated with two floor heating systems which are controlled by thermostats in the kitchen cupboards. The floor heating thermostat uses its temperature probe as a method of reading the air temperature. Therefore, the web-enabled thermostats do not monitor the floor temperature for these zones. Thermocouples are used to monitor both the air temperature and the floor surface temperature for model validation.

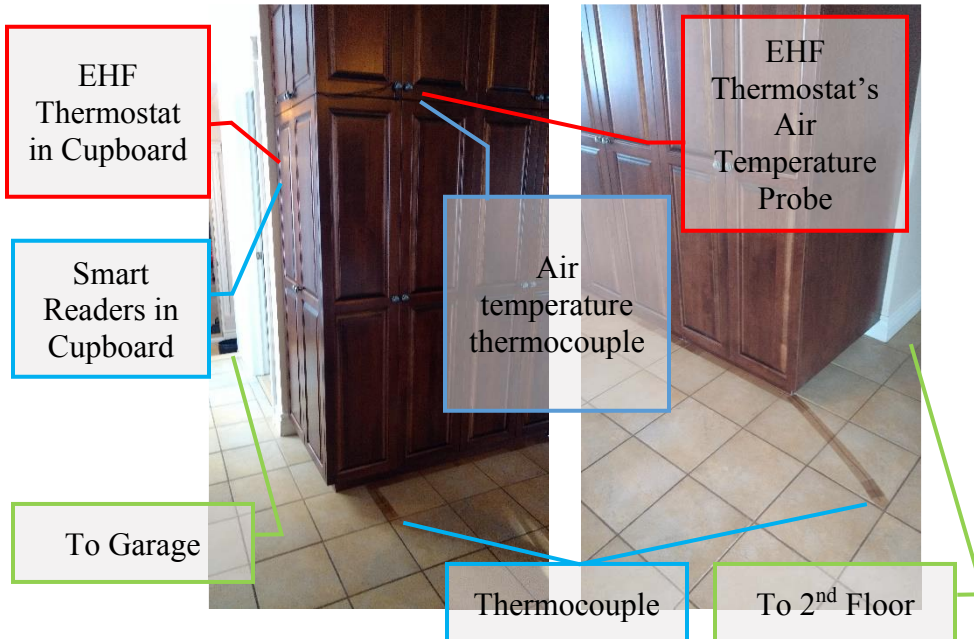


Figure 25 : RDC-CUI Thermostat and Smart Reader Install. Thermostat ID: RDC-CUI-01 (Left) and RDC-CUI-01 (Right)

B.8 RDC-GAR (Ground Floor Garage)

This room is the only one where the locations of the thermostat temperature probe locations are not known. Two Smart Readers are located directly below both thermostats and the thermocouples are placed in line with them on the floor. The left thermostat controls the North section of the garage whereas the right thermostat controls the South section of the garage.

Part of the exterior driveway has electric heating cables, which are controlled by a snow accumulation sensor shown on the right picture below. The current draw from this system was monitored using a Smart Reader and a magnetic current sensor.

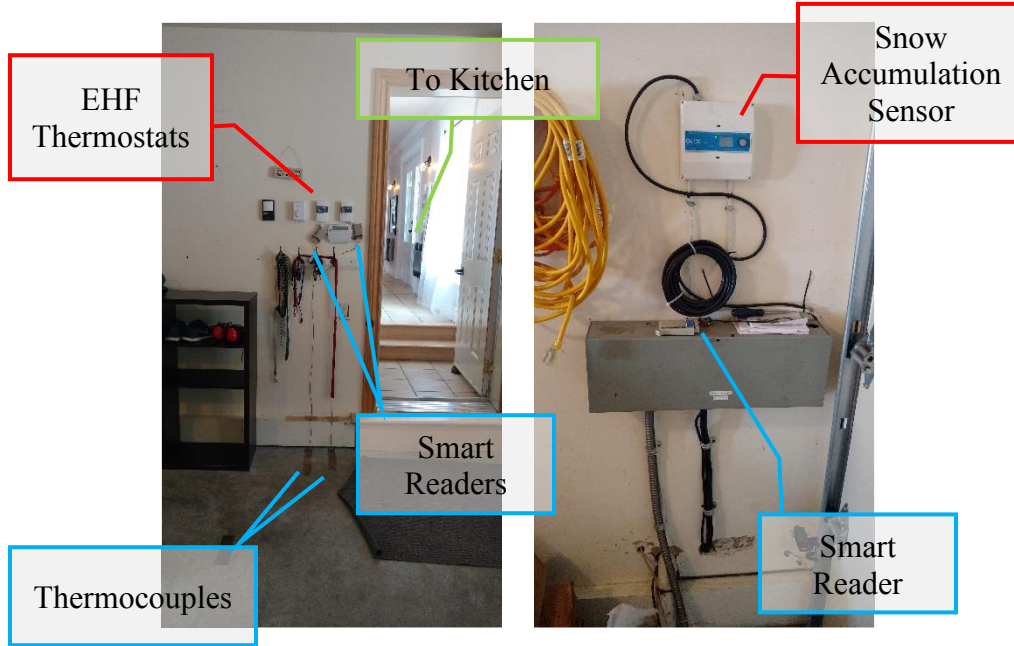


Figure 26 : RDC-GAR Thermostat and Smart Reader Install (Left) and Driveway Smart Reader Install (Right)

B.9 ET-SDB1 and ET-SDB2 (2nd Floor Bathrooms)

In the master's bathroom, there is close proximity between the thermostat and the shower, which does not have a door. This influences the air temperature resulting in momentaneous high peaks. The thermocouple is placed away from the wall close to the center of the room.

For the main bedroom, the thermostat is located very close to the door leading to the hallway. The door is always open except when an occupant is in the bathroom. The air temperature reading is influenced by both the shower and the air currents within the hallway.

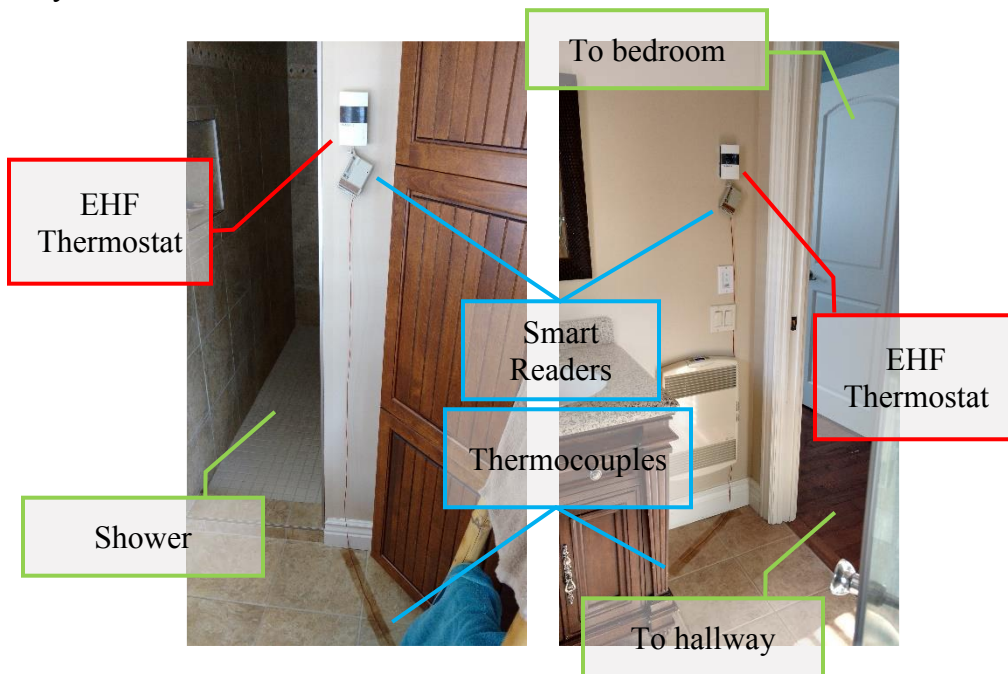


Figure 27 : ET-SDB1 (Left) and ET-SDB2 (Right) Thermostat and Smart Reader Install

B.10 ET-CH1, ET-CH2 and ET-CH3 (2nd Floor Bedrooms)

All three bedrooms on the second floor have their thermostat located directly next to the doorway. The doors are opened most of the time and therefore the temperature read by the thermostat is influenced by the air currents of the hallway. In all cases, the thermostat is located on the opposite wall onto which the heating system is installed. The electric baseboard in all cases is installed directly below or next to a window. Therefore, the air temperature reading is not influenced by the down draft of the window or the updraft of the baseboard.

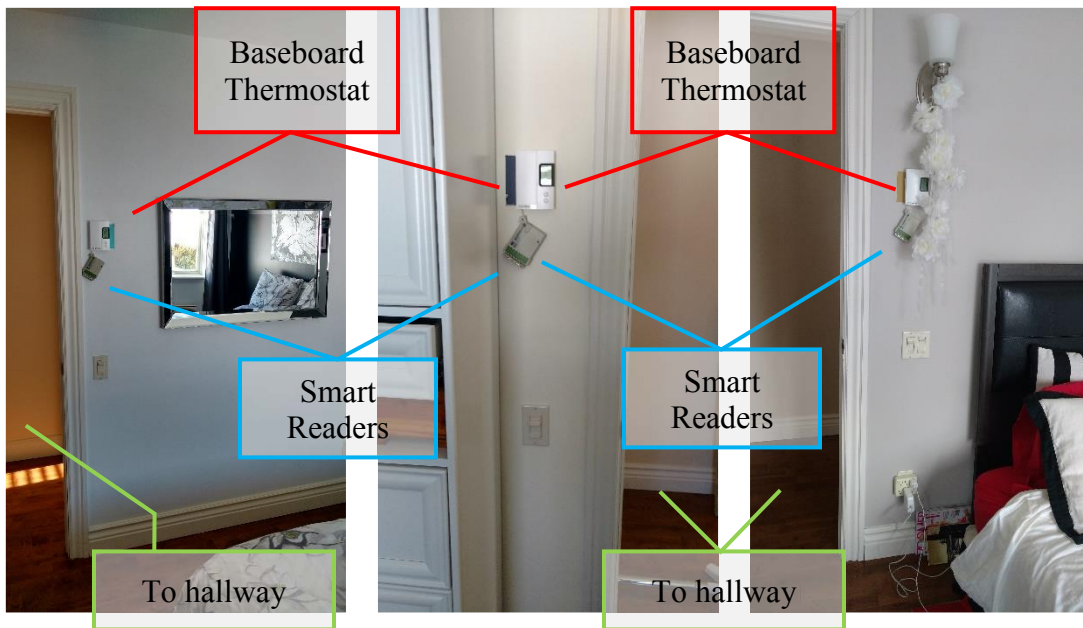


Figure 28 : ET_CH1 (Left), ET-CH2 (Middle) and ET-CH3 (Right) Thermostat and Smart Reader Install

B.11 ET-BUR (2nd Floor Office and Gym)

In this room the two baseboard thermostats are very close to one another. A single Smart Reader was positioned directly below both thermostats. Also, there is close proximity of the thermostats to the door way leading to the staircase and the hallway. The electric baseboards are on the opposite side of the room.

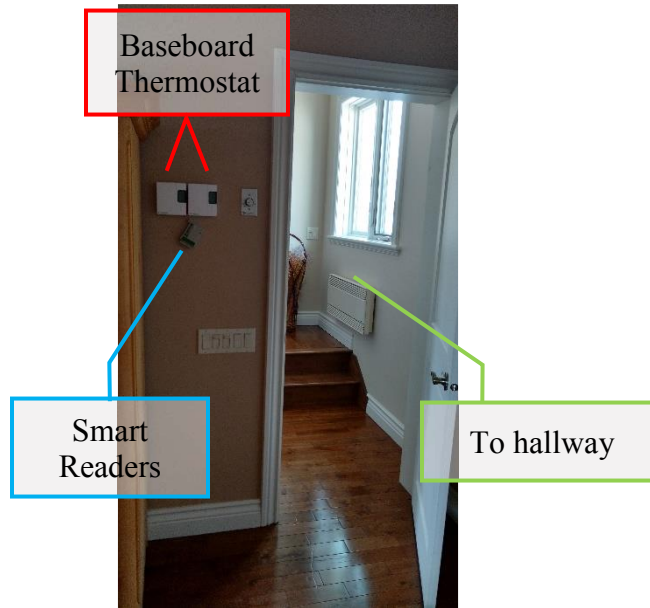


Figure 29 : ET-BUR Thermostat and Smart Reader Install

B.12 ET-COU (2nd Floor Hallway)

The hallway on the 2nd floor is “L” shaped and the thermostat is located on the corner that faces the staircase. Therefore, it is subjected to updrafts coming from the ground floor. The thermostat is placed a certain distance away from the heating baseboard, which is placed directly below a window.

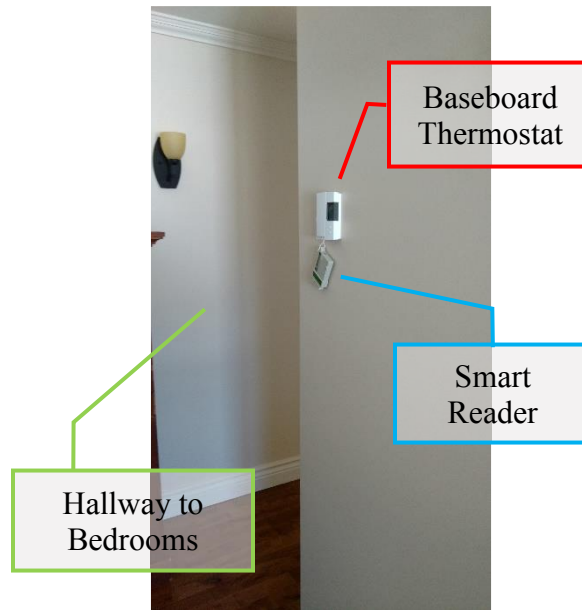


Figure 30 : ET-COU Thermostat and Smart Reader Install

B.13 Hot Water Tank

The following figure shows how the hot water tank was monitored in this study. Only the power consumption to maintain the tank at 140°F is measured. The flow of water to the various house systems is not measured.

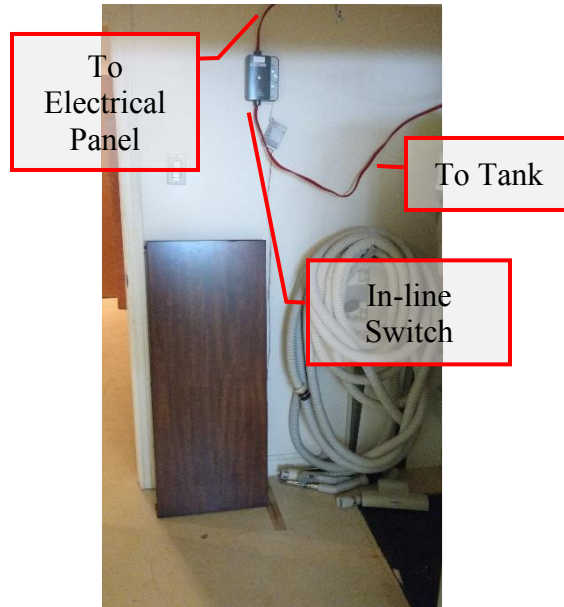


Figure 31 : Sinope In-line Switch Installation

B.14 Heat Exchanger

Only one ventilation system is installed in the residence which is a heat exchanger. This system has two modes of operation which are managed entirely by the heat exchanger module:

1) *Heat Recuperation Cycle*: The fan is activated and moves 97 cfm of fresh air into the room, supplied to the basement living room. In the same process, air is drawn at the same flow rate from all of the bathrooms in the house. Fresh air is pre-heated by the exhaust air being moved to the exterior.

2) *Defrost Cycle*: Air is recirculated within the building. Air is drawn from the basement living room and moved to all bathroom nozzles in the house at a flow rate of 30cfm. This cycle is activated when water condensate freezes in the air exchanger.

The heat exchanger is monitored using two Sinope radiant floor thermostats because they have the ability of recording two temperatures at once. The air flow rate is calculated from the fan electrical motor energy consumption and associating the fan electrical draw to a measured flow rate in the piping. The temperature probe of one of the thermostats is bypassed and connected to a circuit board which converts the fan electrical draw into a signal that the thermostat can measure. The measurement device is shown in Figure 32.

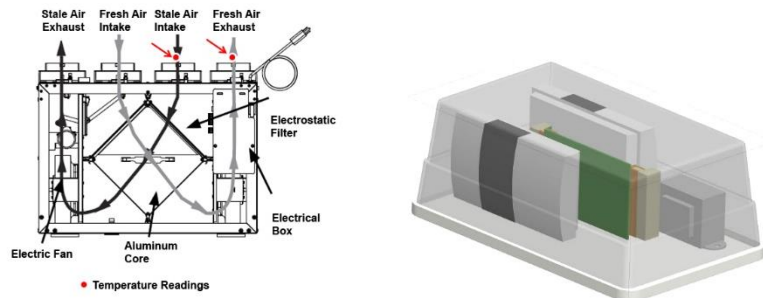


Figure 32 : a) Temperature Reading Locations b) Measurement Device

The right thermostat measures the control box internal temperature and the heat exchanger fresh air outlet. The left thermostat measures the stale air inlet as well as the state of the fan motor. A magnetic current sensor measures the electrical current to the fan

and is connected to the thermostat. The air flow rate of the system was measured for all three modes (off, defrost, active) and correlated to the thermostat temperature reading.

Table 22 : Correlation Between Thermostat Reading and Heat Exchanger Operation

Temperature Reading [°C]	System State	Air Flow Rate [cfm]
3±3	OFF	0
17±3	DEFROST	30
30±3	ACTIVE	97

The following figure shows the EHF thermostat assembly for monitoring the heat exchanger. Once the closet doors are closed, the monitoring unit involves limited intrusiveness for the occupants of the house.

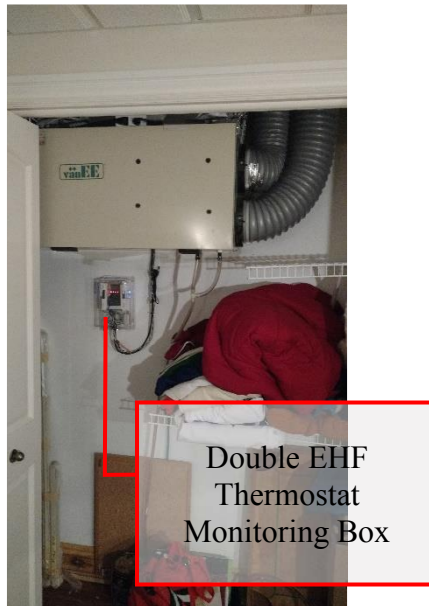


Figure 33 : Thermostat Install for Heat Exchanger

APPENDIX C – Construction Drawings

This appendix presents the construction drawings of the building. These plans are not an exact representation of the actual configuration of the house as some minor changes have been done during the building's construction. Precisions on noted differences between the construction plans and the actual configuration of the house are presented in Appendix F.



L'entrepreneur, le client ou les sous-traitants devront faire part à Jessica Shedy de toute erreur et/ou omission sur les dessins avant d'amorcer les travaux concernés.
 Ce document est la propriété d'Architecture Jessica Shedy et ne doit être réutilisé, réimprimé ou copié sous quelque forme que ce soit.

NO.	DATE	DESCRIPTION
		Revisions

PHASE : **Plan de construction**

CLIENT(S) : Philippe Beaulieu

ADRESSE DU PROJET : 191, des Grenadiers Boischiél Guébec

PROJET : Plan de maison

SUJET : Élévation Avant

ÉCHELLE : DATE : 26 février 2008

DOSSIER : 20070820 FEUILLE : 1



① Avant 5/16" = 1'-0"

FORMAT POUR IMPRESSION A L'ÉCHELLE 11" X 17" SANS MARGE

L'entrepreneur se réfère au les plans et spécifications pour les travaux de construction. Les travaux de construction doivent être effectués conformément aux plans et spécifications et/ou selon les besoins de la construction. Les travaux de construction doivent être effectués conformément aux plans et spécifications et/ou selon les besoins de la construction.

Ce document est la propriété de
 Architecture Jessica Gheey et
 ne doit être utilisé que pour l'usage
 spécifique auquel il est destiné.

NO.	DATE	DESCRIPTION
		REVISIONS

PHASE
Plan de construction

CLIENT(S)
 Philippe Beaulieu

ADRESSE DU PROJET
 191, des Grenadiers
 Boischâtel
 Québec

PROJET
 Plan de maison

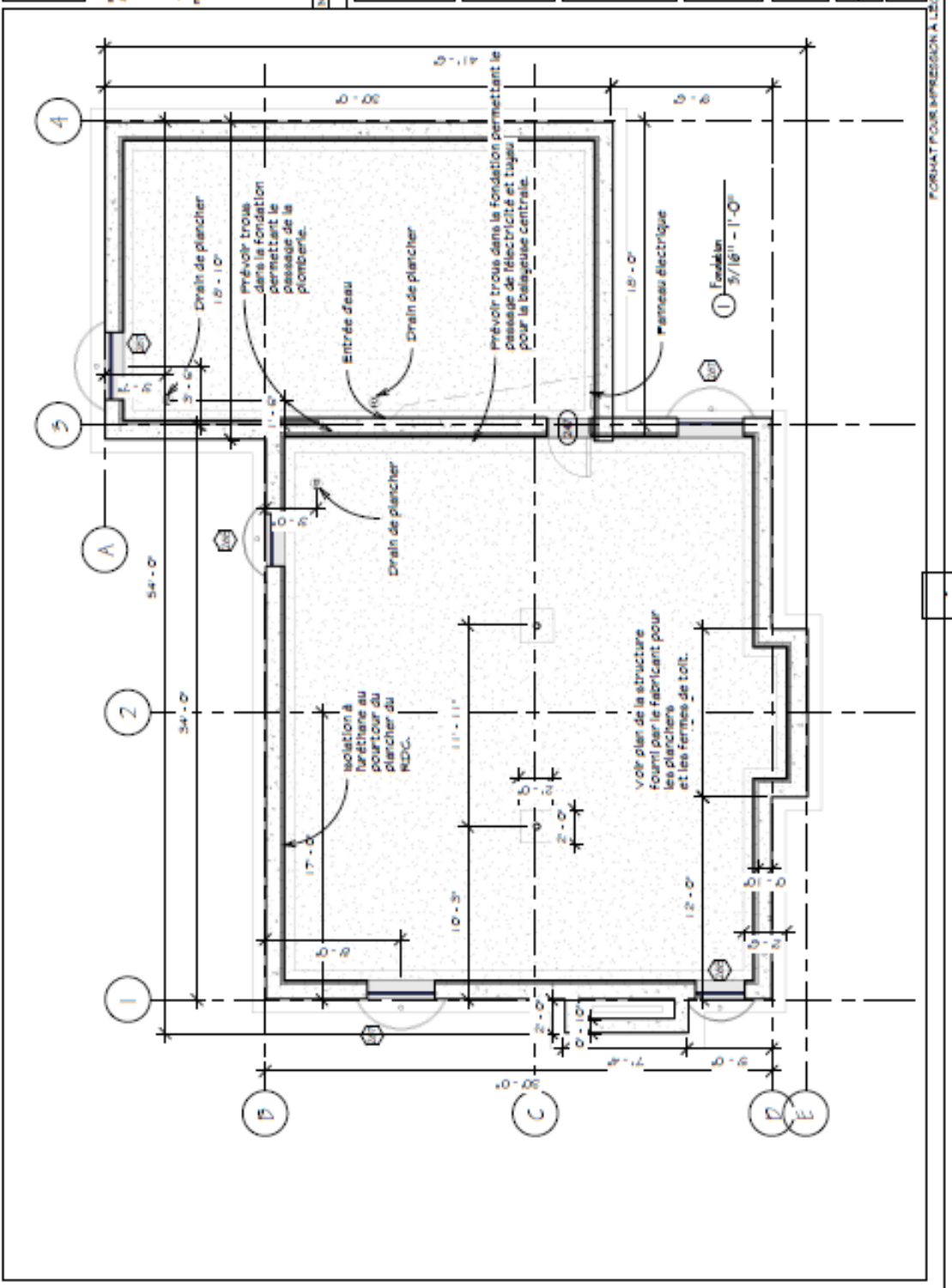
SUJET
 Fondation

ÉCHELLE
 DATE: 26 février 2006

DOSSIER
 20070820

FEUILLE
 2

FORMAT POUR IMPRESSION A L'ÉCHELLE 11" X 17" SANS MARGES



L'entrepreneur, le client ou les sous-traitants, doivent être avisés que Jessica Shedy ne sera pas tenue responsable de toute erreur et/ou omission sur les dessins avant d'aprouver les travaux concernés.
 Ce document est la propriété d'Architecture Jessica Shedy et ne doit être utilisé que pour le projet spécifique auquel il est destiné.

NO.	DATE	DESCRIPTION
		Revisions

PHASE:
Plan de construction

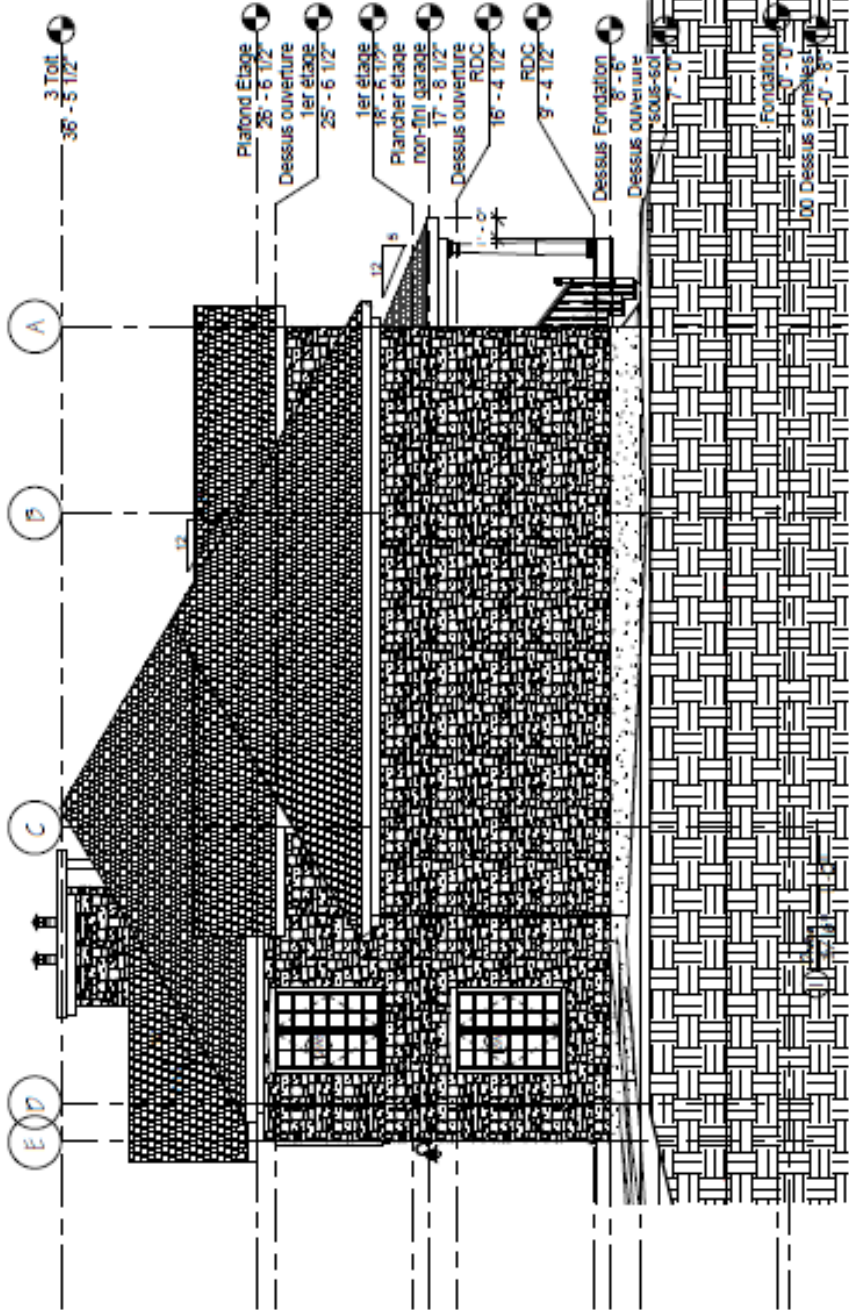
CLIENT(S):
 Philippe Beaulieu

ADRESSE DU PROJET:
 191, des Grenadiers
 Boisbriand
 Québec

PROJET:
 Plan de maison

SUJET:
 Élévation droite

DATE: 26 février 2008
 DOSSIER: 20070820
 FEUILLE: 5



JENNIFER SHEDDY
 Architecte
 418-365-4346
 info@jennifersheddy.com

L'entrepreneur se tient ou les
 sous-traitants doivent faire part
 à Jennifer Shedd de toute erreur
 et/ou omission sur les dessins
 avant d'entamer les travaux
 concernés.
 Ce document est le propriété de
 "Architecte Jennifer Shedd" et
 ne doit être utilisé que pour l'usage
 spécifique auquel il est destiné.

NO.	DATE	DESCRIPTION REVISIONS
-----	------	--------------------------

PHASE :
Plan de construction

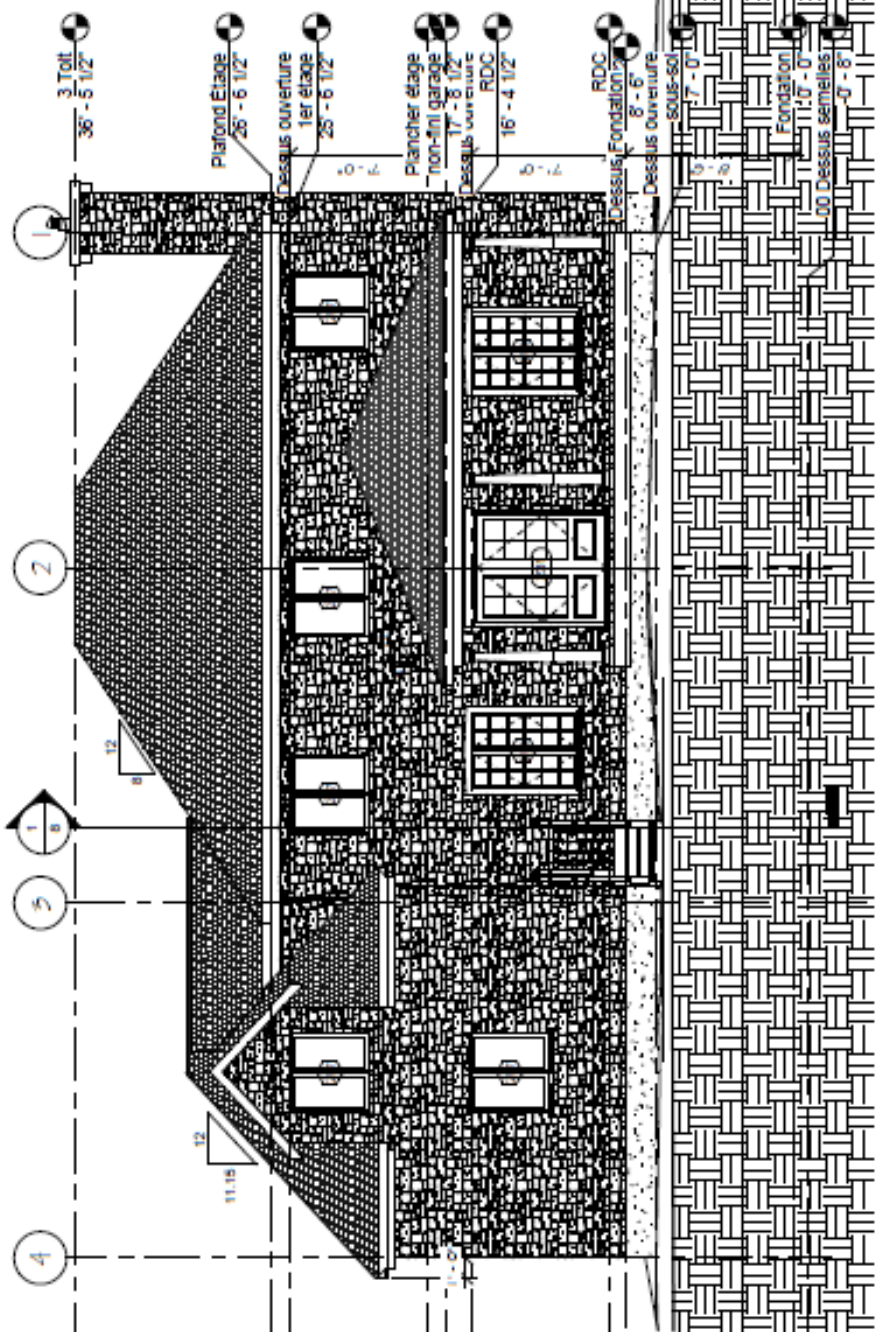
CLIENT(S):
 Philippe Beaulieu

ADRESSE DU PROJET:
 151, des Grenadiers
 Boischatel
 Québec

PROJET:
 Plan de maison

SUJET:
 Élévation arrière

ÉCHELLE:
 DATE: 26 février 2008
 DOSSIER: 20070820
 FEUILLE: 6



1/8" = 1'-0"

L'entrepreneur, le client ou les sous-traitants devront faire part à Jessica Shesley de toute erreur et/ou omission sur les dessins avant d'entreprendre les travaux.
 Ce document est la propriété d'« Architecture Jessica Shesley » et ne doit être utilisé que pour l'usage spécifique auquel il est destiné.

NO.	DATE	DESCRIPTION
		Révisions

PHASE :
Plan de construction

CLIENT(S) :
 Philippe Beaulieu

ADRESSE DU PROJET :
 15 1, des Grenadiers
 Boischatel
 Québec

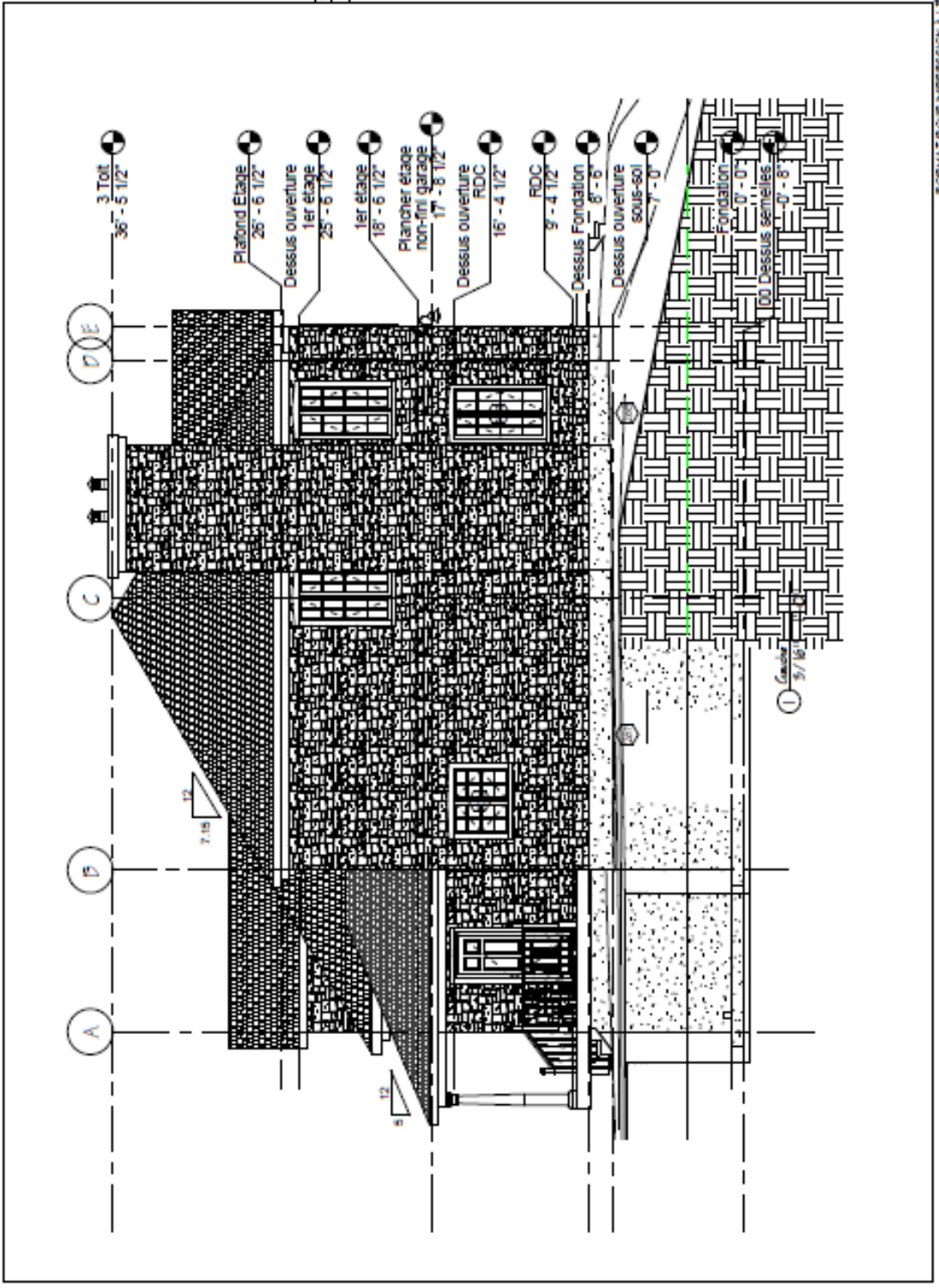
PROJET :
 Plan de maison

SUJET :
 Élévation gauche

DATE : 26 février 2008

DOSSIER :
 20070820

FEUILLE :
 T



Lorsqu'on veut le client ou les sous-traitants doivent faire part à Jessica Shedd de toute erreur et/ou omission sur les dessins avant d'entamer les travaux concernés.
 Ce document est la propriété de l'Architecte Jessica Shedd et ne doit pas être réutilisé sans son accord préalable écrit. Toute réimpression sans son accord préalable est interdite.

NO.	DATE	DESCRIPTION / REVISIONS
-----	------	-------------------------

PHASE :
Plan de construction

CLIENT(S):
 Philippe Beaulieu

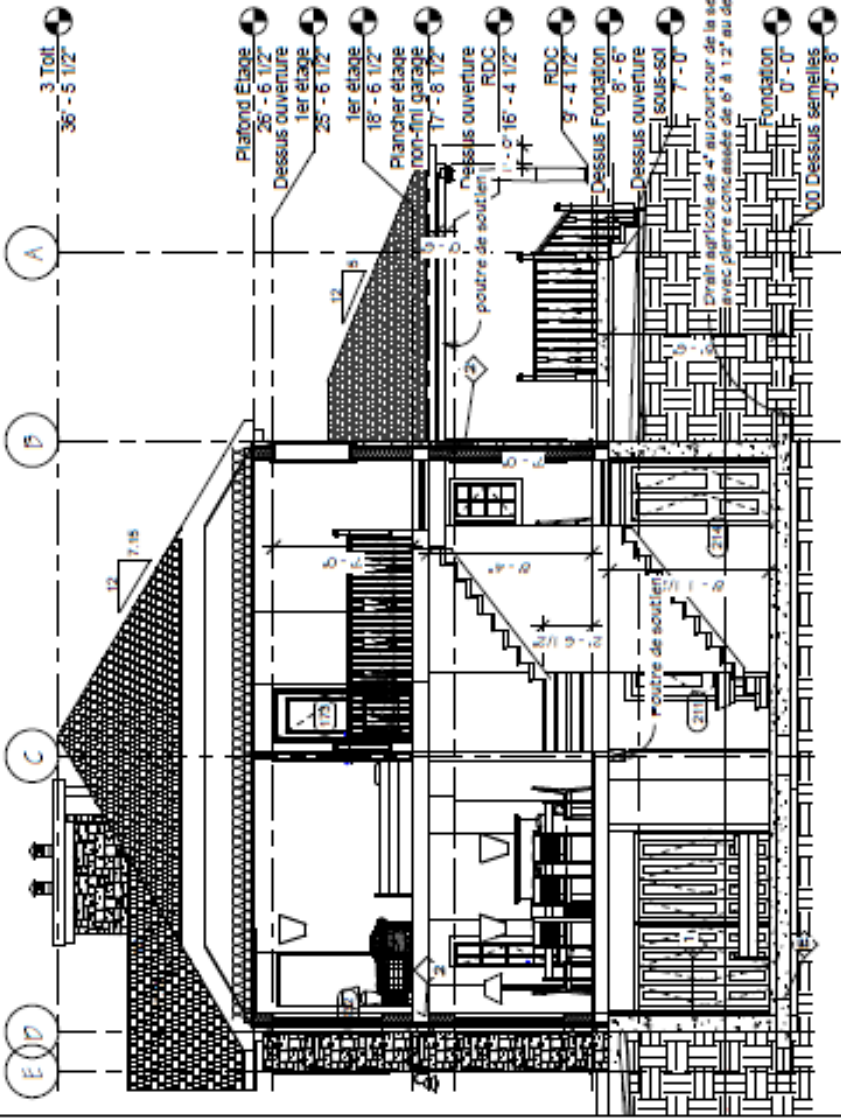
ADRESSE DU PROJET:
 151, des Grenadiers
 Boischi tel
 Gu bec

PROJET:
 Plan de maison

SUJET:
 Devs / Coupe de mur

 CHELLE:
 DATE: 26 f vrier 2006
 DOSSIER:
 20070520
 FEUILLE:
 5

Notes
 Fichier en annexe de tous les plans maison.
 Cuvre-plaque   toiture 1/2" avec arapages en 1/4".
 Membrane d'auvent tout poids selon les tables de l'art.
 Sols en aluminium. (Voir plans pour la couleur)
 Barreaux d'acier 205 mm (r sistance sup rieure   100 lb/ft²)
 Plan d'isolation une combinaison requise d'isolation.



1 Coupe transversale A
 5/16" - 1'-0"



Les renseignements ci-dessus ou les sous-traitants devront être remis à Jessica Shedy de toute urgence et/ou selon les besoins de la clientèle avant d'annoncer les travaux concernés.
Ce document est la propriété de l'Architecture Jessica Shedy et ne doit être communiqué à personne sans l'approbation écrite de l'architecte.

NO.	DATE	DESCRIPTION
REVISIONS		
		PHASE : Plan de construction
		CLIENT(S) : Philippe Beaulieu
		ADRESSE DU PROJET : 151, des Grenadiers Boischnéel Québec
		PROJET : Plan de maison
		SUJET : Tableaux
		ÉCHELLE :
		DATE : 26 février 2008
		DOSSIER : 20070820
		FEUILLE : 09

Tableau des portes vitrées (Voir plans pour détails)

Numéro	Niveau	Largeur	Hauteur
195	Fondation	2' - 6"	6' - 11"
204	Fondation	2' - 6"	6' - 11"
209	Fondation	4' - 0"	7' - 0"
211	Fondation	2' - 6"	7' - 0"
214	Fondation	2' - 6"	7' - 0"
218	Fondation	5' - 0"	6' - 4"
242	Fondation	4' - 0"	7' - 0"
245	Fondation	4' - 0"	7' - 0"
244	Fondation	4' - 0"	7' - 0"
246	Fondation	2' - 6"	7' - 0"
249	Fondation	2' - 6"	6' - 11"
166	RDC	2' - 6"	6' - 11"
224	RDC	1' - 6"	7' - 0"
226	RDC	5' - 11 1/2"	6' - 11"
226	RDC	4' - 0"	7' - 0"
167	1er étage	2' - 6"	6' - 11"
170	1er étage	2' - 6"	6' - 11"
171	1er étage	4' - 0"	7' - 0"
172	1er étage	4' - 0"	7' - 0"
175	1er étage	2' - 6"	6' - 11"
175	1er étage	2' - 6"	6' - 11"
252	1er étage	2' - 7 1/2"	6' - 8 1/2"
245	1er étage	2' - 7 1/2"	6' - 8 1/2"
248	1er étage	2' - 6"	6' - 11"

Tableau des portes dans les murs extérieurs (Voir plans...)

Niveau	Largeur	Hauteur
247	2' - 6"	6' - 11"
199	2' - 6"	6' - 11"
22	12' - 0"	7' - 0"
9	2' - 6"	7' - 0"
0	5' - 11 1/2"	6' - 11"
259	2' - 6"	6' - 11"
25	6' - 0"	6' - 11"

Tableau des fenêtres (voir plans pour le type)

Référence au plan	Niveau	Largeur	Hauteur
267	Fondation	4' - 0"	2' - 0"
268	Fondation	5' - 0"	2' - 0"
267	Fondation	4' - 0"	2' - 0"
268	Fondation	5' - 0"	2' - 0"
267	Fondation	4' - 0"	2' - 0"
248	RDC	6' - 5"	5' - 6"
248	RDC	6' - 5"	5' - 6"
246	RDC	4' - 0"	5' - 6"
246	RDC	4' - 0"	5' - 6"
306	RDC	4' - 0"	5' - 4"
297	RDC	4' - 0"	4' - 0"
305	RDC	5' - 0"	5' - 6"
248	1er étage	6' - 5"	5' - 6"
248	1er étage	6' - 5"	5' - 6"
297	1er étage	4' - 0"	4' - 0"
297	1er étage	4' - 0"	4' - 0"
297	1er étage	4' - 0"	4' - 0"
296	1er étage	4' - 0"	5' - 6"
297	1er étage	4' - 0"	4' - 0"
305	1er étage	5' - 0"	5' - 6"
305	1er étage	5' - 0"	5' - 6"
248	1er étage	6' - 5"	5' - 6"
297	1er étage	4' - 0"	4' - 0"

FORMAT FOUR IMPRESSION A LECHÈLE 11" x 17" SANS MARGE

L'entrepreneur, le client ou les sous-traitants devront faire part à Jessica Sheddly de toute erreur et/ou omission sur les dessins avant d'amorcer les travaux concernés.
 Ce document est la propriété d'Architecture Jessica Sheddly et ne doit être réutilisé sans le consentement écrit de l'architecte.

NO.	DATE	DESCRIPTION / REVISIONS
-----	------	-------------------------

PHASE:
Plan de construction

CLIENT(S):
 Philippe Beaulieu

ADRESSE DU PROJET:
 151, des Grenadiers
 Boisbriand
 Québec

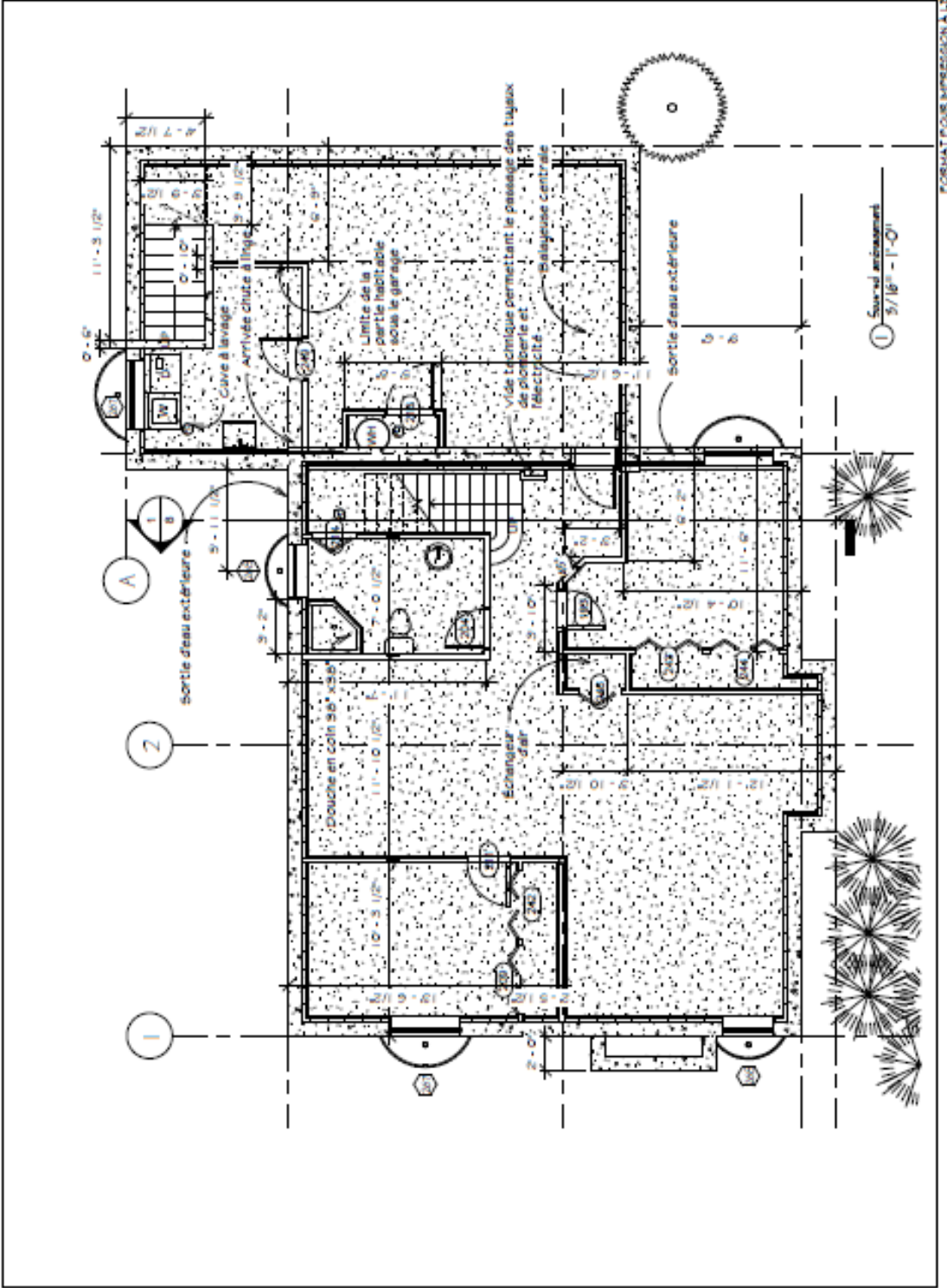
PROJET:
 Plan de maison

SUJET:
 Sous-sol
 Aménagement

ÉCHELLE:
 DATE: 26 février 2006

DOSSIER:
 20070820

FEUILLE:
 q



FORMAT POUR IMPRESSION A L'ÉCHELLE 11\"/>

NO.	DATE	DESCRIPTION
		REVISIONS

PHASE,
Plan de construction

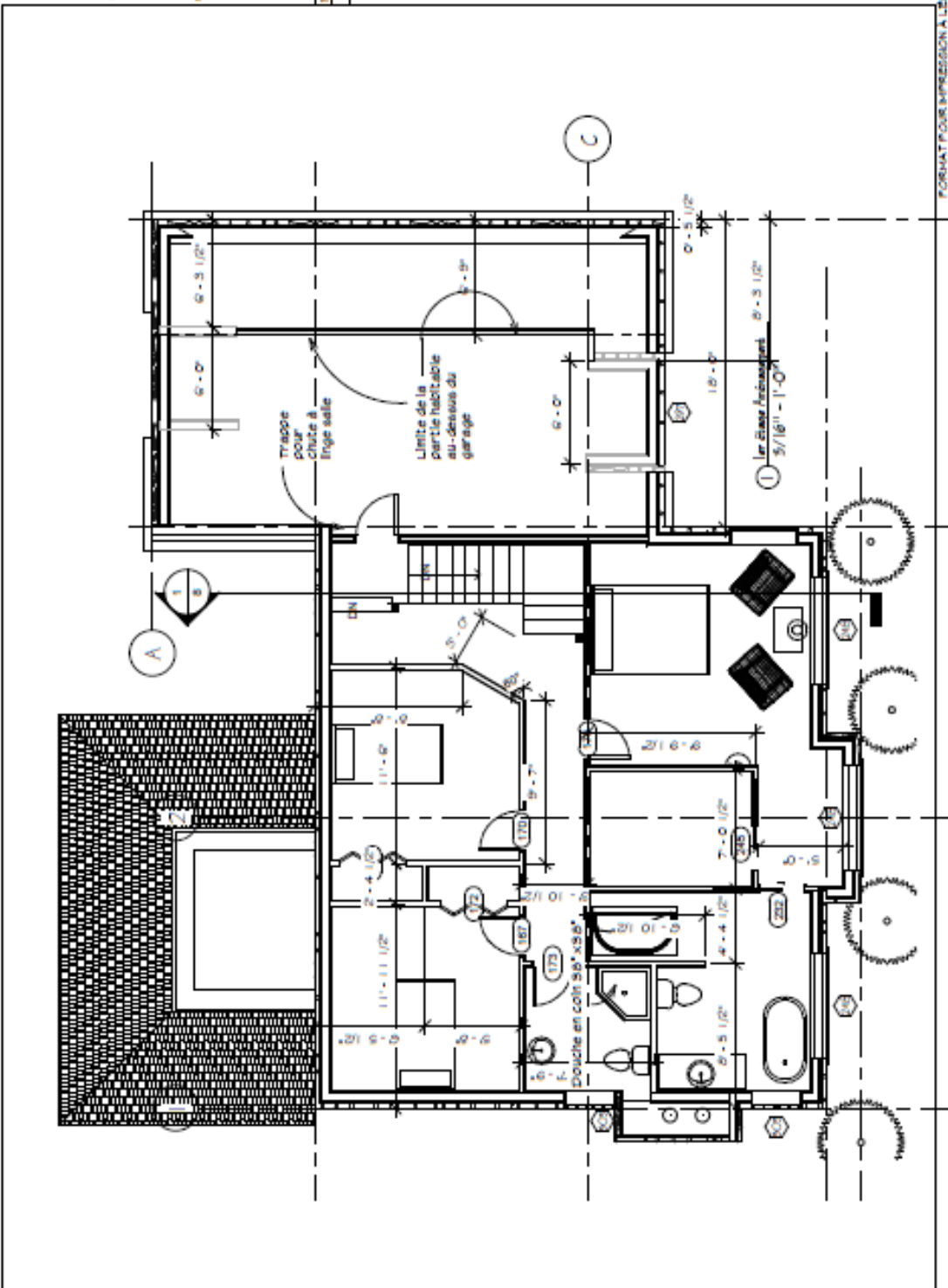
CLIENT(S),
 Philippe Beaulieu

ADRESSE DU PROJET,
 191, des Grenadiers
 Boischâtel
 Québec

PROJET,
 Plan de maison

SUJET,
 Étage aménagement

ÉCHELLE,
 DATE, 26 février 2008
 DOSSIER,
 20070820
 FEUILLE,
 1 1





L'entrepreneur se tient au courant de tous les travaux effectués, ainsi que de la construction de toutes les parties et/ou modification sur les dessins avant d'envoyer les travaux concernés.
Ce document est la propriété de l'Architecte Jessica Ginsbury et ne doit être utilisé que pour l'usage spécifique auquel il est destiné.

NO.	DATE	DESCRIPTION
		Revisions

PHASE : **Plan de construction**

CLIENT(S) : Philippe Beaulieu

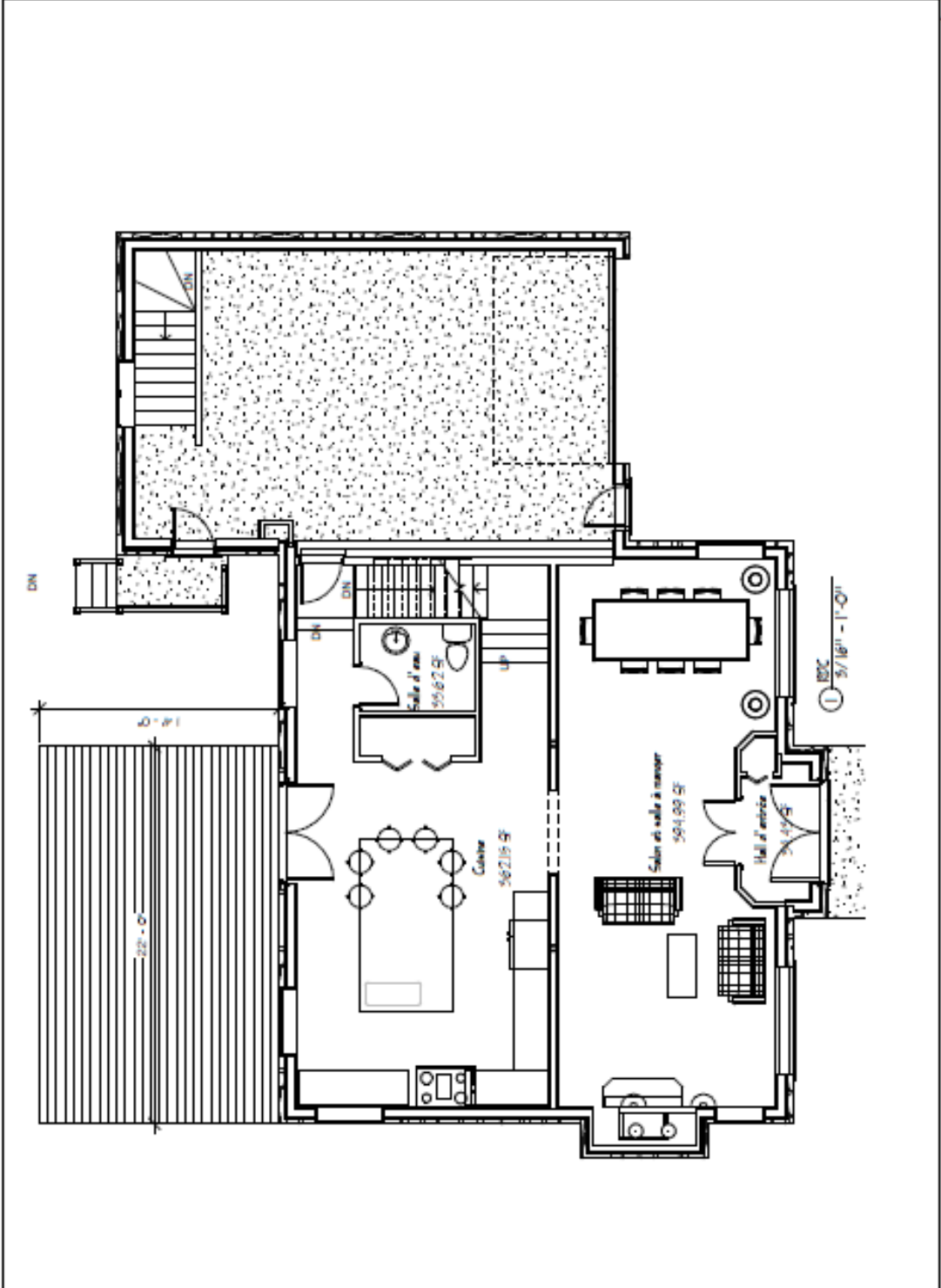
ADRESSE DU PROJET : 191, des Grenadiers Boischatel Québec

PROJET : Plan de maison

SUJET : RDC Finit et super ficés
Echelle :

DATE : 26 février 2006

DOSSIER : 20070620
FEUILLE : 19



FORMAT POUR IMPRESSION A L'ECHELLE 1/8" = 1'-0"

NO.	DATE	DESCRIPTION
		REVISION

PHASE:
Plan de construction

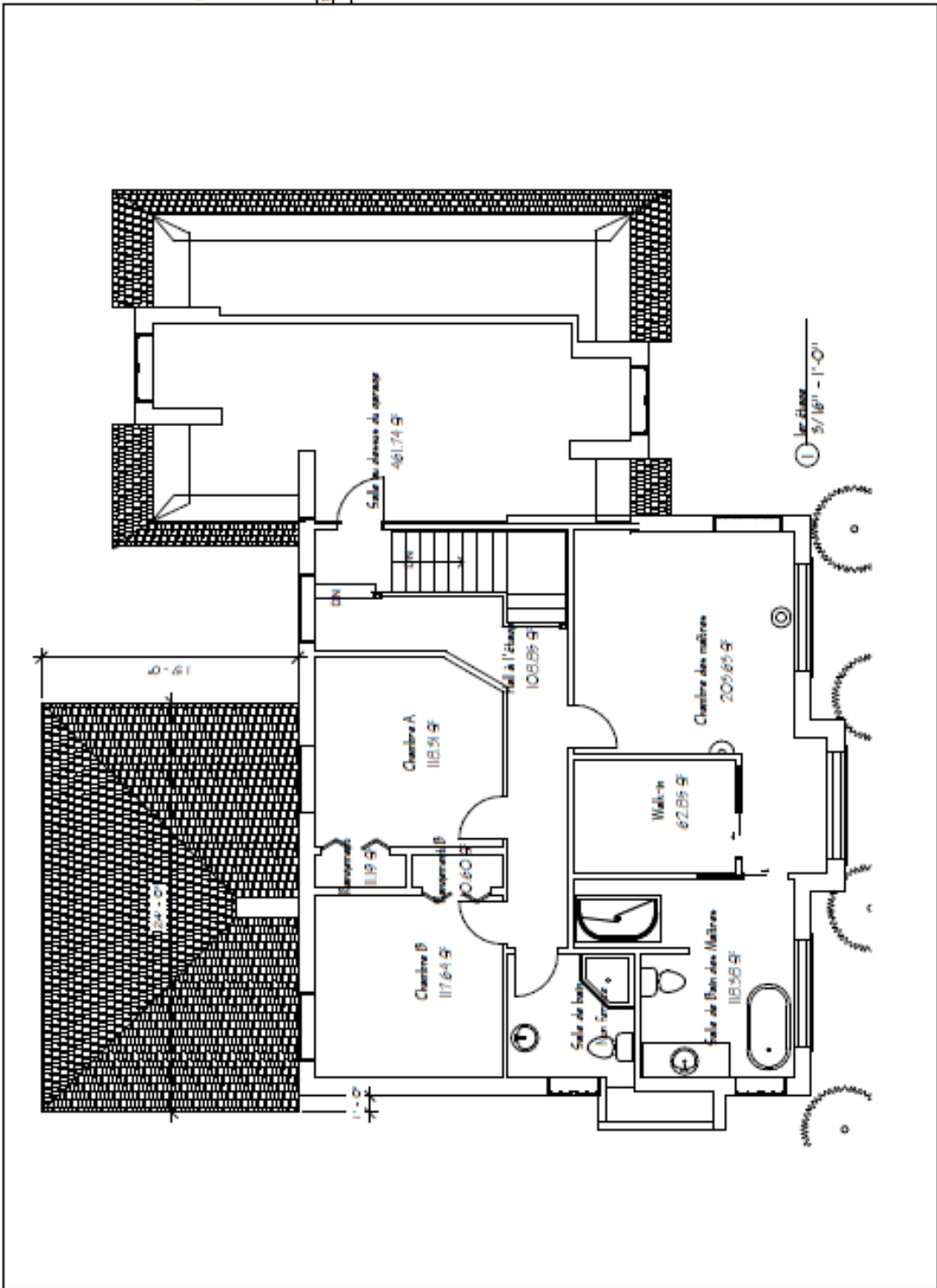
CLIENT(S):
 Philippe Beaulieu

ADRESSE DU PROJET:
 191, des Grenadiers
 Boischâtel
 Québec

PROJET:
 Plan de maison

SUJET:
 Étage Finitions et
 Superficies

ÉCHELLE:
 DATE: 26 février 2008
 DOSSIER:
 20070820
 FEUILLE:
 14



APPENDIX D – Modelling Notes

This appendix presents the details involved in the development of the TRNSYS model used in this thesis work. The description of the building is covered in the methodology section. Nonetheless, important modelling decisions regarding the model have been documented and are presented here.

D.1 Heat Transfer through Walls and Assemblies

All assemblies are assumed to be sufficiently wide and high for the assumption of one-dimensional conduction heat flow to apply. In that regards, TRNSYS Type 56 models all assemblies in this way. The thermal resistance in this case is calculated using the series-parallel method for composite walls. Any layer with multiple materials like air spaces created with furring strips or wood stud walls with insulation are evaluated in this manner.

Several methods are used for the calculation of heat transfer through cavities. For air spaces created from regularly spaced furring strips of 16 mm thick, values already calculated from Hutcheon et al. (1983) are used. These calculated values are based on the ASHRAE Book of Fundamentals. The thermal resistance of the layer is assumed to be the result of a parallel network of the air cavity and the wood furring strips where the equivalent resistance is the area-weighted resistance of the composite layer.

In the case where the cavities are thicker than 92 mm, the average Nusselt number for the cavity is calculated using the correlation from MacGregor and Emery (1969) which applies for vertical cavities with large aspect ratios as is the case in structural wood stud walls constructed from 38 mm x 140 mm dimensional lumber spaced 406 mm apart:

$$Nu = 0.46 Ra_L^{1/3}$$

Where Nu is the average Nusselt number, Ra_L is the Rayleigh of the wall, Pr is the Prandtl number of the air, H is the height of the wall and L is the thickness of the air cavity. This equation can be applied to shape factors (H/L) of up to 40, Prandtl numbers between 1 and 20 and Rayleigh numbers between 10^6 and 10^9 . The resistance of the cavity is assumed to be the result of a parallel network of the air cavity and the wood studs where the equivalent resistance is the area-weighted resistance of the composite layer.

For horizontal cavities created by the floor assemblies, it is assumed that the joists segregate the air contained within the floor into many cavities with a width of 406 mm. For all horizontal cavities found in this home, the Rayleigh number is found to be within the range of 10^5 to 10^9 and therefore the average Nusselt number can be calculated from the correlation presented by Hollands et al. (1975):

$$Nu = 1 + 1.44 \left[1 - \frac{1708}{Ra_L} \right]^+ + \left[\frac{Ra_L^{1/3}}{18} - 1 \right]^+$$

Part of the office on the second floor has a cathedral ceiling within which an air cavity connects the soffit to the attic space. Such cavities have been shown to have an air change per hour of approximately one (Tenwolde & Carll, 1992). Through experiments, it has been shown that the impact of such cavities on heat flow through the wall is negligible. Therefore, the air within the cavity is assumed to be stationary for the purpose of calculating the one-dimensional heat flow through the assembly. The Nusselt number can therefore be approximated by Hollands et al.'s (1975) model for inclined cavities of up to 70° represented by the following equation:

$$Nu = 1 + 1.44 \left[1 - \frac{1708}{Ra_L \cos \theta} \right]^+ \left(1 - \frac{1708 (\sin 1.8 \theta)^{1.6}}{Ra_L \cos \theta} \right) + \left[\frac{(Ra_L \cos \theta)^{1/3}}{18} - 1 \right]^+$$

Where θ is the angle between the horizontal and the cavity and [...]⁺ indicates that if the quantity in the bracket is negative, then the contents of the bracket are set to zero.

D.2 Heat Exchange between Surfaces

All surfaces in contact with air are assumed to transfer heat through both convection and radiation. Surfaces within a room exchange heat through radiation with each other with a magnitude equal to the area weighted average of all surfaces within the room. This simple modeling approach is valid for small temperature differences. This assumption increases the simulation speed considerably.

D.3 Windows and Doors

All window assemblies are modeled in the program WINDOW and imported in TRNSYS. The frame and glass assembly properties are then scale based on the shape and size of individual windows. The thermal properties and geometry of the windows are taken from the manufacturer technical datasheets. Doors are modeled as a wall assembly with a window unit if applicable. With this approach, the radiation between the door and the other surfaces of the room is then taken into consideration. Since the door surface is much colder than other surfaces of the room, this can be of importance in terms of heat losses.

D.4 Attic Thermal Network

Houses in the province of Quebec do not have an insulated attic. Instead, it is the ceiling of the storey right below the attic that is insulated. In addition, ventilation grills are installed in the soffit at the perimeter of the building and ventilation grills are installed at the peak of the roof assembly. This guarantees a good circulation in the attic to remove moisture migrating through the ceiling assembly. If not for this ventilation, moisture would condense on top of the insulation. Therefore, the attic is most often at the same temperature as the outdoor air in the winter time. However, the wind exposure is not the same as exterior walls and the solar radiation is absorbed by roof shingles. The attic in this study is therefore considered as a separate zone in the model. This is the approach that best represents the thermal dynamics of the attic.

D.5 Heat Exchanger

The heat exchanger was not integrated to the model because it was never activated during the monitoring campaign.

D.6 Vertical Air Shafts

The developed TRNSYS model is a thermal model. Only the heat transfer resulting from the airflow can be entered in the modeling environment. The magnitude of the airflow is determined from the general stack effect equation:

$$Q = CA \sqrt{2gh \frac{T_i - T_o}{T_i}}$$

where Q is the inter-storey flow, C is a discharge coefficient, A is the area of the opening, g is the gravitational acceleration, h is the height of the storey, and T_i is the room air temperature of the lower storey whereas T_o is the room air temperature of the storey above. This approach is used to represent staircases as well as the laundry chute

D.7 Integrating Infiltration Test Measurements

An infiltration test is conducted on the house using the ASTM E1827-11. The infiltration test is conducted at two different pressures, 50Pa and 12.5Pa, and a logarithmic curvature connects the results from the two pressure stations, according to a procedure

outlined by the standard. Refer to appendix for a report of the infiltration test results. The test gives the parameters C and n in the following formulae:

$$Q = C * \Delta P^n$$

Yet this equation cannot explicitly be used in a thermal model for several reasons:

- The induced pressure during the test is uniformly distributed on the building envelope which is not representative of actual operating conditions.
- The building induced pressure must be correlated to the wind speed measured at the closest meteorological station where there are no noticeable obstructions because this is where the meteorological conditions used as simulation input are recorded.

Therefore, the above formula requires to be modified to account for this:

$$Q = C * \overline{\Delta P}^n$$

Where $\overline{\Delta P}$ is the average building pressure induced by the stack effect and wind induced pressure. A relationship is set up between the wind speed in the weather file and the average building induced pressure. For low-rise buildings, Shaw et al. (1980) proposes the following formulae:

$$\overline{\Delta P} = \Delta P_{dynamic} + \Delta P_{stack}$$

$$\Delta P_{dynamic} = \frac{1}{2} \rho V^2 \cdot C_e$$

$$\Delta P_{stack} = 117 \cdot \frac{(\beta H)^{1+n}}{1+n} \cdot \left(\frac{1}{T_{out}} - \frac{1}{T_{in}} \right)$$

Where $\Delta P_{dynamic}$ is the wind induced pressure, ΔP_{stack} is the stack pressure, C_e is the exposure coefficient (0.07 for protected site and 0.15 for an exposed site), β is equal to 0.7, V is the measured wind velocity at the meteorological station and H is the height of the building. Also, the density of the air is adjusted as a function of the outdoor dry bulb temperature following the equation presented in the ASTM standard E1827-11:

$$\rho = 1.2041 \cdot \left(1 - \frac{0.0065 \cdot Alt}{293} \right)^{5.2553} \left(\frac{293}{T_{out} + 273} \right)$$

Where Alt is the altitude of the house.

In comparison to the Sherman Grimsrud model for low-rise building infiltration which is the basis for the module Type 75 in the TRNSYS platform, this calculation of house infiltration based on the work of Shaw et al. (1980) is a function of wind speed and therefore wind gusts are represented by the infiltration input to the model. This can be seen in the following figure which shows the output of both infiltration models applied to the current building for an arbitrary time-period during the year. Thus, the model presented by Shaw et al. (1980) will be used in this study.

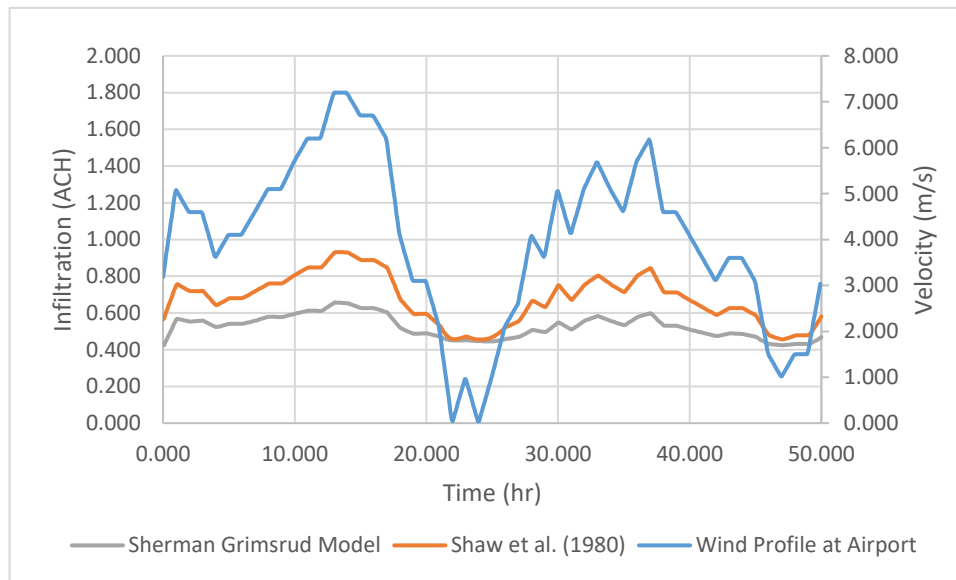


Figure 34 : Comparison of Infiltration Models as A Function of Wind Speed Recorded at Airport and Time

Distributing the infiltration per thermal zone can be a colossal challenge because wind induced pressure on a building envelope can create positive and negative pressures across the envelope depending on the geometric configuration of the building as well as wind obstructions (Lyon & Saldanha, 2016). An assumption is made in the model that the infiltration per room is proportional to the linear distance of potential cracks in the walls. This includes window and door perimeters as well as intersections between walls.

D.8 Modelling Electric Heating Cables in TRNSYS

The electric heating floors are modelled using the approach that was introduced by Thieblemont et al. (2016) which offers much more flexibility than the common active layer method for TRNSYS. This approach takes advantage of the “wall gain” capability of TRNbuild, which enables any surface within the building to receive a heat flux of which the magnitude can be correlated to an input from a thermostat. An inconvenient aspect of this approach is that the wall gain must be applied to the surface of a wall and therefore cannot be located within an assembly as would be the case for electric heating cables lodged in concrete. To go around this problem, a fictitious zone is placed below the heated floor, which includes only two walls; the combination of the two walls represents the electric heating system. A visual representation of this additional zone is shown in Figure 35.

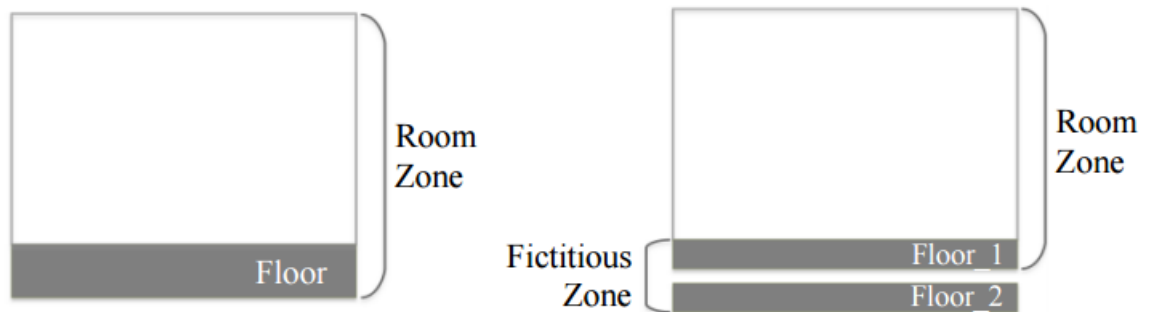


Figure 35 : Conventional Floor Assembly in TRNSYS (Left) And the Discretization of the Floor Assembly with Fictitious Zone (Right)
(Thieblemont, Haghighat, Moreau, et al., 2016)

With this configuration, the power from the electric heating cables can be represented by a uniform heat flux using the wall gain in TRNbuild. A visual representation is presented in the following figure.



Figure 36 : Discretization of Electric Heating Floor into Two Layers and a Wall Gain.
(Thieblemont, Haghighat, Moreau, et al., 2016)

D.9 Convective Heat Transfer Coefficients

The convective heat transfer coefficient between a surface and the surrounding air is highly dependent on the type of fluid flow as well as the difference in temperature

between the surface and the fluid. The TRNSYS platform has two methods of defining the heat exchange: 1) the heat exchange is a pre-defined formula that is a function of the difference of temperature between the surface and the fluid and 2) the coefficient is user-defined.

The first method is used for all assemblies that are heated with electrical heating wires. In this case the following equation is applied:

$$h = 2.11 \cdot (T_s - T_a)^{0.31}$$

The above equation can be considered valid as long as the surface temperature is higher than the air temperature. Note that it agrees with equations found in literature as the following table shows.

Table 23 : Convective Heat Transfer Coefficients for Heated Floors Found in Literature
(Zhang, Liu, & Jiang, 2012)

Equation or Value [W/m ² K]	Reference	Comments
$2.13 \Delta T^{0.31}$	(Min et al., 1956)	$\Delta T = 5 - 8^\circ C, h = 3.5 - 4.1 W/m^2 K$
$\frac{2.175}{D^{0.076}} \Delta T^{0.308}$	(Awbi & Hatton, 1999)	$\Delta T = 5 - 8^\circ C, D = 5m, h = 3.2 - 3.7 W/m^2 K$
5.3	(BS EN 1254-5, 2008)	$h_{tot} = 10.8 W/m^2 K$
5.5	(Olsen et al., 2008)	$h_{tot} = 11 W/m^2 K$
$2.11 \Delta T^{0.31}$	(Klein et al., 2014)	Valid when surface temperature higher than air temperature. $\Delta T = 5 - 8^\circ C, h = 3.48 - 4.02 W/m^2 K$

The second method is used for all other interior convective heat transfers. For interior partitions, the default TRNSYS value was used, which corresponds to 3.056 W/m²K.

Literature is not in agreement as to the appropriate convective heat transfer coefficient for the exterior face of exterior walls. Part of this is due to the numerous experimental procedures including wind tunnels, CFD simulations and full-scale testing. In many full-scale experimental procedures, only several locations on the assembly are monitored which is not representative of the large variation of wind behaviors around a building due to the geometry. Wind tunnel derived values are not representative of the geometry of actual buildings.

In this study, the wind speed and direction are taken from a weather file containing data from the closest meteorological station. The measurements are recorded at a distance of 10m from the ground from a location that is free from any upwind obstructions. A lot of literature is available for the correlation between local wind speed and the convective heat transfer coefficient on a building. Yet, only a handful of papers have proposed correlations between a building's surface averaged convective heat transfer coefficients and airport weather measurements. These include:

Table 24 : Surface Averaged Exterior Convective Heat Transfer Coefficients

Equation [W/m ² K]	Wind Speed Range [m/s]	Building Geometry	Procedure	Reference	Comments
5.15 U ₁₀ ^{0.81} (short wall) 4.84 U ₁₀ ^{0.82} (long wall)	1 - 15	Rectangular (6x8x2.7m)	CFD Simulations	(Emmel et al., 2007)	Wall size influence is almost negligible
4.6 U ₁₀ ^{0.89}	1 - 4	Cubic, 10m high	CFD Simulations	(Blocken et al., 2009)	Wind speed range is too small to use in this study
5.15 U ₁₀ ^{0.89}	0.05 - 5	Cubic, 10m high	CFD Simulations	(Defraeye et al., 2010)	Wind speed is too small to use in this study.
5.01 U ₁₀ ^{0.85} (Windward) 2.27 U ₁₀ ^{0.83} (Leeward)	0.15 - 7.5	Isolated cube	CFD Simulations	(Defraeye et al., 2011)	Leeward coefficient is almost half of windward coefficient.
5.62 U ₁₀ ^{0.84} (Windward)	0 - 5	Isolated cube (20x15x10m)	CFD Simulations	(Montazeri et al., 2015)	Wind speed is too small to use in this study.
1.53 U ₁₀ + 1.43 (Windward) 0.90 U ₁₀ + 3.28 (Leeward)	0 - 16	Rectangular (8.5x8.5x5.6m)	Full Scale Measurements	(Liu & Harris, 2007)	Experimental building is much shorter than building in this study.
$\frac{\sqrt{(0.84 \Delta T^{\frac{1}{3}})^2 + (2.38 U_{10}^{0.89})^2}}{\text{(Windward)}}$ $\frac{\sqrt{(0.84 \Delta T^{\frac{1}{3}})^2 + (2.86 U_{10}^{0.617})^2}}{\text{(Leeward)}}$	0 - 12	Small, single-storey, rectangular	Full Scale Measurement	(Yazdanian & Klems, 1993)	Applies to single storey buildings
2.9 U ₁₀ + 5.3 (Windward) 1.5 U ₁₀ + 4.1 (Leeward)	0 - 12	Tower (20x36x78m)	Full Scale Measurement	(Sharples, 1984)	For high-rise buildings

The interpretation of the above equations is highly subjective as they depend on many parameters that are case specific. All studies enumerated in the above table that determined correlations based on full scale measurements used buildings that are either too

high or too short. On the other hand, CFD simulations account for a single building with total exposure to the wind.

For the model in this study, the house is considered fully exposed because of its location within the neighborhood. In addition, for most equations with building geometries similar to the one modelled here, the surface average convective heat transfer coefficient is proportional to U_{10}^α where α is approximately equal to 0.85. But, there is a difference between windward and leeward surfaces. Therefore, the equations implemented in the model have the following form:

$$h_{WW,average} = 5.01 U_{10}^{0.85} \text{ (Windward)}$$

$$h_{LW,average} = 2.27 U_{10}^{0.83} \text{ (Leeward)}$$

D.10 Hot Water Tank

This house is equipped with a residential electric hot water tank of 279 liters. The standby losses correspond to 89-Watts based on the manufacturer specifications sheet. This is not the total consumption of the heater but only the required energy to maintain the water at 60°C. This corresponds to the gains from the tank to the room in which the heater lies.

The remainder of the heater consumption is monitored with a web-enabled in line switch. Hot water can be used in a variety of applications within the house including kitchen, faucets as well as showers. These activities, however, cannot be monitored during the monitoring campaign. It is assumed that hot water usage dissipates little to no heat to the rooms because most of the sensible heat is lost from the water flowing in the drain.

D.11 Thermostats

For the model to behave exactly like the building, the virtual thermostats must output the same control signal as the real thermostats. This is challenging because the control algorithm of the installed thermostats is unknown. However, one detail is known about them, which is that the basic structure of the control is of the Proportional-Integral (PI) type.

In terms of the TRNSYS model development, care must be taken before setting all virtual thermostats to follow the PI format. As seen on TRNSYS forums, the PI controller

module (Type 23) lacks hysteresis and hence this can cause the FORTRAN solver to crash prematurely. This is due to the assumptions behind conventional thermal modelling of buildings: the thermal zones are assumed to be at a uniform temperature. The influence of energy inputs from heating/cooling equipment are instantaneously seen in the temperature of the zone. In reality, heating/cooling equipment are often not placed directly next to thermostats and therefore there is some time lag between the activation of the conditioning equipment and the associated response of the zone air temperature local to the thermostat. In simulation, controllers that are not developed for this can toggle on and off at a very high frequency which can lead to a TRNSYS simulation crash.

Solutions to this issue exist. One of them involves the addition of a fictional pipe between the PI output and the building module input. This does not influence the total energy balance since the energy input of the pipe corresponds to its output. However, it does prevent the controller from toggling between states at a high frequency. The computational cost of this approach must be taken into consideration though. Another method of implementing a control is using the stage controller (Type 108). This approach is robust because of its simplicity. However, loss of accuracy must be analyzed because of this simplification. Both these approaches are experimented to determine the most feasible virtual controller architecture. If there is no considerable difference in accuracy between the two methods, the stage controller is prioritized because of its lower computational cost and ease of implementation in the TRNSYS environment.

D.11.1 PI-Controller Structure

Type 23 in TRNSYS is a modified version of the “textbook” PID controller. Once discretized, the following architecture represents its implementation:

$$P(t) = K(b \cdot T_{set} - T_{MT}(t))$$

$$I(t) = I(t - 1) + \frac{Kh}{T_i} (T_{set} - T_{MT}(t)) - \frac{h}{T_t} \cdot (I(t - 1) + P(t - 1) - u(t))$$

$$HL(t) = P(t) + I(t)$$

Where $P(t)$ is the proportional component of the control and $I(t)$ is the integral component. Also, K is the controller gain, b is the set point weighing factor, T_{set} is the set

point temperature, $T_{MT}(t)$ is the monitored temperature at time t . Next, h is the time step length, T_i is the integral tracking time, T_t is the anti-windup tracking time, $u(t)$ is the saturate function and $HL(t)$ is the output of the controller. There are therefore four parameters to optimize: the controller gain, set point weighing factor, integral tracking time and anti-windup tracking time.

D.11.2 Stage Controller Structure

Type 108 is a 5-stage controller, where 2 stages are for cooling and 3 are for heating. In this application, only heating stages are utilized. The structure of this controller is very simple, the input temperature signal is compared to three set points, each set point representing an increasingly high output signal. The number of oscillations per time step permitted and dead band are also parameters that can be adjusted for stability of the modelling environment. The following set of equations represents the core of the controller:

$$CS_i(t) = \begin{cases} T_{MT}(t) \leq T_{Set,i} & 1 \\ T_{MT}(t) > T_{Set,i} & 0 \end{cases}$$

$$HL(t) = CS_{1^{st} \text{ stage}}(t) \cdot A + CS_{2^{nd} \text{ stage}}(t) \cdot B + CS_{3^{rd} \text{ stage}}(t) \cdot C$$

Where, T_{MT} is the monitored temperature (either floor temperature or zone air temperature), $T_{Set,i}$ is the set point temperature of stage i , CS_i is the control signal of stage i and $i \in [1,3]$. In addition, HL is the heat level output of the controller, which varies between 0 to 100 (0 being fully deactivated and 100 being fully activated), and A , B and C are the power intensities of stage 1, 2 and 3 respectively subject to the following constraint:

$$A + B + C = 100$$

Thus, 6 parameters are to be optimized: the power intensities of the three stages as well as the set point temperature of the three stages.

D.11.3 Optimisation Process

The optimisation process is conducted independently from the building model. The simulated thermostats need to generate the same output signal as the real thermostat, given the same input. The experimental air set point temperatures as well as the recorded air temperatures are the input to the simulated thermostats.

The above-mentioned controllers are optimized based on minimizing two performance indicators: MBE and CVRMSE. An MBE close to zero indicates that across the simulation, the total energy consumption of the simulated thermostat is similar to the real thermostat. A CVRMSE close to zero is an indicator of the precision of the simulated thermostat across the simulation.

There are several optimisation constraints. First, to reduce the simulation time required for the optimisation, the parameters are permitted to increase only in pre-defined increments. This makes the optimization a mixed-integer linear problem and not all solving algorithms are suited for this kind of application. In addition, due to the high number of parameters to optimize, the solution space is very flat and therefore the gradient of steepest descent is hard to determine for many optimisation algorithms. It causes some algorithms to sometimes search out of initially prescribed boundaries. Of the packages available from the MATLAB software, the genetic algorithm solver is chosen because of its compatibility with the mentioned constraints. In addition, the genetic algorithm is one of the few that can deal with TRNSYS simulations that crash. Certain combinations of parameters, even though they lie between the imposed mathematical optimisation constraints, can be unfeasible from a physical point of view making the TRNSYS solver crash. In this case, the optimisation algorithm needs to skip to a new set combination of parameters.

The optimisation is set to reduce an objective function being a weighted linear combination of the above-mentioned performance indicators. The objective function is defined as the following:

$$\min(f) = \alpha \cdot \overline{MBE} + \beta \cdot \overline{CVRMSE}$$

$$\alpha \in [0,1]; \beta = 1 - \alpha$$

where f is the function to minimize and α and β are the relative weights of each performance indicator. The solution space of this function is quite flat and there are many

combinations of parameters that can produce good performance. Varying the relative importance of each performance indicator modifies the way the algorithm searches the solution-space, and this can generate a portfolio of solutions from which to choose from.

D.11.4 Simulated Thermostats

The optimisation process was using 31 different combinations of NMBE and CVRMSE relative weights when compiling the objective function value. This gives 31 different and independent simulation processes. Every physical thermostat is replicated in the simulation environment. But, the controller parameters are kept the same throughout all simulated thermostats. This is to represent as best as possible actual conditions where the same controller model is installed in various rooms without any pre-defined adjustments as a function of room geometry or thermal mass.

The results of the optimisation are presented in tables Table 26 and Table 27. In both cases, the stage controller had slightly better results than the PI controller. In addition, the PI structure has an integral gain that is low both for baseboard and EHF thermostats. This shows that a proportional type controller can very well be used as a simulated thermostat to represent actual thermostats.

Table 25 : Optimisation Parameter Description

Controller	Parameter	Description
PI	A	Proportional Gain
	B	Integral Gain
	C	Fraction of set point for proportional effect
	D	Anti-windup time for integral gain
Stage	A	Heat level of first stage
	B	Heat level of second stage
	C	Heat level of third stage
	D	Difference between room set point and first stage set point
	E	Difference between room set point and second stage set point
	F	Difference between room set point and third stage set point

Table 26 : Simulated Baseboard Thermostat Optimisation Results

Controller Structure	Parameter Values						Performance		Simulated Parameter Combinations
	A	B	C	D	E	F	CVRMSE	NMBE	
PI	35	0.25	0.85	0.075	N.A.	N.A.	9.20%	2.24%	6911
Stage	18	28	54	-0.05	0.15	0.3	8.57%	1.71%	1141

Table 27 : Simulated EHF Thermostat Optimisation Results

Controller Structure	Parameter Values						Performance		Simulated Parameter Combinations
	A	B	C	D	E	F	CVRMSE	NMBE	
PI	23	2.25	0.8	0	N.A.	N.A.	28.36%	17.12%	7391
Stage	31	31	38	-0.6	0.1	0.5	27.39%	12.82%	2869

The tables above show that there is a negligible advantage to using a PI controller for this thermal energy model. Both the NMBE and CVRMSE show similar performance results. Due to this, the stage controller structure is chosen for its simplicity and stability.

D.12 Internal Heat Gains

The internal heat gains are not explicitly monitored during the monitoring campaign. However, all heating systems are monitored as well as the total electricity consumption is obtained from the utility company. Therefore, the net consumption of appliances and other electrical devices can be obtained from the difference between the total building consumption and the summation of the heating systems.

Not all electrical devices installed on this building's electrical network have thermal heat losses to the interior. As an example, the pool heat pump and exterior lighting. However, most electrical systems installed outdoors can be assumed to have negligible power consumption during the winter season. All but one, which corresponds to an electric heating cables installed in the driveway to melt the snow. However, this system has a high power consumption and can easily be identified. Therefore, by comparing the days with and without snow, the electrical consumption of this system can easily be identified. Figure 37 shows the total space heating consumption as well as the building total power consumption. For most of time, the space heating needs are almost identical to the total building consumption. Figure 38 shows the difference between the total building electricity consumption and the space heating electricity consumption as well as the snow fall during this period, obtained from Environment Canada. The snow fall profile shows two distinct values: 1 and 0, which correspond to either "snow" or "no snow".

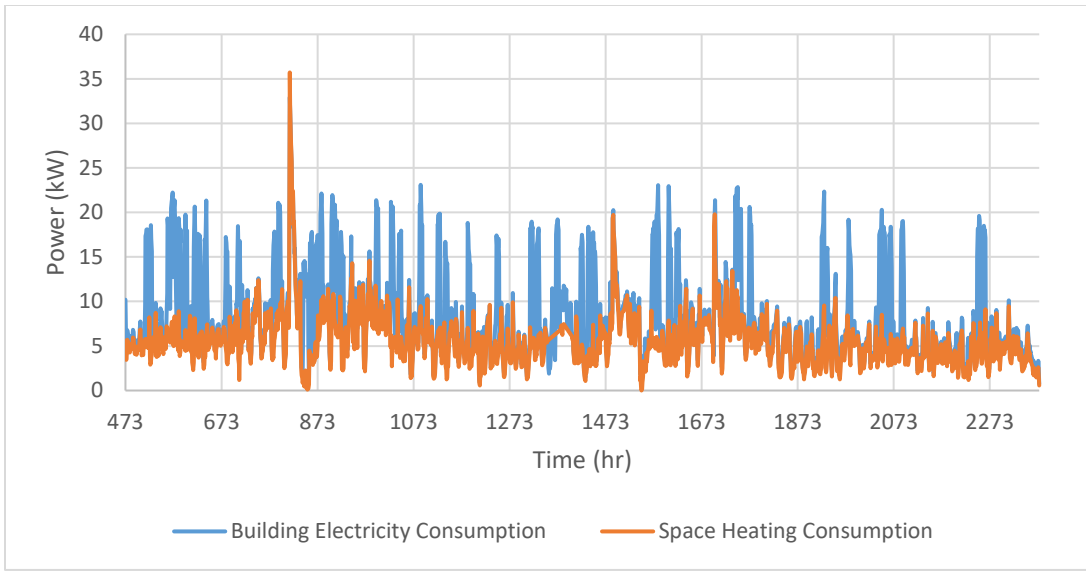


Figure 37 : Total Building Electricity Consumption Versus Space Heating Consumption

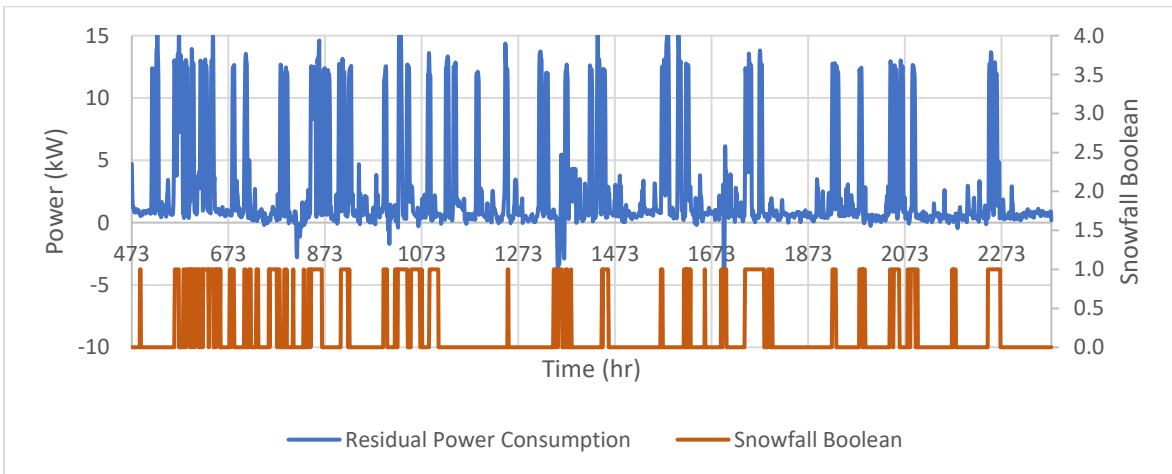


Figure 38 : Residual Electricity Consumption and Snow Fall

The above graph show that every time that there is a snow fall, the electric heating wires trigger shortly after. The energy consumption of interior electrical devices is therefore obtained from instances where the driveway heating system is not activated. The residual energy consumption corresponds to energy consumed by all electric devices inside the house that were not explicitly modelled.

For the purposes of the modelling needs of this thesis, the power consumption of electrical devices is assumed to be converted entirely to heat dissipated inside the building. By sorting the residual power consumption as a function of the hour of the day, a daily

profile can be obtained for the internal heat gains of the building as presented by Figure 39. It is assumed that the heat gains during week days are similar to week end days. This is unusual, yet it represents the habits of the occupants of this building. The internal heat gains are distributed uniformly within the building.

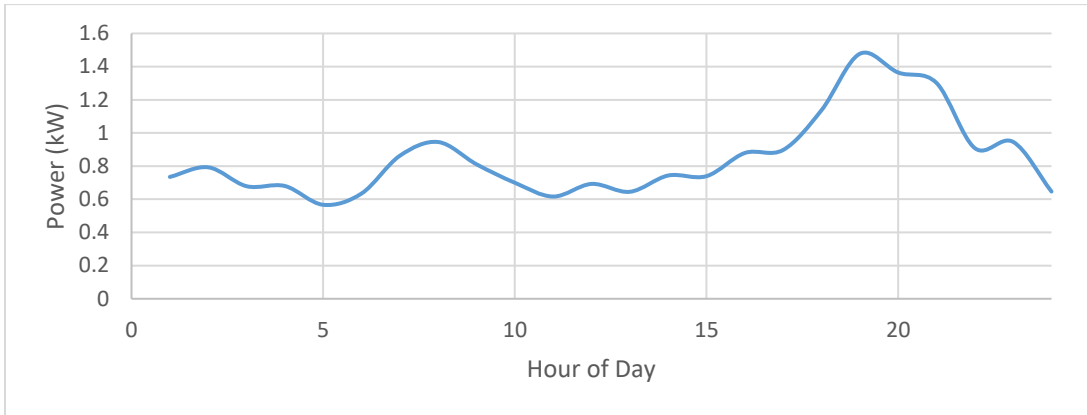


Figure 39 : Residual Consumption as a Function of the Hour of Day

APPENDIX E – Infiltration Test Report

This appendix presents the infiltration test report conducted on the home using the ASTM E1827-11 standard. The format of the report follows the requirements of the standard.

Infiltration Assessment Report



Designation: E1827-11

Dave Olsthoorn¹, H  l  ne Thieblemont¹

¹Department of Building, Civil and Environmental Engineering,
Concordia University, Montreal, Canada, H3G 1M8



E.1. General Information

Test Standard: ASTM E1827-11
Standard Test Methods for Determining Air Tightness of Buildings Using an Orifice Blower

Date of Test: October 26th, 2016

Date of Report: November 3rd, 2016

Building Owner:

Building Representative

During Test:

Test Conducted by: Dave Olsthoorn

Statement: This test was conducted following the above-mentioned ASTM standard procedure for the intent of simulation model input only. In no way can this document be used for any other purpose.

E.2. Building Description

E.2.1 Location

The front facade of the building is oriented south.

E.2.1.1 Elevation

The elevation of the building is 113m from sea level. It was taken from the local meteorological station and confirmed with a GPS activated device.

E.2.2 Construction

E.2.2.1 Date Built

The building was constructed in 2008-2009 based on construction plans.

E.2.2.2 Floor Areas

Table 28 : Livable Space per Room and Storey

Level	Room	Area [m²]
Basement	Bedroom #1	14.26
	Family Room	54.76
	Bathroom	8.61
	Bedroom #2	11.63
	Laundry Room/Storage	52.52
Ground Floor	Kitchen	42.38
	Dining Room/Living Room	38.52
	Garage	42.99
2 nd Floor	Bedroom #3	13.23
	Bedroom #4	12.17
	Bathroom	4.96
	Hallway	14.30
	Master's Bathroom	11.14
	Master's Bedroom	24.72
	Office/Gym Area	42.89

E.2.2.3 Surface Area of Building Envelope

The total building envelope area is 325.04 m². The air barrier system was taken as the envelope area for this test.

E.2.2.4 Volumes of Spaces

Table 29 : Volume per Room and Storey

Level	Room	Volume [m ³]
Basement	Bedroom #1	32.51
	Family Room	124.85
	Bathroom	19.63
	Bedroom #2	26.52
	Laundry Room/Storage	119.75
Ground Floor	Kitchen	102.98
	Dining Room/Living Room	93.60
	Garage	104.47
2 nd Floor	Bedroom #3	32.15
	Bedroom #4	29.57
	Bathroom	12.05
	Hallway	34.75
	Master's Bathroom	27.07
	Master's Bedroom	60.07
	Office/Gym Area	104.22

E.2.3 Condition of Openings in Building Envelope

E.2.3.1 Type of Test Selected

The “occupied” test is selected because this best represents actual conditions under which the simulation will be run.

E.2.3.2 Condition of Building Elements

Table 30 : Recorded Conditions of the Building Elements

Building Component	Test Requirement	Condition During Test	Remarks
Vented combustion appliance	Off	Off	There were 2 slow burning wood stoves. Both had not been used for several days
Pilot light	As found	N.A.	Not applicable
Flue to nonwood combustion appliance	Sealed	N.A.	Not applicable
Flues for fireplaces and wood stoves with dampers	Closed	Closed	Both stove dampers were checked
Flues for fireplaces and wood stoves without dampers	Ashes removed	N.A.	Not applicable
Fireplace and wood stove doors and air inlet dampers	Closed	Closed	Checked
Fireplace without firebox doors	No preparation	Checked	Checked
Furnace room door for furnace outside test zone	Closed	N.A.	Not applicable
Combustion air intake damper for wood stove or fireplace	Closed	N.A.	Not applicable
Make up air intake damper for furnace inside test zone	Sealed	N.A.	Not applicable
Make up air intake for furnace inside test zone without damper	Sealed	N.A.	Not applicable

Exhaust and supply fans	Off	Off	Only one that is connected to outside: the kitchen hood
Fan inlet frills with motorized damper	Closed	N.A.	Not applicable
Fan inlet grills without motorized damper	Sealed	N.A.	Not applicable
Ventilators designed for continuous use	Sealed	Sealed	Air exchanger was disconnected
Supply and exhaust ventilator dampers	Sealed	Sealed	Sealed from outside
Clothes dryer	Off	Off	Turned off during test
Clothes dryer vent	No preparation	Checked	Checked
Ventilation to other zones	Sealed	N.A.	Not applicable
Windows and exterior doors	Latched	Latched	Checked
Window air conditioners	Sealed	N.A.	Not applicable
Openings leading to outside the test zone	Closed	N.A.	Not applicable
Openings within the test zone	Open	Open	Kept open with wood wedges
Floor drains and plumbing traps	Filled	Filled	Checked

E.2.3.3 Initial Pressure

The equipment used during this test is self-adjusting. There is no need to record this parameter.

E.2.4 HVAC System

This building has very few penetrations for HVAC applications because of the fact that it is a NovoClimat certified house. Figure 40 a) shows two penetrations on the East façade. The left grill is the inlet for the wood stoves, which is made of a 5” duct. The right opening is the outlet for the heat exchanger which is made of a 6” duct. Figure 40 b) shows the exhaust for the clothes dryer which is made of a 4” duct. Figure 40 c) shows the exhaust for the kitchen hood which is made of a 6” duct. Figure 40 d) shows the inlet for the heat exchanger which is made of a 6 inch duct. All bathroom fan exhausts pass through the heat exchanger.

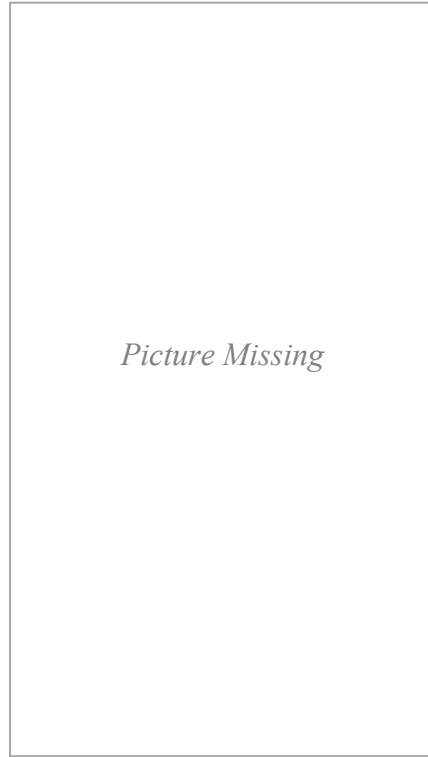
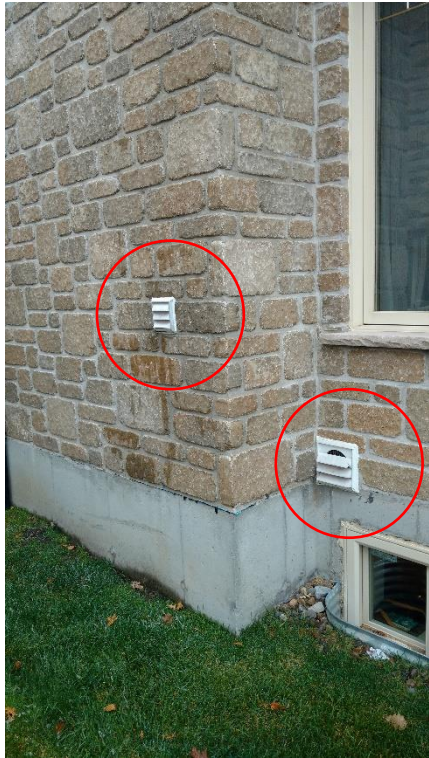


Figure 40 : A) Envelope Penetrations on East Facade (Top Left), B) Envelope Penetration on North Facade (Top Right), C) Other Envelope Penetration on East Facade (Bottom Left) And D) Envelope Penetration on South Facade (Bottom Right)

E.3. Procedure

E.3.1 Technique Employed

The single-point method was conducted for the building owner's personal information as well as for a basis for comparison with the NovoClimat's accepted value. The two-point method was conducted because the output parameters of this method are what is needed as input for the infiltration model used for simulation. The curve obtained from the two-point method is compared with a manual curve obtained from a scatter of points recorded during the test. The building was only depressurized during the test. The blower door apparatus could not maintain the pressure required for pressurization.

E.3.2 Test Equipment Used

The equipment used in this test is a Minneapolis Model-3 Single Fan Blower Door from The Energy Conservatory.

E.3.3 Calibration Date of Fan Pressurization Device

Calibrated on September 29th, 2016.

E.3.4 Calibrated Density

The air density at calibration is 1.204 kg/m³.

E.4. Measurement Data

E.4.1 Fan Pressurization Measurements

E.4.1.1 Inside-Outside Zero Flow Building Pressure Differences

The equipment used during this test is self-adjusting. There is no need to record this parameter.

E.4.1.2 Air Leakage Measurements

E.4.1.2.1 Primary Pressure Station ($P \approx 50\text{Pa}$)

Table 31 : Recorded Air Leakage at Primary Pressure Station

Measurement No.	Measured Pressure [Pa]	Nominal Air Leakage [cfm]	Nominal Air Leakage [m^3/s]
1	52.4	1500	0.708
2	50.1	1508	0.712
3	49.4	1508	0.712
4	49.7	1531	0.723
5	51.3	1508	0.712

E.4.1.2.2 Secondary Pressure Station ($P \approx 12.5\text{Pa} < 16\text{Pa}$)

Table 32 : Recorded Air Leakage at Secondary Pressure Station

Measurement No.	Measured Pressure [Pa]	Nominal Air Leakage [cfm]	Nominal Air Leakage [m^3/s]
1	13.8	961	0.454
2	13.9	949	0.448
3	14.3	949	0.448
4	13.9	884	0.417
5	14.3	1508	0.712

E.4.1.2.3 Other Pressures

Table 33 : Recorded Air Leakage at Various Pressures

Measurement No.	Measured Pressure [Pa]	Nominal Air Leakage [cfm]	Nominal Air Leakage [m^3/s]
1	13.8	961	0.454
2	13.9	949	0.448
3	14.3	949	0.448
4	13.9	884	0.417
5	14.3	911	0.430
6	52.4	1500	0.708
7	50.1	1508	0.712
8	49.4	1508	0.712
9	49.7	1531	0.723

10	51.3	1508	0.712
11	63.9	1561	0.737
12	62.8	1619	0.764
13	62.1	1508	0.712
14	64.3	1668	0.787
15	58.1	1561	0.737
16	54.9	1531	0.723
17	55.3	1515	0.715
18	41.9	1256	0.593
19	42.6	1256	0.593
20	41.9	1362	0.643
21	47.9	1387	0.655
22	48.5	1445	0.682
23	47.7	1421	0.671
24	49.3	1379	0.651
25	37.3	1189	0.561
26	39.0	1274	0.601
27	39.1	1328	0.627
28	40.1	1336	0.631
29	35.7	1328	0.627
30	36.3	1199	0.566
31	32.8	1208	0.570
32	30.6	1256	0.593
33	30.7	1139	0.538
34	28.3	1159	0.547
35	28.2	1208	0.570
36	26.7	1199	0.566
37	22.9	1139	0.538
38	22.1	1086	0.513
39	19.1	1043	0.492
40	11.2	815	0.385
41	11.4	843	0.398
42	9.5	802	0.379
43	8.1	673	0.318

E.4.1.3 Deviations from Standard Procedure

The procedure applied is the one suggested by the standard.

E.4.2 Ancillary Data

E.4.2.1 Weather Measurement Apparatus

No apparatus was set up for the measurement of weather conditions during this test. Instead, the conditions of the local meteorological station were used as an estimate of the conditions that the house is subjected to.

E.4.2.2 Wind Information

The winds for the duration of the test were very low, not exceeding the 2m/s criterion.

E.4.2.3 Inside and Outside Temperature

The outdoor temperature was taken from the local meteorological weather station. It was recorded at the beginning and end of the procedure and its value be equal to 1°C for both. The inside temperature was taken from the thermostats installed throughout the house. Their value were 20°C.

E.5. Calculations

E.5.1 Means and Standard Deviations

E.5.1.1 Primary Pressure Station ($P \approx 50Pa$)

Table 34 : Calculated Means and Standard Deviations of Data Points for Primary Pressure Station

Pressure [Pa]	Nominal Flow Rate [m3/s]	Fan Flow Rate [m3/s]	Envelope Flow Rate [m3/s]
Data			
52.4	0.708	0.689	0.644
50.1	0.712	0.693	0.648
49.4	0.712	0.693	0.648
49.7	0.723	0.703	0.658
51.3	0.712	0.693	0.648
Means			
50.580	0.713	0.694	0.649
Standard Deviations			
1.116	0.005	0.005	0.004

E.5.1.1 Secondary Pressure Station ($P \approx 12.5Pa < 16Pa$)

Table 35 : Calculated Means and Standard Deviations of Data Points for Primary Pressure Station

Pressure [Pa]	Nominal Flow Rate [m3/s]	Fan Flow Rate [m3/s]	Envelope Flow Rate [m3/s]
Data			
13.8	0.454	0.441	0.413
13.9	0.448	0.436	0.408
14.3	0.448	0.436	0.408
13.9	0.417	0.406	0.380
14.3	0.712	0.419	0.391
Means			
14.04	0.439	0.428	0.400
Standard Deviations			
0.2154	0.0136	0.0132	0.0124

E.5.2 One-Point Method

Table 36 : Envelope Leakage Rate and ACH at 50 Pa

Description	Variable	Unit	Value
Envelope Leakage Rate @ 50Pa	Q_{50}	m^3/s	0.646
Air Change Per Hour @ 50Pa	ACH_{50}	hr^{-1}	2.52

E.5.3 Two-Point Method

Table 37 : Logarithmic Coefficients from Two-Point Method

Description	Variable	Unit	Value
Flow Exponent	n	Dimensionless	0.378
Flow Coefficient	C	m ³ /s·Pa ⁿ	0.154
Effective Leakage Area	L	m ²	0.101
Reference Pressure	P _{ref}	Pa	4
Air Leakage Rate @ 50Pa	Q ₅₀	m ³ /s	0.724

Based on the above calculated coefficients, the following equation can be used in order to find the relationship between the building envelope leakage rates as a function of wind-induced pressure:

$$Q = C \cdot \Delta P^n$$

And henceforth giving the following tablature and graph for the studied building:

Blower Induced Pressure [Pa]	Envelope Leakage Rate [m ³ /s]
0	0.000
5	0.286
10	0.371
15	0.433
20	0.483
25	0.525
30	0.563
35	0.596
40	0.627
45	0.656
50	0.682
55	0.708
60	0.731
65	0.754
70	0.775
75	0.796
80	0.815
85	0.834
90	0.852
95	0.870
100	0.887

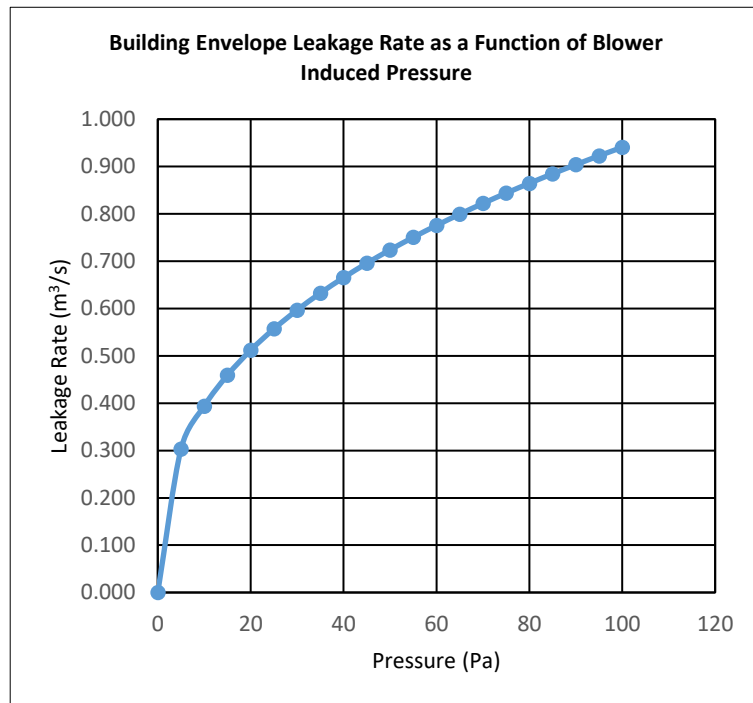


Figure 41 : Building Envelope Leakage Rate as a Function of Blower Induced Pressure

E.5.4 Manual Curve

Note that this section is not part of the original ASTM procedure for the blower door test. This is meant as a comparison between the exponential curve obtained from the two-point method and manually tracing the curve from a scatter of measurements.

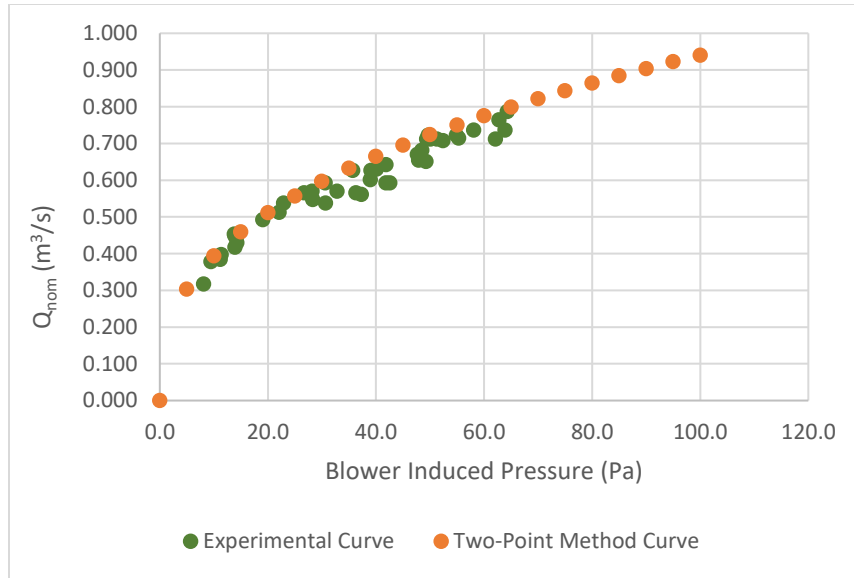


Figure 42 : Comparison of Infiltration Curve as a Function of Test Procedure

We can see from the above figure that there is good agreement between the experimental curve and the exponential curve obtained from the two-point method. One thing to note is that the two-point curve is the upper bound past which there are no points displayed. Of the two procedures, the two-point method is more conservative.

E.5.5 Error Calculations

E.5.5.1 Minimum Assumed Bias

Table 38 : Recommended Bias

Measurement	Recommended Condition	Ideal Condition	Units
Air Flow	3	1	%
Pressure Difference	1	0.1	Pa
Flow Exponent Uncertainty (Single Point Method)	0.15	0.15	Dimensionless
Temperature	0.5	0.5	°C

E.5.5.2 Single-Point Method

Table 39 : Precision Indexes and Estimated Biases from Single-Point Method

PRILIMINARY DATA ANALYSIS			
Measurement	Variable	Unit	Value
Precision Index of the Average of the Measured Flow Rate	$\delta Q_{\text{precision}}$	m ³ /s	0.002
Precision Index of the Average of the Measured Pressure Differential Across the Building Envelope	$\delta P_{\text{precision}}$	Pa	0.499
Estimated Bias of the Flow Rate	δQ_{bias}	m ³ /s	0.007
Estimated Bias of the Pressure Differential Across the Building Envelope	δP_{bias}	Pa	0.580

Table 40 : Measurement Uncertainty of Single-Point Method

Measurement	Variable	Unit	Precision	Bias	Measurement Uncertainty
Envelope Leakage Rate @ 50Pa	Q ₅₀	m ³ /s	0.72%	1.27%	2.36%
Air Change Per Hour @ 50Pa	ACH ₅₀	hr ⁻¹	-	-	5.53%

E.5.2.3 Two-Point Method

Table 41 : Precision Indexes and Estimated Biases from Two-Point Method

PRILIMINARY DATA ANALYSIS			
Measurement	Variable	Unit	Value
Precision Index of the Average of the Measured Flow Rate at the Primary Pressure Station	$\delta Q_{\text{precision},1}$	m ³ /s	0.002
Precision Index of the Average of the Measured Flow Rate at the Secondary Pressure Station	$\delta Q_{\text{precision},2}$	m ³ /s	0.006
Precision Index of the Average of the Measured Pressure Differential Across the Building Envelope at the Primary Pressure Station	$\delta P_{\text{precision},1}$	Pa	0.499
Precision Index of the Average of the Measured Pressure Differential Across the Building Envelope at the Primary Secondary Station	$\delta P_{\text{precision},2}$	Pa	0.096
Estimated Bias of the Flow Rate at the Primary Pressure Station	$\delta Q_{\text{bias},1}$	m ³ /s	0.007
Estimated Bias of the Flow Rate at the Primary Secondary Station	$\delta Q_{\text{bias},2}$	m ³ /s	0.004
Estimated Bias of the Pressure Differential Across the Building Envelope at the Primary Pressure Station	$\delta P_{\text{bias},1}$	Pa	0.580
Estimated Bias of the Pressure Differential Across the Building Envelope at the Primary Secondary Station	$\delta P_{\text{bias},2}$	Pa	1.540

Table 42 : Measurement Uncertainty of Two-Point Method

Measurement	Variable	Unit	Precision	Bias	Measurement Uncertainty
Flow Exponent	n	Dimensionless	1.16%	3.43%	4.71%
Flow Coefficient	C	m ³ /s·Pa ⁿ	4.43%	13.25%	18.07%
Effective Leakage Area	L	m ²	-	-	-
Reference Pressure	P _{ref}	Pa	2.83%	8.51%	11.58%

E.6. Calibration Certificates

E.6.1 Statement of Means of Calibration

The report of calibration is unavailable for this test apparatus. However, a statement of calibration is identified on the Digital Pressure and Fan Flow Gauge (Model DG-3) as shown in the picture below.



Figure 43 : Statement of Calibration of Test Apparatus

E.6.2 Statement of Precision and Bias of Instruments

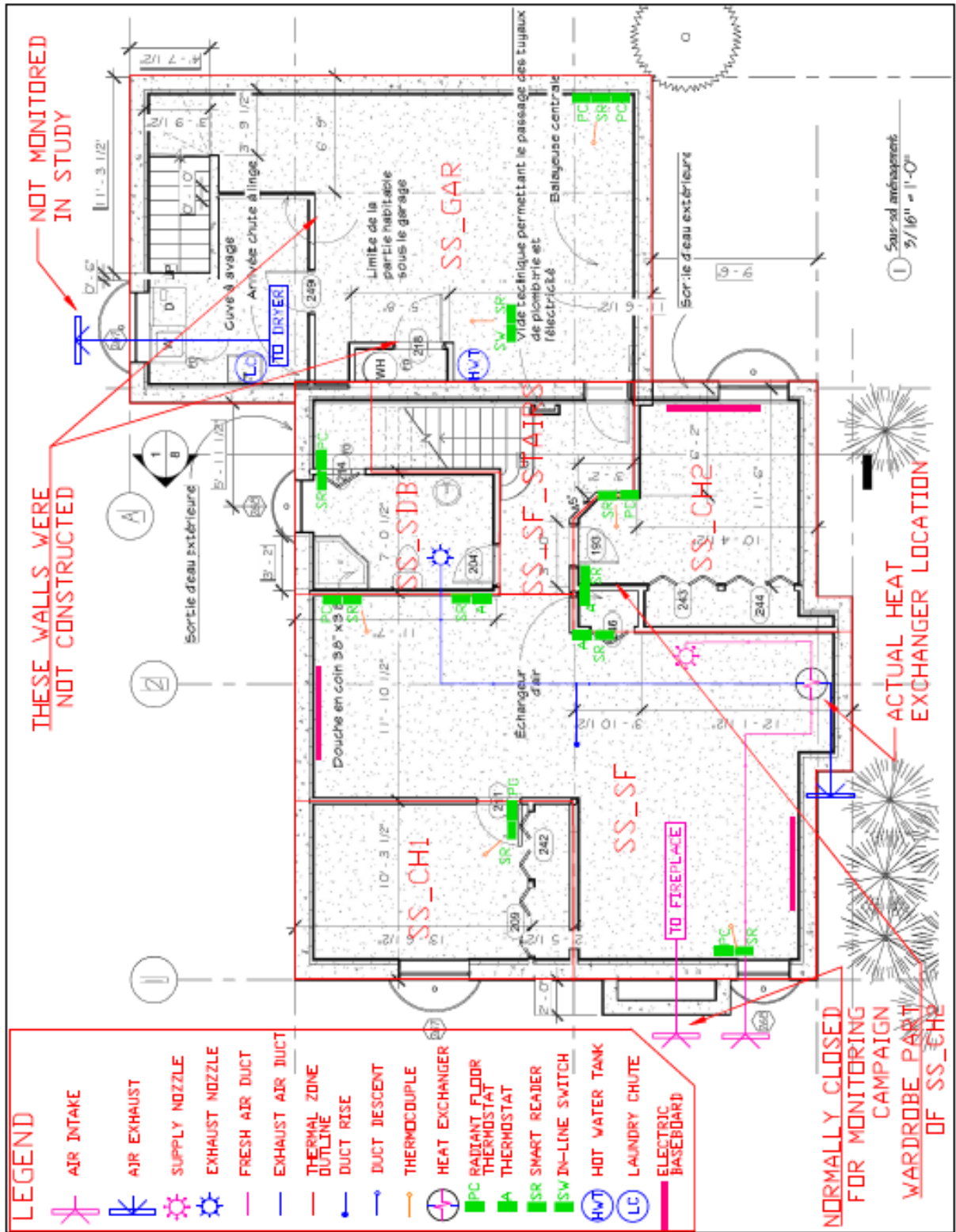
The precision and bias were assumed for this infiltration test. Minimum values suggested by the standard were utilized in the calculation of errors.

APPENDIX F – House Parameters

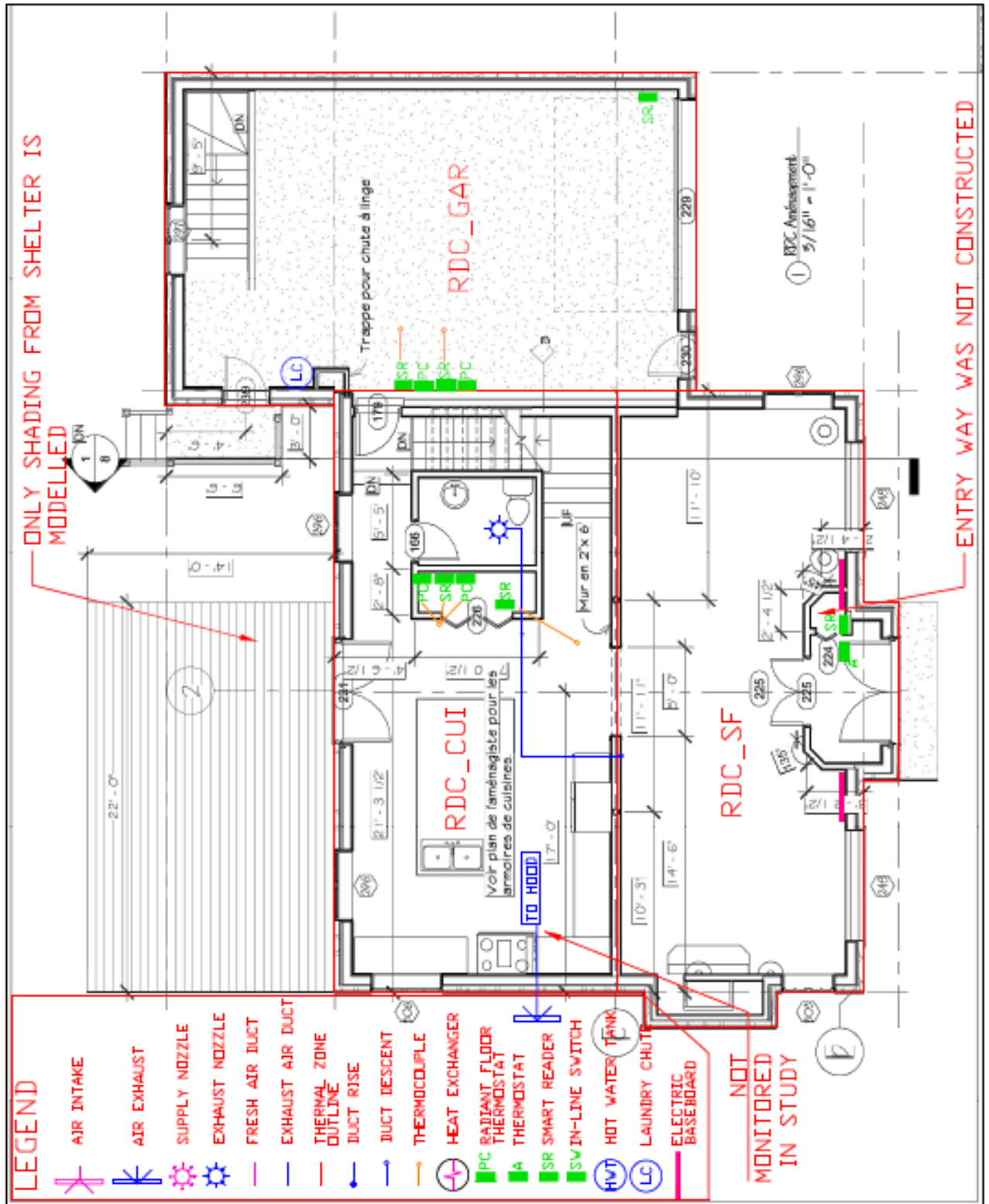
This appendix presents technical details of the house that was monitored. Differences between the constructed building and the architectural plans are highlighted. The thermal zones used for the model are presented as well as the zone labels used for the TRNSYS thermal model. All ventilation and heating equipment is presented and detailed. Please note that these drawings are not presented to scale.

F.1 House Plans

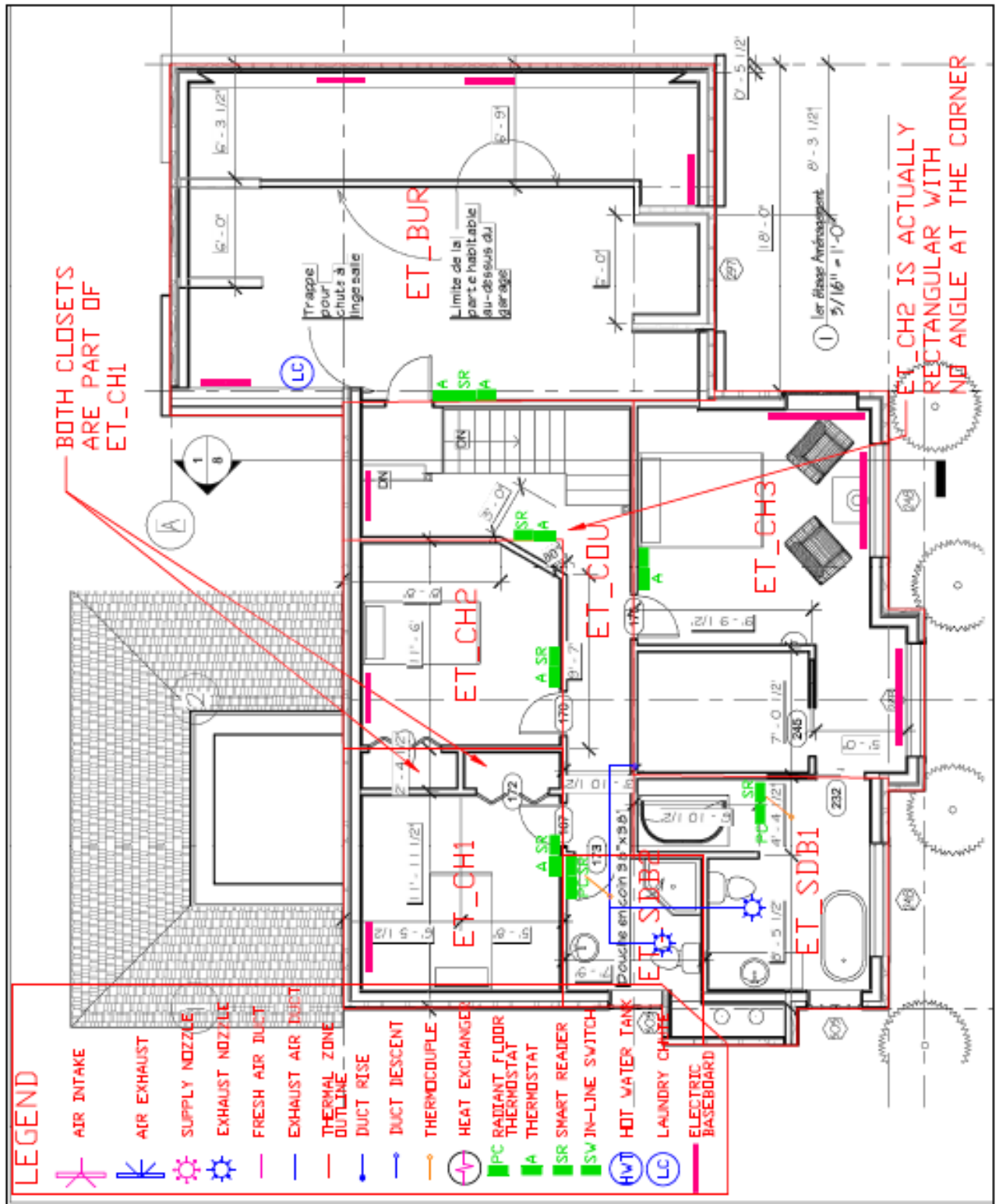
F.1.1 Basement



F.1.2 Ground Floor



F.1.3 Second Floor



F.2 Heated Floor Construction

This section presents pictures of the construction of the basement slab. The pictures are to highlight the position of the heating cables and temperature probes with respect to the rooms and exterior walls. Figure 44, for instance, shows the heating cable configuration for room SS-CH2. As can be seen, there are no cables underneath the wardrobes. The main section of the room has a bed with a base in direct contact with the ground. Therefore, a considerable portion of the heat from the cables are underneath furniture with a limited convective heat transfer coefficient. The electric heating cables stretch out of the room and partly heat the hallway leading to the stairs.



Figure 44 : Heating Cables for SS-CH2, SS-SF-STAIRS and SS-SF

Figure 45, on the other hand, shows the EHF for rooms SS-SF, SS-SDB and SS-CH1. There is no overlap of the heating systems in between rooms. No heating cables are located in the bedroom wardrobe. Room SS-CH1 has a similar issue to SS-CH2 where a bed with a large base limits the convective heat transfer between the floor and the room.



Figure 45 : Heating Cables for SS-SDB, SS-SF and SS-CH1

Figure 46 shows how the electric heating system supply cables are grouped near the junction box. Because of this arrangement, the temperature probe length is longer than manufacturer recommendations.

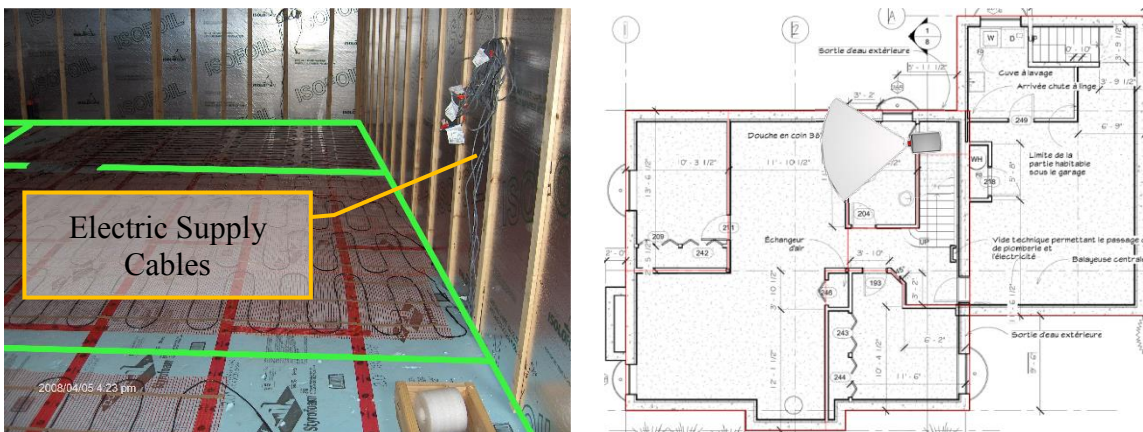


Figure 46 : Heating Cables for SS-SF and SS-CH1

Figure 47 shows the temperature probe for SS-SF-04. The manufacturer recommendations for installing the probe is to place the tip of the wire at least four cable rows away from the wall in order to get rid of the influence of the perimeter of the slab, which was not applied in this case.

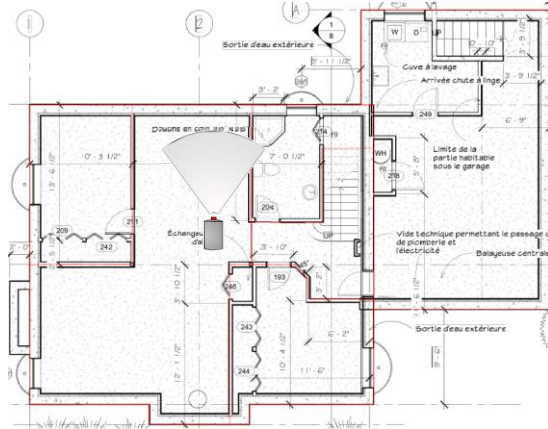
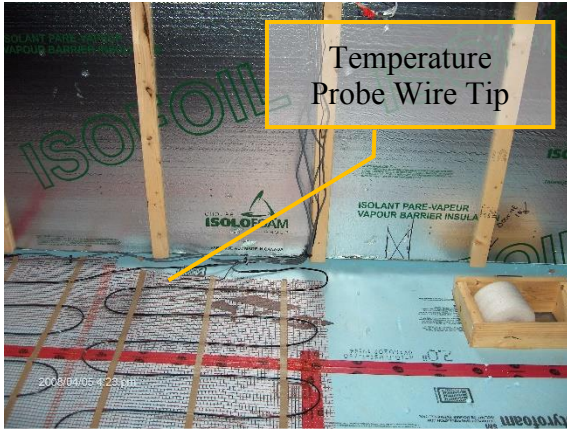


Figure 47 : Temperature Probe for SS-SF-04

Figure 48 shows the temperature probe for the basement bathroom. This probe was also not placed sufficiently far from the exterior wall. There are no heating cables placed beneath the shower or toilet.

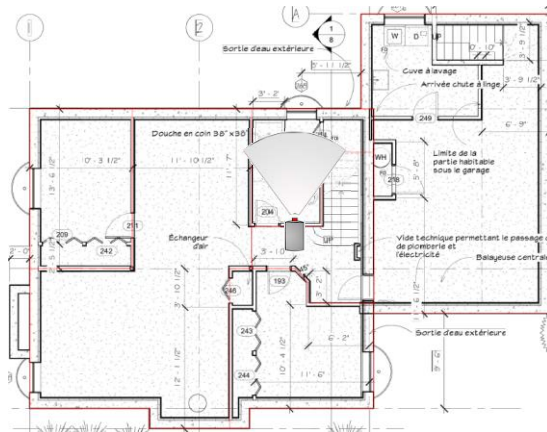
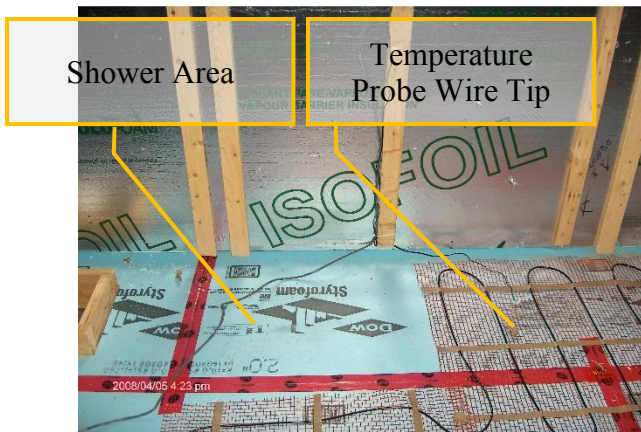


Figure 48 : Temperature Probe for SS-SDB-01

Figure 49 highlights a case where the temperature probe is very far from the thermostat. The EHF thermostat for SS-CH1 is near the doorway whereas the temperature probe is at the other end of the room in close proximity to an exterior wall.



Figure 49 : Temperature Probe for SS-CH1

Figure 50 shows the cable disposition near thermostat SS-SF-01. Here again, that the temperature probe is very close to the exterior wall. In addition, the insulation in periphery of the basement slab does not stretch all the way down to the floor insulation. This further strengthens the fact that the perimeter of the basement slab has higher thermal losses, influencing the floor temperature readings.

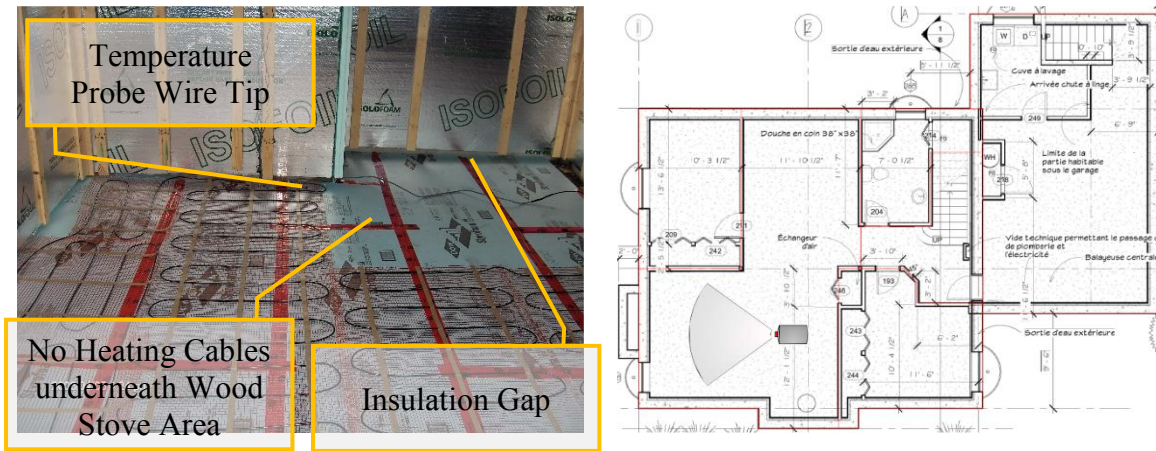


Figure 50 : Temperature Probe for SS-SF-01

Figure 51 shows the temperature probe location for room SS-GAR which further highlights the fact that the probes are placed too close to the exterior wall.



Figure 51 : Temperature Probes for SS-GAR-01 and SS-GAR-02

Furthermore, all rooms have their floor surface area partially heated, because no electric heating cables were placed underneath interior partitions, wardrobes and other objects such as showers, bathroom countertop, etc. In the TRNSYS model however, the heating power is uniformly distributed across the room.

F.3 Hot Water Tank

The following picture shows the make and model of the electric domestic hot water tank installed in the home. The maximum electrical power draw is 4500W for a 61.4 imperial gallon tank.



Figure 52 : DHW Tank Label

F.4 Air Exchanger

The following picture shows the installed air exchanger in its current location in the basement. The unit is completely new, it was purchased and installed on the day of the first visit, October 26th, 2016.



Figure 53 : Heat Exchanger Installation (Left) and Label (Right)

F.6 Laundry Chute

The laundry chute connects the 2nd floor office to the basement laundry room. The chute is not open to the ground floor garage but merely passes through it. The dimensions of the channel are 30cm x 30 cm. The air flow through the chute from the stack effect is not monitored.



Figure 54 : Laundry Chute Spanning All Storeys: Basement Laundry Room (Left), Ground Floor Garage (Middle) and 2nd Floor Office (Right).

F.7 Assemblies

The assemblies of this house are presented in the following table as well as their thermal properties. The thermal conductivity is a calculation which is based on a framing factor of 15% for structural light weight wood walls. Certain assemblies do not have density or heat capacity displayed in the table. The TRNSYS simulation environment is based on explicit finite difference formulations and therefore assemblies are bound to certain density/capacity ratios to ascertain convergence of the FORTRAN solver. Assemblies that cannot guaranty the convergence of the solver are described as massless layers and only a thermal resistance is prescribed.

Table 43 : Assemblies of the Monitored Building and Their Constituting Materials and Properties

Description	Materials	L [m]	ρ^1 [kg/m ³]	c_p^1 [kJ/kg·K]	k^1 [kJ/h·m·K]
Basement slab below heating wires	Concrete	0.1143	2240	0.9	7.02
	Extruded Polystyrene	0.05	25 ⁵	1.47	0.1023
Basement slab above heating wires	Stratified wood flooring	0.0095	650	1.2	0.504
	Concrete	0.1143	2240	0.9	7.02
Basement slab above heating wires in bathroom	Porcelain Tiles	0.0064	2000	1	4.32
	Ceramic adhesive	0.0064	1920	0.84	5.04
	Concrete	0.1143	2240	0.9	7.02
Foundation wall in contact with earth	Concrete	0.254	2240	0.9	7.02
	Expanded polystyrene	0.0508	16	1.2	0.144
	Air space	0.0159	-	-	0.3378 ³
	Gypsum panel	0.0127 ⁶	480 ⁶	1.09 ⁶	0.571 ⁶
Foundation wall adjacent to exterior	Stucco	0.0064	1857	0.9	2.592
	Concrete	0.254	2240	0.9	7.02
	Expanded polystyrene	0.0508	16	1.2	0.144
	Air space with furring strips	0.0159	-	-	0.3378
	Gypsum panel	0.0127 ⁶	480 ⁶	1.09 ⁶	0.571 ⁶
Interior wall, 2x6 assembly	Gypsum panel	0.0127 ⁶	480 ⁶	1.09 ⁶	0.571 ⁶
	Air space with 2x6 @ 0.406m	0.1397	54.86	1.047	1.264
	Gypsum panel	0.0127 ⁶	480 ⁶	1.09 ⁶	0.571 ⁶
Interior wall, 2x4 assembly	Gypsum panel	0.0127 ⁶	480 ⁶	1.09 ⁶	0.571 ⁶
	Air space with 2x4 @ 0.406m	0.0889	54.86	1.047	0.161
	Gypsum panel	0.0127 ⁶	480 ⁶	1.09 ⁶	0.571 ⁶
Fictitious division of concave room to convex room	Massless Layer	-	-	-	-
Floor assembly with hardwood cover	Hardwood flooring	0.0191	670	1.63	0.5904
	Tung and groove plywood	0.0159	800	1.2	0.5400
	Air space with wood open-web joists @ 0.406m	0.3937	126.41	1.092	1.546
	Acoustic tile	0.0127	288	1.34	0.206
Floor assembly with ceramic cover, heated floor	Porcelain tile	0.0064	2000	1	4.32
	Ceramic adhesive	0.0064	1920	0.84	5.04
	Self-leveling concrete with heated wires	0.0064	400	0.84	0.36
	Tung and groove plywood	0.0318	800	1.2	0.5400
	Air space with wood open-web joists @ 0.406m	0.3937	126.41	1.092	1.546
	Acoustic tile	0.0127	288	1.34	0.206
Structural concrete wall	Gypsum panel	0.0127 ⁶	480 ⁶	1.09 ⁶	0.571 ⁶
	Air space	0.0159	-	-	0.3378 ³
	Concrete	0.254	2240	0.9	7.02
2 nd storey floor assembly, ceramic cover	Porcelain tile	0.0064	2000	1	4.32
	Ceramic adhesive	0.0064	1920	0.84	5.04
	Self-leveling concrete with heated wires	0.0064	400	0.84	0.36
	Tung and groove plywood	0.0318	800	1.2	0.5400
	Air space with wood open-web joists @ 0.406m	0.3366	126.41	1.092	1.500
	Gypsum panel	0.0127 ⁶	480 ⁶	1.09 ⁶	0.571 ⁶
2 nd storey floor assembly, hard wood cover	Hardwood flooring	0.0191	670	1.63	0.5904
	Tung and groove plywood	0.0159	800	1.2	0.5400
	Air space with wood open-web joists @ 0.406m	0.3366	126.41	1.092	1.500
	Gypsum panel	0.0127 ⁶	480 ⁶	1.09 ⁶	0.571 ⁶

Floor assembly, ceramic cover, no heated floor	Porcelain tile	0.0064	2000	1	4.32
	Ceramic adhesive	0.0064	1920	0.84	5.04
	Tung and groove plywood	0.0318	800	1.2	0.5400
	Air space with wood open-web joists @ 0.406m	0.3937	126.41	1.092	1.546
	Acoustic tile	0.0127	288	1.34	0.206
Garage structural concrete floor	Concrete	0.2286	2240	0.9	7.02
	Extruded Polystyrene	0.0254	25 ⁵	1.47	0.1023
	Air space	0.0159	-	-	0.4293 ³
	Gypsum panel	0.0127 ⁶	480 ⁶	1.09 ⁶	0.571 ⁶
Interior division, ceramic cover on one side	Porcelain tile	0.0064	2000	1	4.32
	Ceramic adhesive	0.0064	1920	0.84	5.04
	Gypsum Panel	0.0127	800	1.09	0.5787
	Air space with 2x4 @ 0.406m	0.0889	54.86	1.047	0.161
	Gypsum panel	0.0127 ⁶	480 ⁶	1.09 ⁶	0.571 ⁶
Attic floor	Mineral Wool with 2x4@0.609m	0.254	-	-	0.01398
	BP Enermax & airspace	0.0286	-	-	0.0376 ⁴
	Gypsum panel	0.0127 ⁶	480 ⁶	1.09 ⁶	0.571 ⁶
Cathedral ceiling	Asphalt Shingles	-	-	-	0.0214
	Roofing O.S.B.	0.0110	-	-	0.468
	Airspace with stud @ 0.609m	0.0254	36.94	1.035	0.188
	Mineral wool & joist @ 0.609m	0.254	44.81	0.874	0.166
	BP Enermax & airspace	0.0286	-	-	0.0376 ⁴
	Gypsum panel	0.0127 ⁶	480 ⁶	1.09 ⁶	0.571 ⁶
Uninsulated exterior wall	Brick	0.0889	2002	0.92	4.8
	Air space	0.0254	-	-	0.439 ³
	Asphalt impregnated fiber board	0.0127	288	1.3	0.547
Insulated exterior wall	Brick	0.0889	2002	0.92	4.8
	Air space	0.0254	-	-	0.439 ³
	Asphalt impregnated fiber board	0.0127	288	1.3	0.547
	Mineral wool with 2x6 @ 0.4064m	0.1397	62.42	0.891	0.170
	BP Enermax & airspace	0.0286	-	-	0.0376 ⁴
	Gypsum panel	0.0127 ⁶	480 ⁶	1.09 ⁶	0.571 ⁶
Attic roof	Asphalt Shingles	-	-	-	0.0214
	Roofing O.S.B.	0.0110	-	-	0.468

1) Values taken from Çengel et al. (2011); 2) Thermal resistance calculated by TRNBUILD module 3) Values taken from Hutcheon et al. (1983); 4) Values from www.bpcan.com (Building Products of Canada Corp., 2016) 5) Values taken from www.building.dow.com (Dow Building Solutions, 2017) 6) Values taken from www.usg.com (Sheetrock, 2017)

F.8 Heating Systems

The following table shows the heating systems monitored in the building as well as their identifier.

Table 44 : Heating Systems Installed in the Residence

Storey	Zone	Zone Description	Thermostat Name	Nominal Power [W]	Equipment Type Controlled	Prescriptive Parameter
Basement	SS_SF	Living Room	SS-SF-01	1992	B.F.H.S.	F.S.T.
			SS-SF-02	1000	C.H.S.	Z.A.T.
			SS-SF-03	1000	C.H.S.	Z.A.T.
			SS-SF-04	2640	B.F.H.S.	F.S.T.
	SS_SF_STAIRS	Living Room & Stairs	N. A.	N. A.	N. A.	N. A.
	SS_CH1	Bedroom	SS-CH1-01	1296	B.F.H.S.	F.S.T.
	SS_SDB	Bathroom	SS-SB-01	672	B.F.H.S.	F.S.T.
	SS_GAR	Storage	SS-GAR-01	2280	B.F.H.S.	F.S.T.
			SS-GAR-02	2352	B.F.H.S.	F.S.T.
SS_CH2	Bedroom	SS-CH2-01	624	B.F.H.S.	F.S.T.	
		SS-CH2-02	1000	C.H.S.	Z.A.T.	
Ground Floor	RDC_SF	Living Room	RDC-SF-01	3444	C.H.S.	Z.A.T.
	RDC_CUI	Kitchen	RDC-CUI-01	1560	S.F.H.S.	Z.A.T.
			RDC-CUI-02	840	S.F.H.S.	Z.A.T.
	RDC_CUI_STAIRS	Kitchen & Stairs	N. A.	N. A.	N. A.	N. A.
	RDC_SDB	Bathroom	N. A.	N. A.	N. A.	N. A.
	RDC_GAR	Garage	RDC-GAR-01	2352	B.F.H.S.	F.S.T.
RDC-GAR-02			2304	B.F.H.S.	F.S.T.	
2 nd Floor	ET_SDB1	Bathroom	ET-SDB1-01	648	S.F.H.S.	Z.A.T.
	ET_SDB2	Bathroom	ET-SDB2-01	288	S.F.H.S.	Z.A.T.
	ET_CH1	Bedroom	ET-CH1	1000	C.H.S.	Z.A.T.
	ET_CH2	Bedroom	ET-CH2-01	1250	C.H.S.	Z.A.T.
	ET_COU	Hallway	ET-COU-01	1000	C.H.S.	Z.A.T.
	ET_CH3	Bedroom	ET-CH3-01	2250	C.H.S.	Z.A.T.
	ET_BUR	Office & Gym	ET-BUR-01	2308	C.H.S.	Z.A.T.
ET-BUR-02			2175	C.H.S.	Z.A.T.	